Natural Convective Heat Transfer from Interrupted Rectangular Fins

by

Golnoosh Mostafavi
B. Sc., University of Tehran, 2010

THESIS SUBMITTED IN PARTIAL FULFILLMENT OF
THE REQUIREMENTS FOR THE DEGREE OF

MASTER OF APPLIED SCIENCE

in the
School of Engineering Science
Faculty of Applied Sciences

SIMON FRASER UNIVERSITY
Fall 2012

Approval

Name: **Golnoosh Mostafavi**

Degree: **Master of Applied Science**

Title of Thesis: **Natural convective heat transfer from interrupted rectangular fins**

Examining Committee:

Chair: **Dr. Siamak Arzanpour**
Assistant Professor of Engineering Science

_____

Dr. Majid Bahrami
Senior Supervisor
Associate Professor of Engineering Science

_____

Dr. John Jones
Supervisor
Associate Professor & Acting Director
School of Engineering Science

_____

Dr. Ash Parameswaran
Internal Examiner
Professor of Engineering Science (Burnaby)

Date Defended/Approved: November 29, 2012

Partial Copyright Licence

Abstract

Heatsinks are widely used in various industrial applications to cool electronic, power electronic, telecommunications, and automotive components. Those components might be either high-power semiconductor devices, e.g., diodes, thyristors, IGBTs and MOSFETs, or integrated circuits, e.g. audio amplifiers, microcontrollers and microprocessors. More precisely, the passive cooling heatsinks are widely used in CPU cooling, audio amplifiers and power LED cooling.

In the work herein, steady-state external natural convection heat transfer from vertically-mounted rectangular interrupted finned heatsinks is investigated. After regenerating and validating the existing analytical results for continuous fins, a systematic numerical, experimental, and analytical study is conducted on the effect of the fin array and single wall interruption. FLUENT and COMSOL Multiphysics software are used in order to develop a two-dimensional numerical model for investigation of fin interruption effects. To perform an experimental study and to verify the analytical and numerical results, a custom-designed testbed was developed in Simon Fraser University (SFU). Results show that adding interruptions to vertical rectangular fins enhances the thermal performance of fins and reduces the weight of the fin arrays, which in turn, can lead to lower manufacturing costs. The optimum interruption length for maximum fin array thermal performance is found and a compact relationship for the Nusselt number based on geometrical parameters for interrupted walls is presented using a blending technic for two asymptotes of interruption length.

Keywords: natural convection; air cooling; thermal management; heat transfer; fluid flow; numerical modeling; heatsink design; experimental study; passive cooling; electronic cooling; power electronics; modeling

Executive Summary

Heatsinks are widely used in various industry applications to cool down electronic components. Those components might be either high-power semiconductor devices, e.g., diodes, thyristors, IGBTs and MOSFETs, or integrated circuits, e.g. audio amplifiers, microcontrollers and microprocessors. More precisely, the passive cooling heatsinks are widely used in CPU cooling, audio amplifiers and power LED cooling. The constitutive element that defines the geometry of a heatsink is its fins. A fin is usually a flat plate that extends from a heatsink; it is used to increase the rate of heat transfer to or from the environment by increasing the convective heat transfer surface area. Some of the common fin geometries that are being used in the industry and studied in the literature include: straight, circular, and pin-shaped. Interrupted fins are a more general form of fins and they can include both, continuous rectangular and pin fins, see Fig. 1-2. At a closer look, continuous fins and pin fins are two extreme cases of interrupted fins.

A proper selection of interruption length leads to a higher thermal performance. This expectation is based on the fact that interrupted fins disrupt the thermal boundary layer growth, thus, maintaining a thermally developing flow regime along the fins, which, in turn, leads to a higher natural heat transfer coefficient. Additionally, fin interruption results in a considerable weight reduction and that can lead into lower manufacturing costs. On the other hand, adding interruptions leads to a heat transfer surface area reduction, which decreases the total heat transfer. These two competing effects clearly indicate that an “optimum” fin interruption exists that provide the maximum heat transfer rate from naturally-cooled heatsinks.

Despite numerous existing studies in the area of the natural convective heat transfer from fins, as shown in the literature review Chapter 1, no in-depth study has been performed to investigate the natural convection heat transfer from interrupted fins for external natural convective heat transfer.

Motivation

The work herein has been impelled by a collaborative research project with Analytic Systems Ware (ASW), a local company that manufactures electronic power conversion systems located in Delta, BC. Some of the company products, which are cooled via naturally-cooled enclosures (heatsinks), experienced an excessive heating which created reliability and performance issues for ASW's clients. The company contacted Dr. Bahrami and a research venture was initiated to resolve the thermal management problem.

As the first step, a testbed was designed and built at Simon Fraser University (SFU) and six enclosure heatsinks made by ASW were tested; the electronic enclosures were made of aluminum by extrusion process. Three enclosures were finned, the original ASW design at three different lengths, while the others had the fins milled off, down to the bottom of the fin base, as shown in Fig. I. During the milling process, no alterations were made to affect the enclosure dimensions. The thermal test results did not show any noticeable heat transfer enhancement between the finned and un-finned enclosures with the same length; however, the enclosure weight, and its production cost, in bare enclosures was reduced by almost 84%. The reason for that indistinguishable difference in the cooling capacity of the two enclosures resided in the improper design of the fin geometry on the heatsink.

After proper thermal analysis, testing, and heatsink prototyping, several new fin designs for ASW enclosures were proposed by SFU, an enclosure made by ASW based on the findings of this project, which led to a significant average surface temperature reduction, 22°C, under the maximum operational power as well as to an average 26% weight reduction, when compared to the original ASW design.

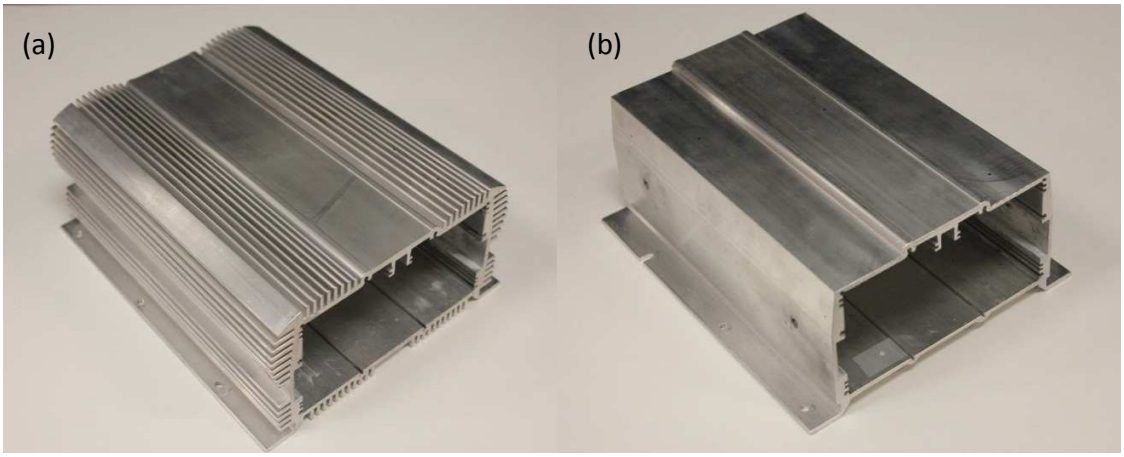

Figure I: The enclosure designed by the industrial collaborator, Analytic System Ware (ASW), a) finned enclosure manufactured via extrusion, b) bared (the fins were machined down to the base) of the enclosure. The length of both enclosures was 6 inches.

Research Objectives

- To develop new models for natural convection heat transfer from interrupted rectangular fins based on geometrical parameters.
- To predict the optimum value for fin interruption lengths in fin arrays for maximum heat transfer rate.

Methodology

In this study, a systematic approach is adopted to study the natural convection heat transfer from the interrupted rectangular, vertically-installed fins. The natural heat convection heat transfer is complex since the momentum and energy equations are highly coupled and non-linear, which makes finding a general analytical solution highly unlikely. As such, the following methodology has been adopted.

The focus of this study is on developing compact easy-to-use thermal models that can predict the natural convective heat transfer from interrupted, rectangular walls to the ambient. Two asymptotes are specified and a blending technique is implemented to devise a compact relationship for the Nusselt number based on a new characteristic length scale, which is called the effective fin length.

The fin array problem is numerically studied, using Fluent and COMSOL Multiphysics software, and a relationship for the optimum fin array interruption length is developed to obtain the maximum natural convective heat transfer.

Two new experimental test beds have been designed and built at SFU to verify the developed models and the proposed correlations. Experimental studies with various testing samples at different scales were performed. Figure II shows the project road map and the deliverables of this thesis.

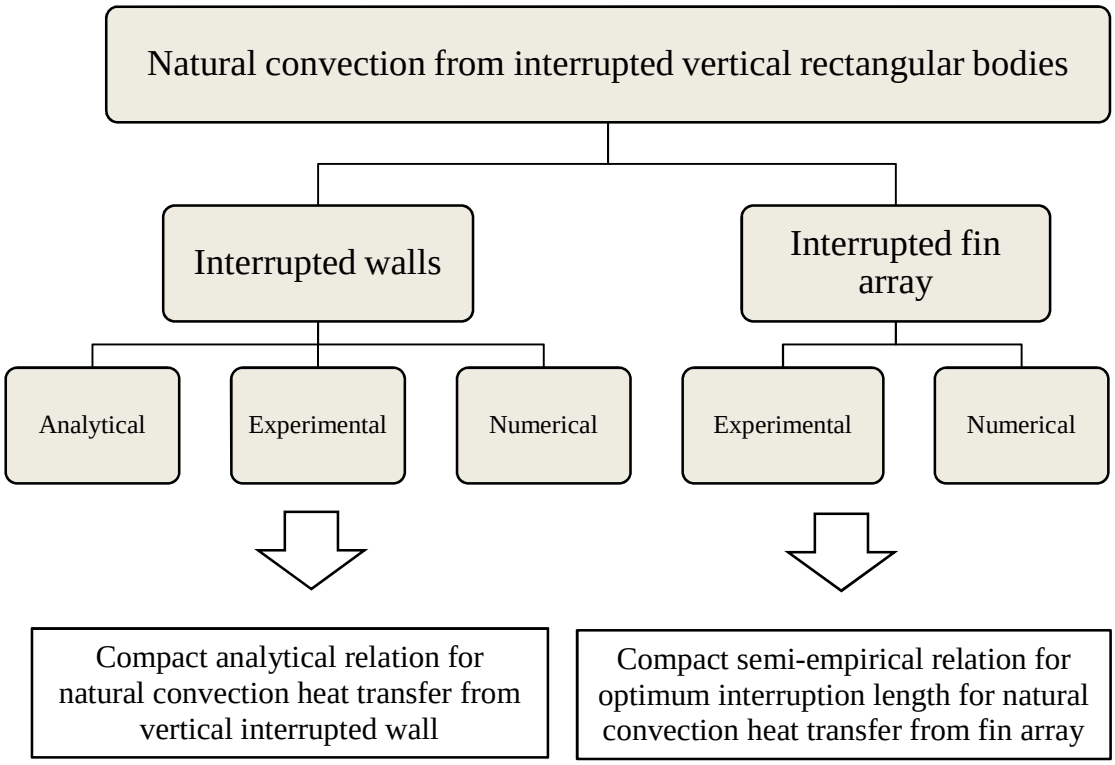

Figure II: Research road map.

This dissertation is divided into five chapters. Chapter 1 includes an introduction including a background on the natural convective heat transfer from rectangular fins. The numerical procedure is presented in Chapter 2. This chapter includes the problem

definition, the governing equations, boundary conditions, assumptions, mesh size, and numerical results. The present experimental study is described in Chapter 3; where, the two test-beds and the experimental procedure are explained in detail, and an uncertainty analysis is performed. The effects of fin interruptions on thermal boundary layer and the relationships for the Nusselt number are presented in Chapter 4. Summary and conclusions of the dissertation is presented in Chapter 5. This last chapter also includes potential future work endeavours. Appendix 1 includes all the experimental and numerical data collected from various sources and used in the dissertation. Appendix 2 contains the reports prepared for ASW for the new enclosure design.

Acknowledgements

I would like to thank my supervisor, Dr. Majid Bahrami, for his excellent support during my graduate studies. His professional attitude and positive personality have continually inspired me and his encouragements have refreshed me when I needed the most. I would also like to thank Dr. John Jones and Dr. Ash Parameswaran for kindly reviewing this thesis.

I would like to thank my colleagues and lab mates at the Laboratory of Alternative Energy Conversion (LAEC) at Simon Fraser University. Their helpful comments and assistance played an important role in the development of this dissertation. In particular, I want to thank Mr. Marius Haiducu and Mehran Ahmadi for their invaluable support.

This project has been financially supported by the Mathematics of Information Technology and Complex Systems (MITACS) and the Natural Sciences and Engineering Research Council of Canada (NSERC). I would also like to acknowledge Analytic System Ware (ASW) Ltd. for providing their financial support and helpful technical feedbacks during the project.

Contents

Approval ii
Partial Copyright Licence iii
Abstract iv
Executive Summary v
Acknowledgements x
Contents xi
List of Figures xiii
Glossary xvi

Chapter 1. Introduction 1
1-1 Power Electronics Cooling 1
1-2 Passive cooling solutions 2
1-3 Background 4
1-3-1 Vertical walls 6
1-3-2 Vertical rectangular fin arrays 7
1-4 Objectives 15

Chapter 2. Numerical Analysis 17
2-1 Problem statement 18
2-2 Governing Equations 19
2-3 Summary of Assumptions 23
2-4 Computational domain and boundary conditions 24
2-5 Mesh independency 30
5.4 Numerical results validation 33

Chapter 3. Experimental Study 36
3-1 Testbed design 36
3-2 Sample Preparation 40
3-3 Test procedure and data collection 43
3-4 Uncertainty analysis 50

Chapter 4. Results and Discussion 52
4-1 Continuous finned heatsinks 53
4-2 Effect of fin spacing on heat transfer rate 55
4-3 Effects of fin interruption on natural convection heat transfer 58
4-4 Model development for interrupted vertical walls 62

Chapter 5. Conclusion 73
Future Work 75

Bibliography 76

Appendices 81
Appendix 1. Experimental Data 81
Appendix 2. ASW Reports 94

List of Figures

Figure 1-1: Different fin types, a) rectangular b) radial c) pin fins. 3

Figure 1-2: Heatsink with continuous rectangular fins. 4

Figure 1-3: geometrical parameters and boundary layers of a vertical wall. 6

Figure 1-4: geometrical parameters and schematic thermal and hydrodynamic boundary layers on vertical fin array. 7

Figure 1-5 : Fujii's [21] considered geometry for inclined interrupted fins. 10

Figure 1-6: Comparison of the data and analytical models in literature. 14

Figure 1-7: Continuous and Interrupted rectangular fins 16

Figure 2-1: Schematic of the considered heatsink geometry: a) continuous rectangular finned heatsink and b) interrupted rectangular finned heatsink. 18

Figure 2-2: Effect of adding interruptions on the boundary layer growth in natural heat transfer from vertical fins. 19

Figure 2-3: Schematic of the considered numerical domain: a) continuous fins; b) interrupted fins; c) boundary conditions for continuous fins; d) boundary conditions for interrupted fins. 22

Figure 2-4: Grid used in the numerical model for a) continuous and b) interrupted fin array. 26

Figure 2-5: Temperature distribution contours of fin arrays, and the effect of interruption length on thermal boundary layer. The thermal boundary and its growth can be seen in the temperature contours. 27

Figure 2-6: Numerical simulation, temperature contours, for fin arrays, and the effect of multiple interruptions on thermal boundary layer. 28

Figure 2-7: a) Schematic of the numerical domain and boundary conditions for interrupted single vertical walls. b) Grid used in the model for interrupted walls. 29

Figure 2-8: Grid independency study, Ra = 1.6· 103; in vertical direction 31

Figure 2-9: Numerical simulation validation; continuous fin, single channel (s = 9.5 mm, L = 305 mm, H = 17 mm). 35

Figure 2-10: Numerical simulation validation; interrupted finned heatsink (n = 8, s = 9.5 mm, L = 305 mm, H = 17 mm, l = 37 mm, G = 30 mm). 35

Figure 3-1: Schematic of the heatsink test-bed. 37

Figure 3-2: A continuous fin in the heatsink test-bed. 38

Figure 3-3: The testbed components: a) Extech 430 multimeter, b) SC-20MVariac, c)NI 9214DAQ system. 39

Figure 3-4: a) Schematic of the single wall test-bed; b) an interrupted single wall shown in the testbed. 39

Figure 3-5: Examples of tested samples, a) continuous fins heatsink and b) interrupted fins heatsink. 42

Figure 3-6: Experimental results for interrupted fins heatsinks. 47

Figure 3-7: Experimental results for interrupted single walls. 49

Figure 4-1: Comparison of the present experimental data with the theoretical predictions of [15] for different fin heights-continuous finned heatsinks; see Table 3-1 for the dimensions of the heatsinks. 54

Figure 4-2: Comparison of the present experimental data with the theoretical predictions of [1] for different fin spacing-continuous finned heatsinks; see Table 3-1 for the dimensions of the heatsinks. 55

Figure 4-3: Heat transfer rate and heatsink mass versus fin spacing for different average surface temperatures, fin base lengths L = 305 mm, heights H = 17 mm; see Table 3-1 for more detail on samples. 57

Figure 4-4: Comparison between the present experimental data and numerical results for different fin interruption lengths (i.e., 20, 30 and 40 mm) for constant number of fins in a row N = 4 interruptions; see Table 3-2 for more detail on samples. 59

Figure 4-5: Comparison between experimental data and the present numerical results for different number of interruptions (N) for constant interruption value of G = 20 mm; see Table 3-2 for more detail on samples. 60

Figure 4-6: Effect of the interruption length on the total natural convection heat transfer from the fins (numerical results): a) fin length l = 5 mm and b) fin length l = 12.5 mm. ($\Delta T = Ts - Tamb$) 61

Figure 4-7: Numerical data and asymptotes for natural convective heat transfer from interrupted walls. 67

Figure 4-8: Numerical data and analytical relationship - natural convective heat transfer from interrupted walls. 68

Figure 4-9: Comparison between the present numerical data and the proposed compact relationship for Nusselt number of interrupted walls. (ζ = l / t) 70

Figure 4-10: Comparison between the present numerical and experimental data against the new compact relationship for the natural convective heat transfer from interrupted walls. ($\zeta = l/t$) 72

Figure A1-1: Testbed configuration for heatsinks with fin array (both continuous and interrupted) 81

Figure A1-2: Testbed configuration for heatsinks with interrupted walls 89

Glossary

A	Surface area, m^2
F	Surface view factor
g	Gravitational acceleration, m^2/s
G	Fin interruption length, m
Gr	Grashof number
h	Convection heat transfer coef. W/m^2K
H	Fin height, m
I	Electrical current, A
k	Thermal conductivity, $W/m\ K$
l	Fin length, m
L	Enclosure length, m
L_{eff}	Effective length, m
n	Number of interruptions
N	Number of fins per row
Nu	Nusselt number
P	Pressure, Pa
P_{input}	Input power, W
Pr	Prandtl number
$\dot{Q}$	Heat transfer rate, W
Ra	Rayleigh number
s	Fin spacing, m
t	Fin thickness, m
T	Temperature, K
u	Flow velocity in x direction, m/s
v	Flow velocity in y direction, m/s
V	Electrical voltage, V
V_{in}	Inlet velocity, m/s

W	Enclosure width, m
x	Direction normal to fin surface, m
y	Direction along fin surface, m

Greek symbols

α	thermal diffusivity
β	Coefficient of volume expansion, 1/K
γ	Interruption length to wall length ratio
ζ	Wall length to wall thickness ratio
μ	Fluid viscosity, Ns/m^2
ρ	Density, kg/m^3

Subscripts

amb	ambient
atm	Atmosphere
low	Lower side of the fin/wall
NC	Natural convection
opt	Optimum
R	Radiation
s	surface
up	Upper side of the fin/wall
w	wall

Chapter 1.

Introduction

1-1 Power Electronics Cooling

The design of efficient cooling strategies is essential for reliable performance of high power density electronics. A number of failure mechanisms in electronic devices, such as inter-metallic growth, metal migration, and void formation, are related to thermal effects. In fact, the rate of such failures nearly doubles with every 10°C increase above the operating temperature (~80°C) of high power electronics [1]. Besides the damage that excess heat can cause, it increases the movement of free electrons within semiconductors, causing an increase in signal noise [2]. Consequently, electronics thermal management is of crucial importance as is reflected in the market. Thermal management products show a growth from about $7.5 billion in 2010 to $8 billion in 2011, and it is expected to grow to $10.9 billion in 2016, a compound annual growth rate increase of 6.4%. Thermal management hardware, e.g. fans and heat sinks, accounts for about 84% of the total market. Other main cooling product segments, e.g. software, interface materials, and substrates, each account for between 4% and 6% of the market, respectively. The North American market will maintain its number one position throughout this period, with a market share of about 37%, followed by Asia-Pacific with approximately 23% to 24% [3].This power dissipation generates heat, which is a by-product in many engineering

applications. This unwanted by-product can decrease the performance of the systems since almost every engineering system is designed to work within a certain temperature limits. Exceeding these limits by overheating, could lead to a system failure.

Currently, the thermal losses of power electronic devices are increasing. At the same time, their sizes are decreasing. Consequently, heatsinks have to dissipate higher heat fluxes in every new design. Therefore, devising efficient cooling solutions to meet these challenges is of paramount importance and has direct impacts on the performance and reliability of electronic and power electronic devices.

1-2 Passive cooling solutions

The techniques used in the cooling of high power density electronic devices vary widely, depending on the application and the required cooling capacity. The heat generated by the electronic components has to pass through a complex network of thermal resistances to the environment. Passive cooling methods are widely preferred for electronic and power electronic devices since they provide low-price, noiseless, and trouble free solutions. Some passive cooling techniques include: heat pipes, natural convection air cooling, and thermal storage using phase change materials (PCM). Heat pipes can efficiently transfer heat from heat sources in high power density converter components to a heatsink based on phase change of a working fluid [4, 5]. Air-cooling also is recognized as an important technique in the thermal design of electronic packages, because besides its availability, it is safe, does not contaminate the air and does not add vibrations, noise and humidity to the system in which it is used [6]. Such features of natural convection stimulated considerable research on the development of optimized

finned heatsinks and enclosures [7, 8, 9]. Using fins is one of the most inexpensive and common ways to dissipate unwanted heat and it has been successfully used for many engineering applications.

Fins come in various shapes; such as rectangular, circular, pin fin rectangular, pin fin triangular, etc., see Fig. 1-1, depending on the application. Rectangular fins are the most popular fin type because of their low production costs and high thermal effectiveness.

Figure 1-1: Different fin types, a) rectangular b) radial c) pin fins.

Natural convective heat transfer from vertical rectangular fins, shown in Figure 1-2, and from pin fins is a well-studied subject in the literature. It has been investigated analytically, numerically and experimentally. The following paragraphs provide an overview on the pertinent literature on the subject; the previous studies are grouped into analytical, numerical, and experimental works; more detailed reviews can be found elsewhere, see for example [10].

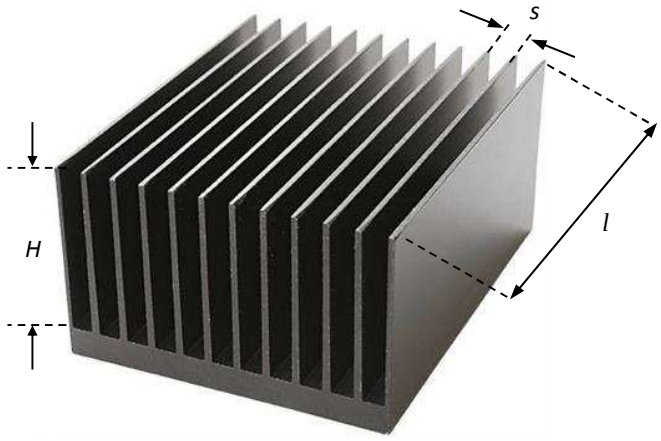

Figure 1-2: Heatsink with continuous rectangular fins.

1-3 Background

The focus of this study is on natural convection heat transfer from interrupted, vertical and rectangular fins. However, a more general overview on pertinent literature in the area of natural heat transfer from fins is provided in this section. A variety of theoretical expressions, graphical correlations and empirical equations have been developed to represent the coefficients for natural convection heat transfer from vertical plates and vertical channels. These studies were mostly focused on geometrical parameters of the heatsinks and fins, such as fin spacing, fin height, fin length, as well as, fin directions.

Table 1-1Table 1-1 presents a summary of the literature review as it pertains to analytical, numerical or experimental type of work.

Three dimensionless numbers are important in heat transfer: the Nusselt (*Nu*) number, the Prandtl (*Pr*) number and Rayleigh number (*Ra*). These three non-

dimensional numbers are used extensively in the heat transfer literature for analytical purposes. The Nusselt number is the ratio of convection heat transfer to the fluid conduction heat transfer under the same conditions.

$$Nu_l = \frac{h\,l}{k}, \tag{1-1}$$

where l is fins length, h is the convective heat transfer coefficient, and k is the fluid thermal conductivity, respectively. The Prandtl number is the ratio of momentum diffusivity (kinematic viscosity) to thermal diffusivity.

$$Pr = \frac{\nu}{\alpha}, \tag{1-2}$$

where ν is the kinematic viscosity, α is the thermal diffusivity of the fluid.

Rayleigh number, *Ra,* is a dimensionless number associated with buoyancy driven flow. Ra is defined as the product of Grashof number, Gr, which describes the relationship between buoyancy and viscosity within a fluid, and the Prandtl number, for cases of both, uniform surface heat flux and uniform surface temperature.

$$Nu_L = \left\{ 0.825 + \frac{0.387 Ra_L^{\frac{1}{6}}}{\left[1 + (0.492/Pr)^{\frac{9}{16}}\right]^{\frac{8}{27}}} \right\}^2, \tag{1-3}$$

$$Ra_L = \frac{g\beta\,\Delta T L^3}{\alpha\vartheta}, \tag{1-4}$$

$$Gr_L = \frac{g\beta\,\Delta T L^3}{\vartheta^2}, \tag{1-5}$$

where g is the gravitational acceleration and β is the thermal expansion coefficient, respectively. ΔT is the temperature difference between the fins and ambient.

1-3-1 Vertical walls

The considered vertical wall geometrical parameters are shown in Figure 1-3.

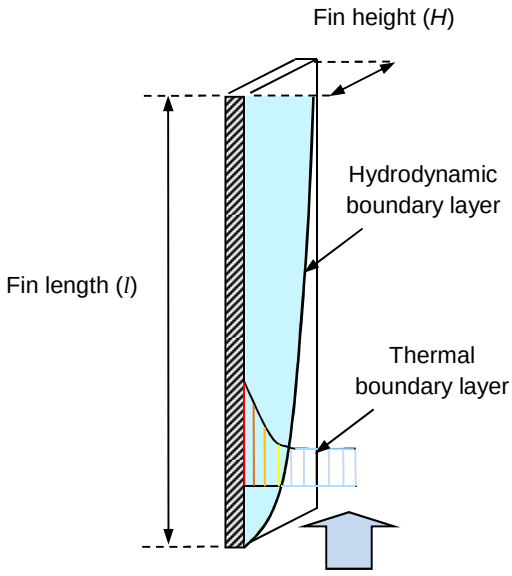

Figure 1-3: geometrical parameters and boundary layers of a vertical wall.

Ostrach [11] made an important contribution on analysing the natural convective heat transfer from vertical fins. He analytically solved laminar boundary layer equations through similarity methods for uniform wall temperature condition and developed a relationship for the Nusselt number for different values of Prandtl number. As well, Sparrow and Gregg [12] used similarity solutions for boundary layer equations for the

cases of uniform surface heat flux. Churchil and Chu [13] also developed an expression for Nusselt number for all ranges of the *Ra*, and *Pr* numbers,

1-3-2 Vertical rectangular fin arrays

A schematic of a vertical rectangular fin array and its geometrical parameters along with the thermal and hydrodynamic boundary layers are shown in Figure 1-4.

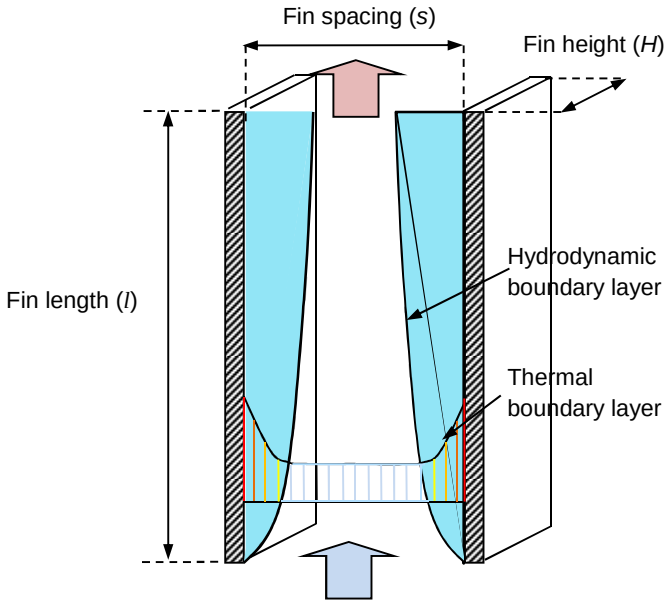

Figure 1-4: geometrical parameters and schematic thermal and hydrodynamic boundary layers on vertical fin array.

1-3-2-1 Analytical approach

Pioneering analytical work on vertical channels was carried out by Elenbaas [14]. He investigated analytically and experimentally the isothermal finned heatsinks. The analytical study resulted in general relations for natural convective heat transfer from vertical rectangular fins.

Bar-Cohen and Rohsenow [15] also performed an analytical study to investigate the natural convective heat transfer from two parallel plates. They developed a relationship for Nusselt number in terms of the Ra number for both, isothermal and isoflux plate cases and reported a correlation for the optimum fin spacing. They claimed that the value of the Nusselt number lies between two extremes that are associated with the separation between the plates, or, in other words, the channel width. For wide spacing, the plates appear to have little influence upon one another looking like they are isolated; the Nusselt number in this case approaches its isolated plate limit. On the other hand, for closely spaced plates or for relatively long channels, the fluid velocity attains its fully developed value and the Nusselt number reaches its fully developed limit:

$$Nu_s = \frac{h\,s}{k} = \left[\frac{576}{\left(\frac{Ra_s s}{L}\right)^2} + \frac{2.873}{\left(\frac{Ra_s s}{L}\right)^{0.5}}\right]^{-0.5,} \qquad 1\text{-}6$$

where Ra_s is the Rayleigh number, which is based on fin spacing between two adjacent fins, s, L is fins length, $h$is the convective heat transfer coefficient, and k is the fluid thermal conductivity, respectively. Most of the aforementioned coefficients are shown in Fig. 1-2.

Culham *et al*. [16] correlated the Nusselt number with characteristic length scale based on the squared root of the wetted area for the three dimensional bodies [17] and [18]. The wetted area of a fin is the surface that is exposed to the air flow. An agreement of less than 9% between the proposed relationship and the numerical data showed that the selection of the squared root of area as the characteristic length for natural convection from rectangular fins was a suitable choice.

1-3-2-2 Numerical approach

Bodoia and Osterle [19] used a numerical approach to investigate the developing flow in the channel and the heat transfer between symmetrically heated, isothermal plates. They aimed to predict the channel length required to achieve a fully developed flow as a function of the channel width and wall temperature. Ofi and Hetherington [20] used a finite element method to study the natural convective heat transfer from open vertical channels with uniform wall temperature. They observed that fluid velocity may be vertical only. Culham *et al.* [16] also used a numerical code, META, to simulate the natural convective heat transfer from a vertical fin array, and compared their results to their experimental data and the models of [17] and [18] as mentioned in the previous section.

1-3-2-3 Experimental approach:

Several researchers studied the natural convection heat transfer in vertical channels experimentally. Fujii [21] studied the heat transfer from inclined interrupted fin channels. In this study, it is claimed that the thermal boundary layers were interrupted by the fins; a correlation, as shown in Eq. 1-7, was fitted to the experimental results.

$$Nu_s = \frac{1}{24} Ra_s . \left(\frac{S}{l}\right) \left\{ 1 - e^{-12.5/\left[Ra_s . \left(\frac{s}{l}\right)\right]^{3/4}} \right\}, \qquad 1\text{-}7$$

As it can be seen from this relationship, the characteristic length is chosen to be the fin spacing. The interruption length is kept constant and it does not play any role in the calculation of the Nusselt number; those features make the above relationship applicable for a specific interruption length. Figure 1-5 shows the fin geometry used by Fujii.

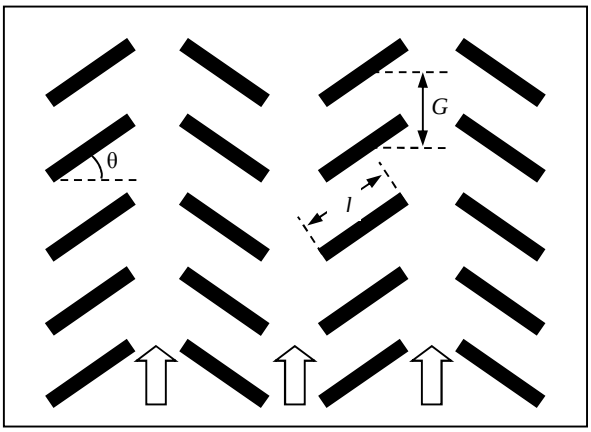

Figure 1-5 : Fujii's [21] considered geometry for inclined interrupted fins.

Starner and McManus [22] calculated natural heat transfer coefficients for four different fin arrays and three different base plates. Flow patterns for each case were observed by using smoke filaments. Parameters that were varied in their study were the fin spacing and the height, respectively. Welling and Wooldridge [23], who investigated large arrays with comparable fin heights, confirmed the findings of [22] for the vertically based fin array orientation. They provided an equation for optimum value of the ratio of fin height to fin spacing and showed the importance of the fin spacing in their results. The way the ratio of fin height to fin spacing varies with temperature was also reported.

Chaddock [24] investigated the natural convection and radiation heat transfer from twelve large vertically based fin arrays. Only one value of base-plate width to the fin length ratio was employed while the fin thickness was kept constant. The fin spacing and the fin height were varied and they showed the importance of the radiation in calculations of total heat transfer, about 20% of the total heat transfer. The outcome of that study was a report on the optimum fins-spacing Yazicioglu and Yuncu [8] also

carried out an experimental investigation on natural convection heat transfer from rectangular fin arrays on a vertical surface to determine the effects of fin height, fin spacing and temperature difference between the fin base and the surroundings on heat transfer. They developed a correlation for optimum fin spacing and discussed the effect of fin height, fin length and fin spacing on the interference of boundary layers, flow pattern, and heat transfer.

Aihara [25, 26] investigated the natural convection and radiation heat transfer from eleven large vertically based fin arrays. In the former work [25], He conducted an experimental study of the heat transfer from the base plate. The effect of fin geometry and temperature on average heat transfer coefficient has been studied and an empirical correlation was obtained. In their latter work [26], a series of experiments focused on heat transfer from the fins reported. Based on their experimental data, they proposed a correlated average Nusselt number.

Leung *et al*. [27, 28, 29, 30, 31]and Van de Pol and Tierney [32] were mostly focused on the effects of varying fin geometric parameters, the array, and base plate orientation; they proposed a relationship for the Nusselt number based on fin spacing for different ranges of *Ra* number.

Radiation heat transfer plays an important role in the heat transfer from fin arrays. This has been shown by Edwards and Chaddock [33], Chaddock [24], Sparrow and Acharya [34], Saikhedkar and Sukhatme [35], Sparrow and Vemuri [36, 37], Azarkish *et al*. [38], and Dharma Rao *et al*. [39]. The common conclusion of the aforementioned

studies was that the radiation heat transfer contributes between 25–40% to the total heat transfer from fin arrays in naturally cooled heatsinks.

There are also studies performed by Karki and Patankar [40] and Cengel and Ngai [41] that dealt with naturally cooled vertical shrouded fins. The authors conducted an experimental study and investigated the effect of shrouds on fins performances. A summary of the above-mentioned studies is presented in Table 1-1.

Table 1-1: Literature review on natural convective heat transfer from vertical rectangular fin.

Ref. #	Method	Ra range	CorrelationNu	Conditions	Highlights
[21]	Exp.		$Nu_s = \frac{1}{24} Ra_s . \left(\frac{s}{l}\right) \left\{1 - e^{-12.5/\left[Ra_s \cdot \left(\frac{s}{l}\right)\right]^{3/4}}\right\}$		● Interrupted fins ● Model cannot see the effect of *G*
[13]	Analytical	all	$Nu_L = \left\{0.825 + \frac{0.387 Ra_L^{\frac{1}{6}}}{\left[1 + (0.492/Pr)^{\frac{9}{16}}\right]^{\frac{8}{27}}}\right\}^2$	Isothermal and isoflux	● Applicable for plates with inclination up to 60°
[33]	Empirical	$10^4 - 10^9$	$Nu_L = 0.59\, Ra_L^{1/4}$		
[14]	Analytical Exp.	$10^{-1} - 10^5$	$Nu_s = \frac{1}{24} Ra_s \left[1 - \exp\left(-\frac{35}{Ra_s}\right)\right]^{\frac{3}{4}}$	Symmetric isothermal	● Reported s_{opt}= f (*H*)
[15]	Analytical	all	$Nu_s = \left[\left(\frac{24}{Ra_s}\right)^2 + \left(\frac{1}{0.59\, Ra_s^{0.25}}\right)^2\right]^{-0.5}$ $Nu_s = \left[\left(\frac{6}{Ra_s}\right)^2 + \left(\frac{1}{0.59\, Ra_s^{0.25}}\right)^2\right]^{-0.5}$	Symmetric isothermal Asymmetric isothermal	● Reported s_{opt}

Ref. #	Method	Ra range	CorrelationNu	Conditions	Highlights
[24]	Exp. & Num.		$Nu_s = \left[\left(\frac{12}{\frac{s}{L}Ra_s}\right)^2 + \left(\frac{1}{0.619\left(\frac{s}{L}Ra_s\right)^{0.25}}\right)^2\right]^{-0.5}$	Asymmetric isothermal	●fins are 2D problem Developing+developed flow
[34]	Exp.	s < 50mm	$Nu_s = 6.7 \times 10^{-4} Ra_s \left[1 - \exp\left(\frac{7460}{Ra_s}\right)^{0.44}\right]^{1.7}$	Symmetric isothermal horizontal	● Reported s_{opt}= f (H, s)
		s > 50mm	$Nu_s = 0.54 Ra_s^{0.25}$		
[42]	Exp.	Ra<10^6	$Nu_s = 0.135\, Ra_s^{0.5}$ Ra<250 $Nu_s = 0.423\, Ra_s^{\frac{1}{3}}$ 250<Ra<10^6		
[42]	Exp.	Ra<10^6	$Nu_s = 0.144\, Ra_s^{0.5}$ Ra<250 $Nu_s = 0.490 Ra_s^{\frac{1}{3}}$ 250<Ra<10^6	Small fin heights	

Figure 1-6 shows the comparison of the data and analytical models existing in literature for the external natural convective heat transfer from isothermal vertical rectangular continuous fins. Unfortunately most of the literature found for the rectangular interrupted fins were limited to the forced convection and intenal natural convection which is not our case study. Fujii [21] studied the external natural convective heat transfer from isothermal vertical rectangular interrupted fins and reported a fitted correlation, but the effect of interruptions, G, can not be seen in his correlation.

Figure 1-6 shows that:

- The experimental data is successfully validated with the current models
- [15] Predicts the data more accurately than the other models in literature

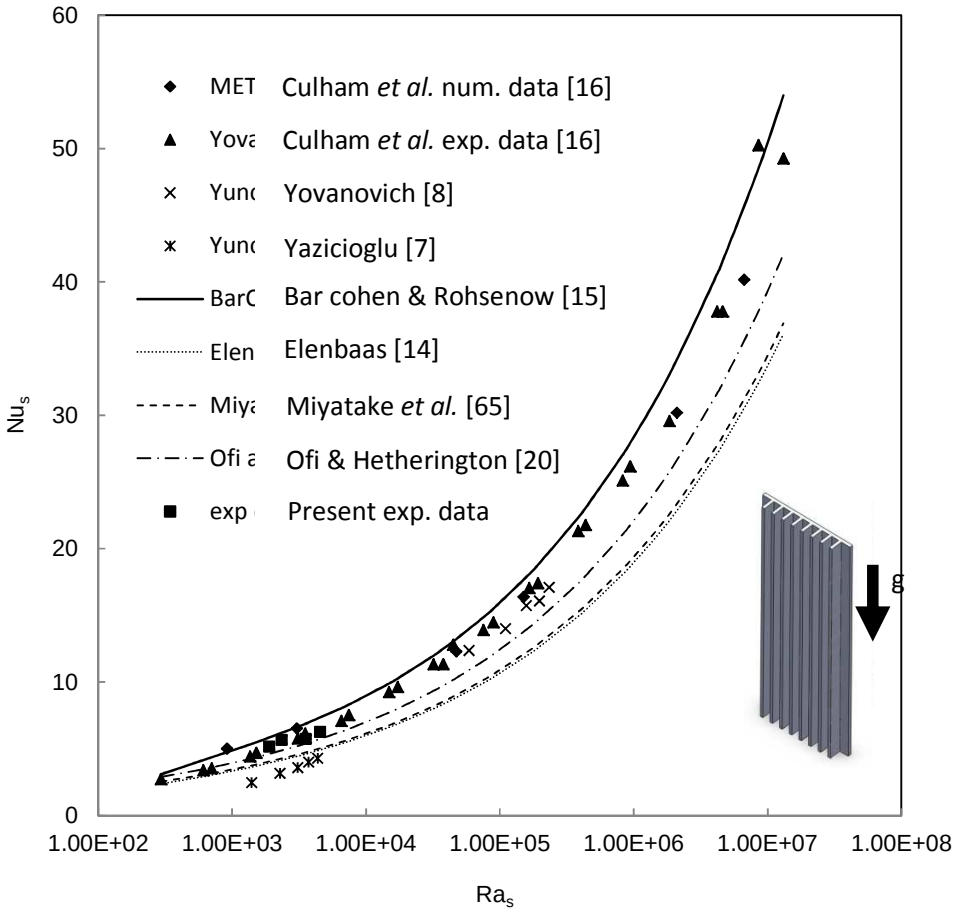

Figure 1-6: Comparison of the data and analytical models in literature.

1-4 Objectives

The previous section on literature review indicated that the focus of the pertinent research in the area of the natural convective heat transfer from fins has been mostly on continuous fins and pin fins, and no in-depth study has been performed to investigate the natural convection heat transfer from interrupted fins for external natural convective heat transfer. Interrupted fins have been mostly studied for internal natural convection [43], [44] and forced convection, e.g., [45].The present study aims to address this shortcoming by investigating the effect of fin interruption on the efficiency with which the heat is transferred from the heatsink to the environment.

Interrupted fins are a more general form of fins and can include both continuous and pin fins at the limit where the fin interruption approaches zero, as it can be seen in Fig. 1-7. At a closer look, continuous fins and pin fins are two extreme cases of the targeted interrupted fins. We started our analysis expecting that a proper selection of fin spacing and interruption sizes can lead to a higher thermal performance. This expectation was based on the fact that interrupted fins exhibit a thermal boundary layer interruption, which help increase the heat transfer [21], see the next chapter for more details on the concept. Additionally, fin interruption leads to significant weight reduction, which in turn, can lower the manufacturing costs. On the other hand, adding interruptions leads to a heat transfer surface area reduction, which decreases the total heat transfer. These two competing effects clearly indicate that an “optimum” fin interruption exists that provide the maximum heat transfer rate from naturally-cooled heatsinks.

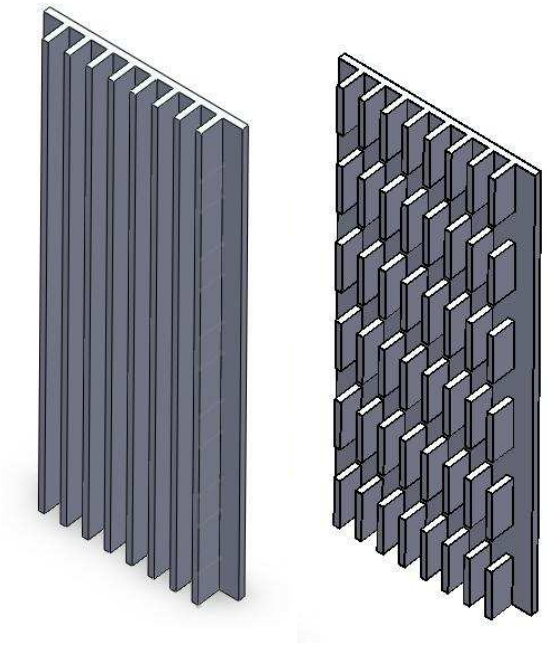

Figure 1-7: Continuous and Interrupted rectangular fins

The goal of this study is to investigate the effects of adding interruptions to fins and determine an optimum value for different geometrical parameters of the fin array. Our focus will be mainly on the fin length and fin interruption length. Also, in order to study the natural convective heat transfer from interrupted fins, a new concept, effective length, is introduced and a new relationship for the Nusselt number is developed based on the non-dimensional geometrical parameters.

Chapter 2.

Numerical Analysis

Our literature survey indicates that there is a lack of in-depth understanding of the effects of various fin parameters, as shown in Figure 2-1, on the thermal performance of interrupted fin arrays. This thorough understanding is a cornerstone of any comprehensive modeling and development program. As such, we will investigate natural convection heat transfer in the general interrupted fin array shown in Figs. 2-1 and 2-2. It should be noted that the targeted fin array has all the relevant and salient geometrical fin parameters and covers the targeted fins ranging from continuous straight rectangular fins to pin fins. In the following paragraphs, the physical effect of adding interruptions to the fins on natural convective heat transfer is discussed. On the following subsections, the governing equations, numerical domain and the corresponding boundary conditions, the assumptions and the mesh independency are discussed. Some of the present numerical results are also presented in this chapter and compared against well-established analytical model available in the literature. The validation of the numerical data with our experimental data is done at the end of this chapter; the details for the experimental procedure are discussed in the next chapter.

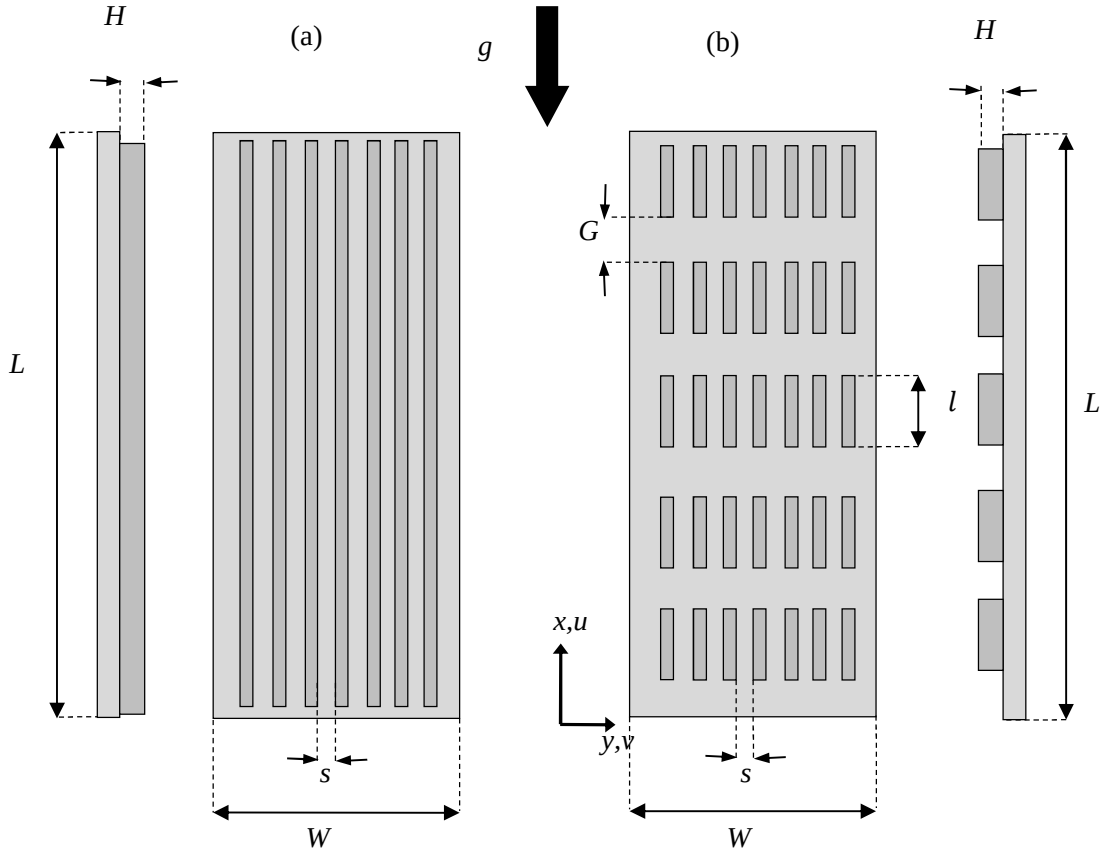

Figure 2-1: Schematic of the considered heatsink geometry: a) continuous rectangular finned heatsink and b) interrupted rectangular finned heatsink.

2-1 Problem statement

When a vertical heatsink is heated, the buoyancy force causes the surrounding fluid to start moving and, as a result, thermal boundary layers start to develop at the bottom edges of the opposing surfaces of the neighboring fins; the boundary layers eventually merge if the fins/channels are sufficiently long, creating a fully developed channel flow [46]. Interrupted fins disrupt, and ideally reset the thermal boundary layer growth, maintaining a thermally developing flow regime, which, in turn, leads to a higher natural heat transfer coefficient; this concept is schematically shown in Fig. 2-2.

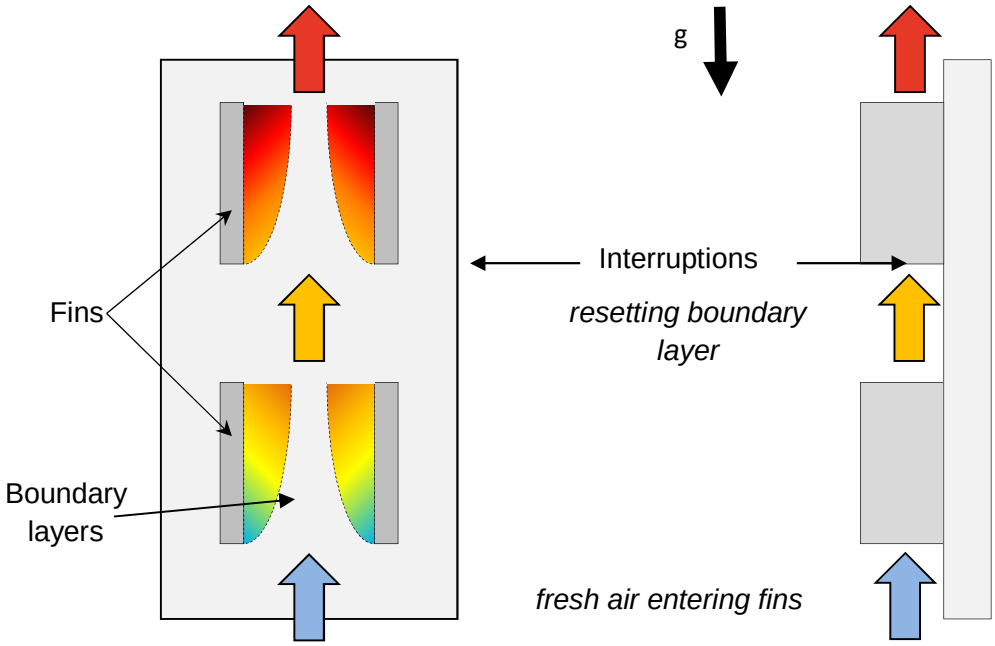

Figure 2-2: Effect of adding interruptions on the boundary layer growth in natural heat transfer from vertical fins.

2-2 Governing Equations

We seek a solution for steady-state laminar natural convective heat transfer from an interrupted vertical wall and fins. Figure 2-1 shows the geometry of the considered interrupted fin array. The conservation of mass, momentum and energy in the fluid are based on assuming a fluid with constant properties and the Boussinesq approximation [46] for density-temperature relation:

$$\frac{\partial u}{\partial x}+\frac{\partial v}{\partial y}=0 \qquad 2\text{-}1$$

$$\rho\left(u\frac{\partial u}{\partial x}+v\frac{\partial u}{\partial y}\right)=-\frac{\partial P}{\partial x}+\mu\nabla^2 u \qquad 2\text{-}2$$

$$\rho\left(u\frac{\partial v}{\partial x}+v\frac{\partial v}{\partial y}\right)=-\frac{\partial P}{\partial y}+\mu\nabla^2 v-\rho g \qquad 2\text{-}3$$

$$\left(u\frac{\partial T}{\partial x}+v\frac{\partial T}{\partial y}\right)=\alpha\nabla^2 T, \qquad 2\text{-}4$$

where y is the direction parallel to the gravitational acceleration and x is the direction normal to the gravitational acceleration, u is the flow velocity in x-direction and v is the flow velocity in y-direction, respectively. ρ, μ, and α are the fluid's density, dynamic viscosity and thermal diffusivity, respectively.

Since the pressure is only a function of longitudinal position only [46] we have:

$$\frac{\partial P}{\partial y}=\frac{\partial P_\infty}{\partial y} \qquad 2\text{-}5$$

Further that $\partial P_\infty/\partial y$ is the hydrostatic pressure gradient dictated by the reservoir fluid of density ρ_∞, therefore:

$$\frac{\partial P_\infty}{\partial y}=-\rho_\infty\times g \qquad 2\text{-}6$$

Plugging equations 2-5 and 2-6 into momentum equation 2-3 yields:

$$\rho\left(u\frac{\partial v}{\partial x}+v\frac{\partial v}{\partial y}\right)=\mu\nabla^2 v-(\rho-\rho_\infty)g \qquad 2\text{-}7$$

To express the net buoyancy force, which is equal to $-(\rho-\rho_\infty)g$, in terms of temperature difference, the volumetric thermal expansion coefficient, β should be defined first. This parameter represents the variation of the density of a fluid with temperature at constant pressure:

$$\beta=-\frac{1}{\rho}\left(\frac{\partial\rho}{\partial T}\right)_P \qquad 2\text{-}8$$

In natural convection studies, the condition of the fluid located sufficiently far away from the hot or cold surface is indicated by the subscript "infinity". That subscript serve as a

reminder that this is the value of a certain entity at a distance where the presence of the surface is not felt [47]. Equation 2-8 can be rewritten as:

$$\beta \approx -\frac{1}{\rho}\frac{\Delta\rho}{\Delta T} = -\frac{1}{\rho}\left(\frac{\rho_\infty - \rho}{T_\infty - T}\right) \qquad at\ constant\ P \tag{2-9}$$

Plugging the expression of β into Eq. 2-7 yields to:

$$\rho\left(u\frac{\partial v}{\partial x} + v\frac{\partial v}{\partial y}\right) = \mu\nabla^2 u - g\beta\rho_\infty(T - T_\infty) \tag{2-10}$$

where in the numerical simulation using COMSOL the term, $-g\beta\rho_\infty(T - T_\infty)$, is inserted as a body force.

Isothermal boundary conditions have been assumed on the walls, i.e.,

$$T = T_w \quad \text{at} \quad x = \mp\frac{s}{2}, 0 < y < l, \tag{2-11}$$

where T_s is the surface temperature.

A symmetry boundary condition is assumed for the interruption region, as shown in Fig. 2-3:

$$\frac{dT}{dx} = 0 \quad \text{at} \quad x = \mp\frac{s}{2}, l < y < l + G. \tag{2-12}$$

The inlet and outlet boundary conditions for the domain considered are the following:

$$P = P_{atm} \quad \text{at} \quad y = L, y = 0. \tag{2-13}$$

Boundary conditions used to solve the domain are also shown schematically in Fig. 2-3.

Radiation heat transfer from a surface to the surroundings, at an ambient temperature T_{amb}, can be calculated from Eq. 2-13. More details on the subject can be found in Rao *et al* [34]:

$$\dot{Q}_{rad} = \sigma\varepsilon({T_w}^4 - {T_{amb}}^4)\sum_{i=1}^{3} A_i F_{i4} \quad [W], \tag{2-14}$$

where F is the surface view factor, ε is the surface emissivity coefficient, and σ is the Stefan–Boltzmann constant $5.67 \times 10^{-8}\ W/m^2.K^4$, respectively.

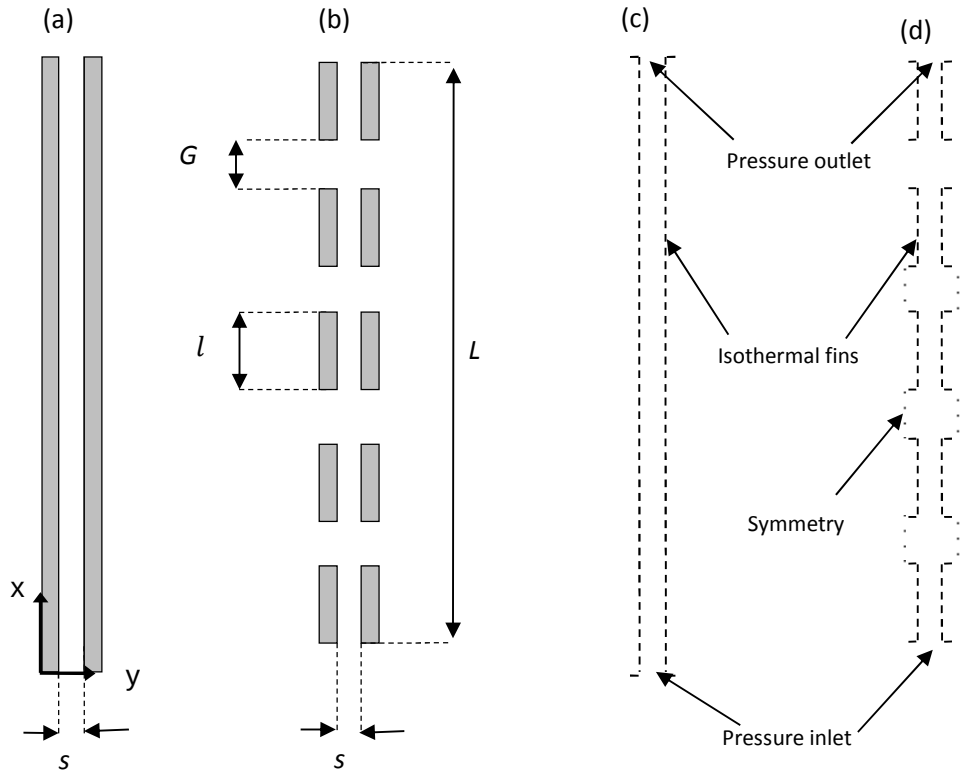

Figure 2-3: Schematic of the considered numerical domain: a) continuous fins; b) interrupted fins; c) boundary conditions for continuous fins; d) boundary conditions for interrupted fins.

2-3 Summary of Assumptions

The following is a summary of the assumptions made to model the fluid flow and heat transfer in a vertical finned heatsink.

- steady state, laminar flow, i.e., Rayleigh number Ra $<10^9$, [47]
- incompressible flow, i.e., Ma < 0.30);

(Ma, Mach number is a dimensionless quantity representing the ratio of speed of an object moving through a fluid and the local speed of sound. [47])

- two-dimensional flow and heat transfer inside the channels; [24]
- symmetric flow and identical heat transfer in all the channels;
- isothermal boundary condition for the base plate and fins;
- negligible air entrance in side channels. (The fresh air inflow and outflow from the open sides of the outmost channels was small compared to the air flow entering from the bottom of the fin array. [48])

The effect of fin interruption is investigated using a two dimensional numerical simulation using FLUENT [49] and COMSOL Multyphysics [50] for the fins and walls. In order to investigate the effects of fin interruption and to determine an optimum interruption ratio, we started by using the existing analytical models as reported in [15]. Based on the models, the optimum fin spacing *s* can be calculated. The idea is to decouple the effect of fin spacing from the fin interruption. Our strategy is to keep the fin spacing constant, at its optimum value calculated by the model of [15]. The present numerical simulation results have been validated by our experimental data; the simulation

results were within a mean relative difference of 4.6 % and the maximum relative difference 14 % of experimental values.

2-4 Computational domain and boundary conditions

2-4-1 Fin array simulation

For modeling the channel, since the geometry repeats itself, a single channel has been chosen to represent the computational domain, as shown in Fig. 2-3, According to the flow visualization and velocity measurement of the flow field for a finned plate reported in [48], as mentioned in the assumptions, the fresh air inflow and outflow from the open sides of the outmost channels was small compared to the air flow entering from the bottom of the fin array. Therefore, the effect of the side fins exposed to the ambient is not expected to be significant and the selection of a single channel instead of whole domain is justified. Additionally, the influence of the flow in the direction normal to the base plate was shown to be negligible [48]. Thus, a two-dimensional analysis (instead of three dimensional) is adequate for the purpose of our simulation. For the domain dimension selection, the optimum fin spacing, *s*, is estimated using the existing analytical model of [15]. The effect of fin spacing was decoupled for the simulation of interruptions in interrupted fins, keeping the fin spacing constant at the optimum value, which is determined with the following relationship for the symmetric isothermal plates [15]:

$$s_{opt} = 2.71(Ra_s/s^3L)^{-0.25} \qquad \text{[m]}, \tag{2-15}$$

where *Ra* is the Rayleigh number, *s* is the fin spacing and *L* is fins length, respectively.

In Eq. 2-15, the s_{opt} changes with the temperature difference; the value of $dT = 22℃$ is chosen to calculate the fin spacing by substituting it in *Ra*.

$$Ra_s = \frac{g\beta\Delta T s^3}{\alpha\vartheta}, \qquad 2\text{-}16$$

The pressure inlet boundary condition is applied to the fin array's inlet, the bottom of the fin array channel, and that defines the static/gauge pressure at the inlet boundary. The value of that pressure is interpreted as the static pressure of the environment from which the flow enters.

For the top of the domain, i.e., the outlet of the fin array channel, the outlet boundary condition is applied. The symmetry boundary condition which is equivalent to a no-heat flux in the direction normal to the fins surface plane was chosen for the interruption region. A no-slip flow with isothermal solid surface is considered for the walls. Figure 2-3 shows a schematic of the domain considered for the numerical simulation, along with the chosen boundary conditions for continuous and interrupted fins.

For solving the system of partial differential equations introduced in *Chapter 3*, ANSYS-Fluent 12.1.4 [49] has been employed; as well, GAMBIT 2.3.16 was used for mesh generation. Boundary layer mesh was used for regions that are closer to the fin surface, in order to capture the flow behaviour with a higher resolution. Figure 2-4 shows a segment of the domain and the generated mesh for continuous and interrupted fins.

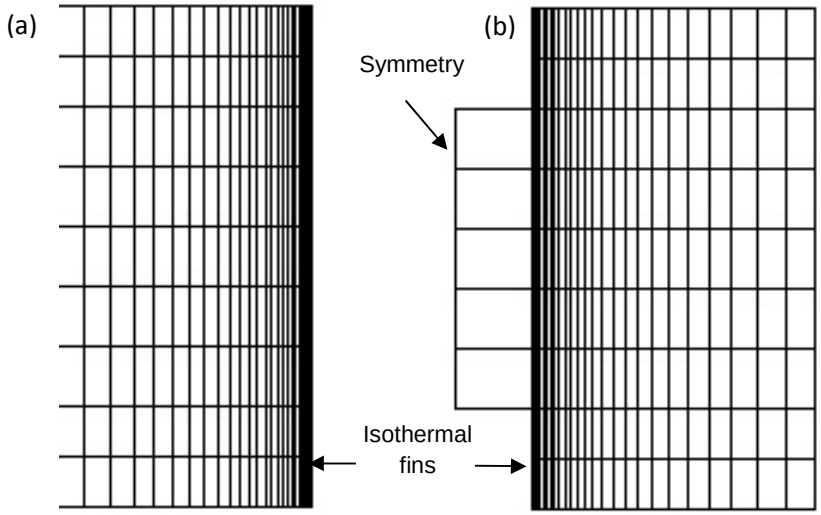

Figure 2-4: Grid used in the numerical model for a) continuous and b) interrupted fin array.

In order to investigate the effect of interruptions on natural convective heat transfer, a comprehensive parametric study has been performed and the experimental data and the numerical results are discussed in Chapter 4 accordingly

Table 2-1 presents the geometrical specifications, i.e., the fin and interruption lengths of the numerical domain geometry. Fin lengths have been varied in the following sequence : $l = t$, $2t$, $5t$, $10t$ and $15t$, where t is the fin thickness; similarly, interruption lengths have been varied as per: $G = l/2$, l, $2l$, $5l$, $10l$, in some cases G was varied up to $20l$, $40l$, $80l$ and $225l$. As a result, thirty six different heatsink geometries have been investigated overall. The selection of the range for both l and G were arbitrary selections to cover a wide range for each parameter. The chosen fin and interruption lengths are given in 2-1.

This set of geometries is meant to cover a wide range of $\gamma = G/l$.

Table 2-1: Geometrical dimensions of the considered interrupted fin array in numerical analysis.

Considered numerical Geometry case studies#	$\gamma = G/l$	t (mm)	s (mm)
1-5	0.5	2.5	9.5
6-10	1	2.5	9.5
11-15	2	2.5	9.5
16-20	5	2.5	9.5
21-25	10	2.5	9.5
26-28	20	2.5	9.5
29-32	40	2.5	9.5
33-35	80	2.5	9.5
36	255	2.5	9.5

Fin length and fin width is constant in all the geometries, L = 1.4 m and s = 9.5 mm.

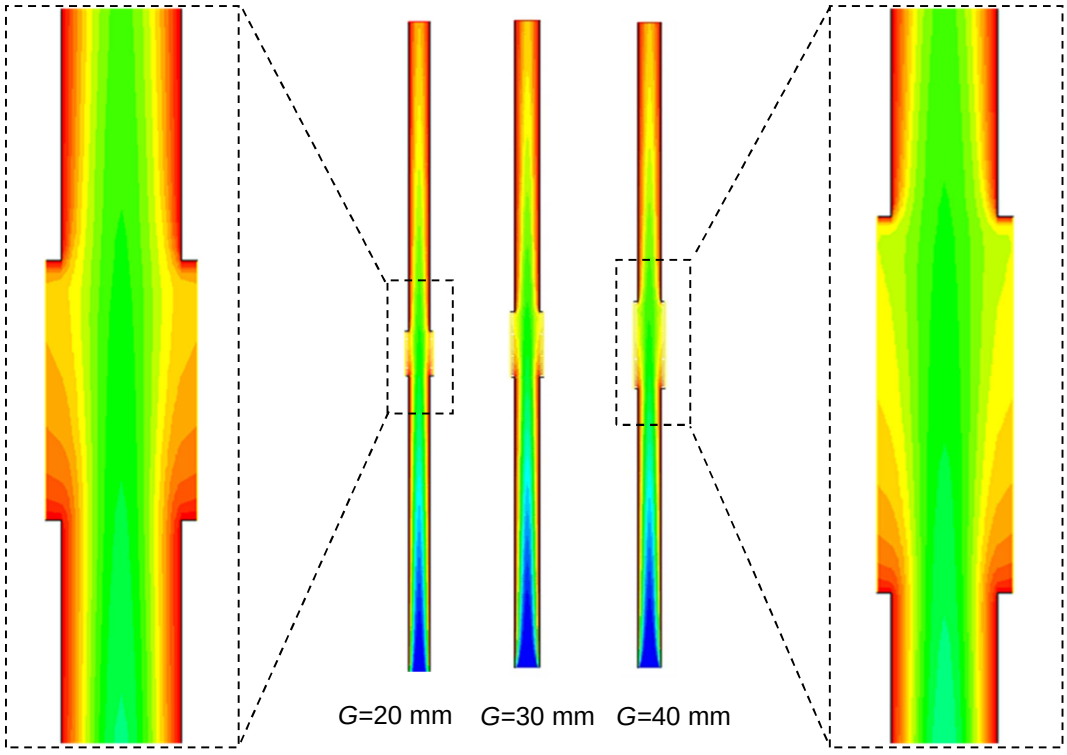

Figure 2-5: Temperature distribution contours of fin arrays, and the effect of interruption length on thermal boundary layer. The thermal boundary and its growth can be seen in the temperature contours.

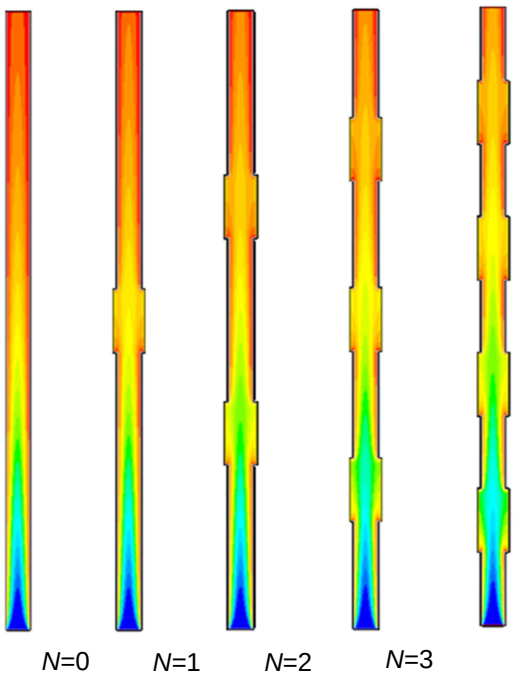

Figure 2-6: Numerical simulation, temperature contours, for fin arrays, and the effect of multiple interruptions on thermal boundary layer.

Figure 2-5 shows the temperature contours, and the effect of interruption length on resetting the thermal boundary layer could be clearly observed. Figure 2-5 also shows the effect of frequent interruption on resetting the thermal boundary layer and temperature distribution in the channels. The frequent resetting causes a delay in flow to get to the fully-developed condition.

2-4-2 Interrupted single vertical wall simulation

Interrupted vertical walls are simulated in order to be used in developing a new compact relationship for the natural convective heat transfer and the corresponding Nusselt number. The domain is shown in Fig. 2-7. The pressure inlet boundary condition is applied to the bottom of the domain. For the top and sides of the domain, an outlet boundary condition is applied. For the interruption region, the symmetry boundary

condition was chosen. This type of boundary condition is equivalent to a no-heat flux in the direction normal to the wall surface plane. Similar to the fin arrays, a no-slip isothermal solid surface is considered for the walls. Figure 2-7 shows a schematic of the domain considered for the numerical simulation, along with the chosen boundary conditions for walls.

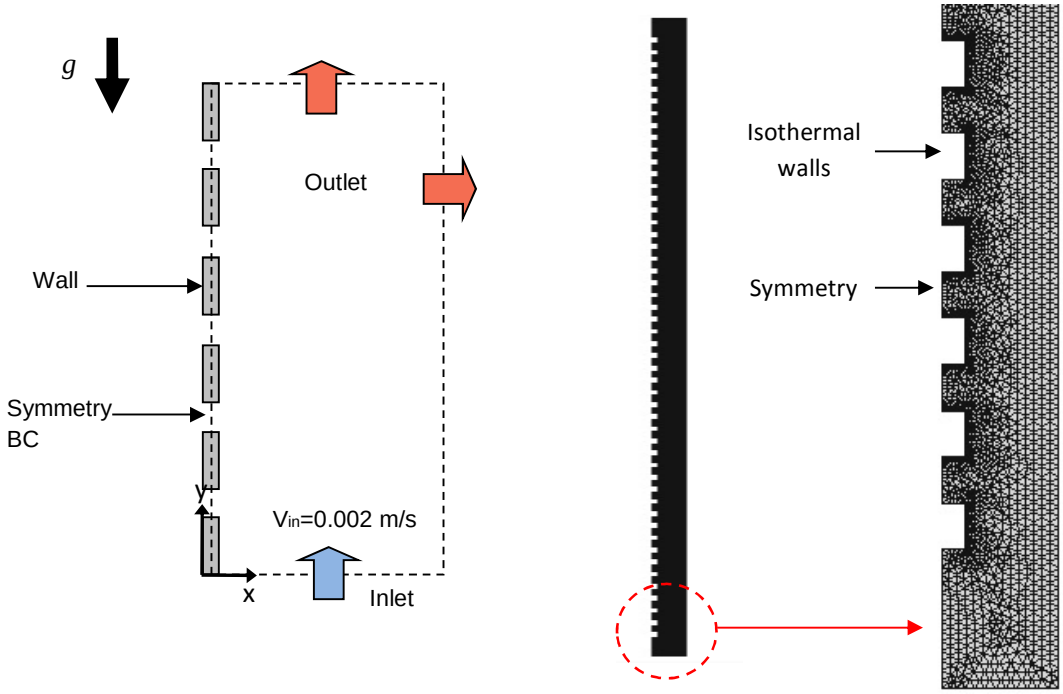

Figure 2-7: a) Schematic of the numerical domain and boundary conditions for interrupted single vertical walls. b) Grid used in the model for interrupted walls.

For solving the system of partial differential equations introduced in Section 2-2 and also for mesh generation, COMSOL software has been employed.

Table 2-2 shows the specifications of the numerical domain geometry. The wall length and the interruption length have been varied, respectively, in the following order: $l = t$, $5t$, $7.5t$, $10t$, $15t$, where t is the wall thickness. The interruption length ratio to the

wall length, γ, was varied from 0.5 to 120. Forty four different wall geometries have been investigated overall. In this set of simulations the number of walls where kept constant, *n* = 50; however, due to the above considerations, the total length of the walls was varied. The selection of the range for both *l* and *G* was an arbitrary selection to cover a wide range.

Table 2-2: Geometrical dimensions of the considered interrupted walls in numerical analysis.

Considered numerical Geometry case studies#	l (mm)	$\zeta = l/t$	$\gamma = G/l$
1-10	2.5	1	[0.5-60]
11-21	12.5	5	[0.5-60]
22-31	7.5	7.5	[0.5-50]
25-34	12.5	10	[0.5-40]
35-44	37.5	15	[0.5-38]

General note: Fin numbers and fin thickness were kept constant in all the geometries, *n* = 50 and *t* = 2.5 mm.

2-5 Mesh independency

2-5-1 Fin array simulation

A mesh independency study has been performed for a continuous fin case, with seven different mesh sizes in the *y*-direction, i.e., parallel to the gravitational acceleration direction, shown in Fig. 2-3, and four different mesh sizes in the *x*-direction, i.e. normal to the gravitational acceleration direction. Figure 2-8 shows the results of the mesh independency study along and normal to the walls, respectively. According to this study, the optimum size for vertical meshes has been chosen to be 1 mm. For mesh sizes smaller than 1 mm, the increase in the Nusselt number is of only 0.5%; therefore, the accuracy will not improve significantly thereafter. As for the mesh number, 50 has been used in the

horizontal space between two fin surfaces in order to have less than 0.5% error and still save significant computational time. It should be noted that the mesh structure was distributed unequally on the horizontal space; it is denser in the vicinity of walls in order to increase the accuracy of the results.

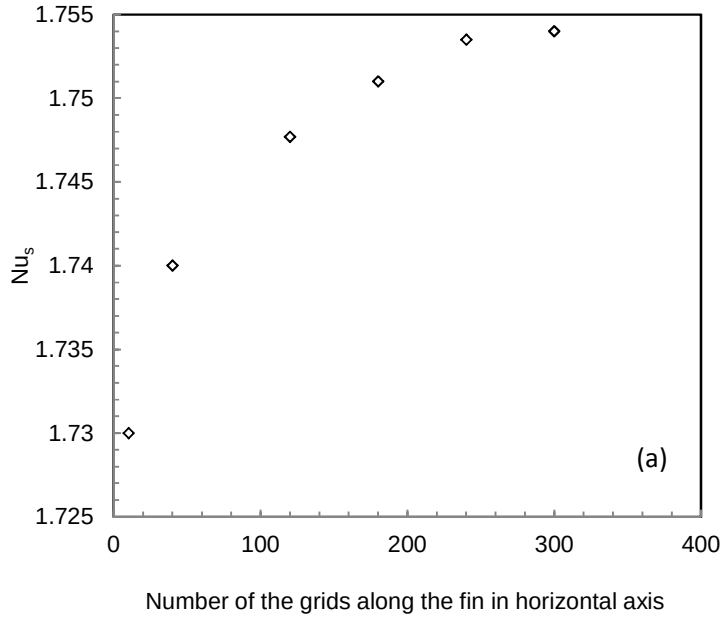

Figure 2-8-a: Grid independency study, *Ra* = $1.6 \cdot 10^3$; in vertical direction (horizontal grid number = 50).

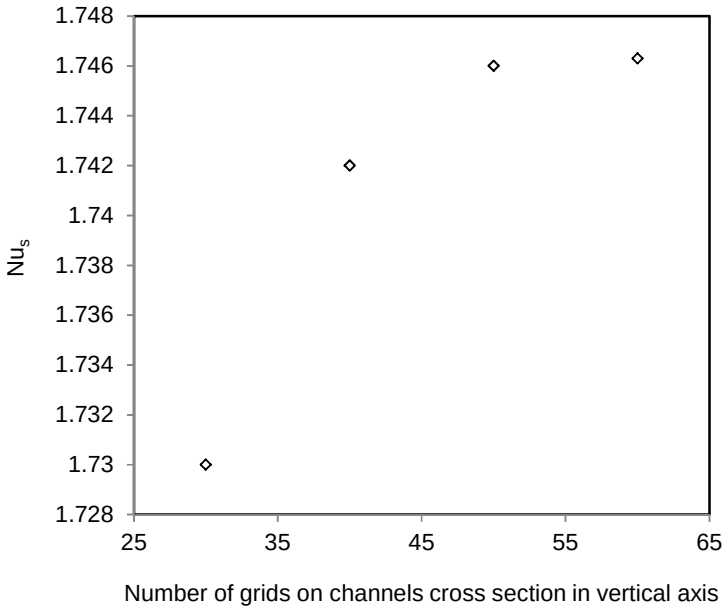

Figure 2-8-b: Grid independency study, *Ra* = 1.6· 10^3; in horizontal direction (vertical grid number = 300).

2-5-2 Interrupted wall simulation

The computational domain, shown in Figure 2-7, for simulating the heat transfer in the walls was created in COMSOL Multiphysics [48]. Three different number of mesh elements were used for each different geometry cases and compared in terms of local temperature and total heat transfer rate to ensure a mesh independent solution. Accordingly, for the case of $\zeta = l/t = 1$, i.e., pin fins, and $\gamma = G/l$ =1, choosing a mesh number of 2.3×10^4 , we found that the simulation of walls gives approximately 2% deviation in heat transfer rate from walls as compared to the simulation of walls with mesh number of 5.0×10^5. Similarly, the heat transfer rate for the simulation of walls with 1.0×10^4 mesh elements deviate up to 9% as compared to those from the finest one. Therefore, we chose a mesh size of 2.3×10^4 elements considering that it was sufficient for the numerical investigation purposes. As mentioned before, in the ANSYS meshing, a

finer mesh size was applied near the wall to resolve with an enhanced accuracy the boundary layer and an increasingly coarser mesh was chosen in the middle of the domain in order to reduce the computational time.

5.4 Numerical results validation

Figure 2-9 and 2-10 show the validation of the present numerical simulation. Simulation results for only one continuous fin channel, experimental sample called cont-1-10-17, with s = 9.5 mm, L = 305 mm, H = 17 mm, are compared to our experimental data and to the analytical model presented by [15]; see Chapter 3 for more details on the experimental procedure. As mentioned before, the radiation is deduced from the experimental data analytically, based on the average temperature measured via the thermocouples. The emissivity was considered 0.75, Prandtl number equal to 0.7, air thermal conductivity, k equal to 0.026 W/m.K and the average temperature measured via the thermocouples was considered as the wall temperature. Natural convective heat transfer is calculated after deducting the base plate and radiation heat transfer from the data. Figure 2-9 and 2-10 show the results for both continuous and interrupted fins. As it can be seen, there is a good agreement between our numerical simulation results and both analytical and experimental results with a mean relative difference of 4.6 % and a maximum relative difference of 14 %. Similarly in Figure 2-10 it can be seen that there is a good agreement between our numerical simulation results and both analytical and experimental results with a mean relative difference of 3.5 % and a maximum relative difference of 4.6 %.

In Figs 2-9 and 2-10, the shown measured temperatures have been averaged to

calculate a wall temperature for the experimental data. To calculate the experimental data, convective heat transfer from the base plate is computed based on an analytical relation as reported in the literature for vertical plates, Eq. 2-17, by [13]; the natural convective heat transfer is then deducted from the total heat transfer rate so that only the heat transfer from the fins is considered. In addition, the radiation heat transfer, which can be as high as 40% according to [51], has been calculated based on Eq. 2-20 and deducted from the data. This operation was done because the simulation was performed for convection heat transfer only.

$$Nu_L = \left\{ 0.825 + \frac{0.387 Ra_L^{\frac{1}{6}}}{\left[1 + (0.492/Pr)^{\frac{9}{16}}\right]^{\frac{8}{27}}} \right\}^2, \quad 2\text{-}17$$

$$\dot{Q}_{NC} = \dot{Q}_{total} - \dot{Q}_{rad}[W], \quad 2\text{-}18$$

$$\dot{Q}_{fins} = \dot{Q}_{NC} - \dot{Q}_{base}[W], \quad 2\text{-}19$$

$$\dot{Q}_{rad} = \sigma\varepsilon\left({T_w}^4 - {T_\infty}^4\right)\sum_{i=1}^{3} A_i F_{i4}\,[W], \quad 2\text{-}20$$

where Ra_L is Rayleigh number based on the base plate length, Pr is the Prandtl number, $\dot{Q}_{rad}$ is the radiation heat transfer rate, $\dot{Q}_{NC}$ is the natural convective heat transfer rate, ε is the surface emissivity, and F is the radiation shape factor, and A is the radiative area. $\dot{Q}_{base}$is the heat transfer rate from the base plate, and $\dot{Q}_{fins}$ is the heat transfer rate from the fins.

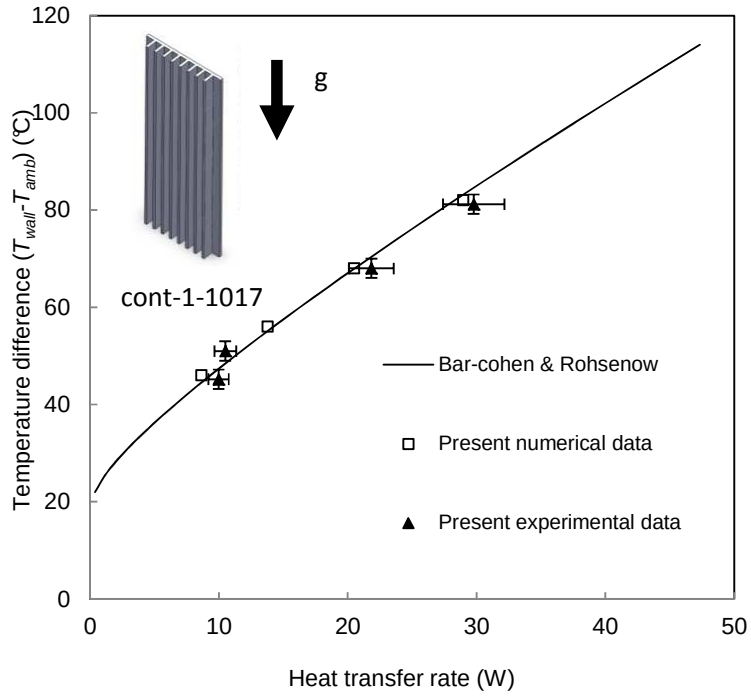

Figure 2-9: Numerical simulation validation; continuous fin, single channel (*s* = 9.5 mm, *L* = 305 mm, *H* = 17 mm).

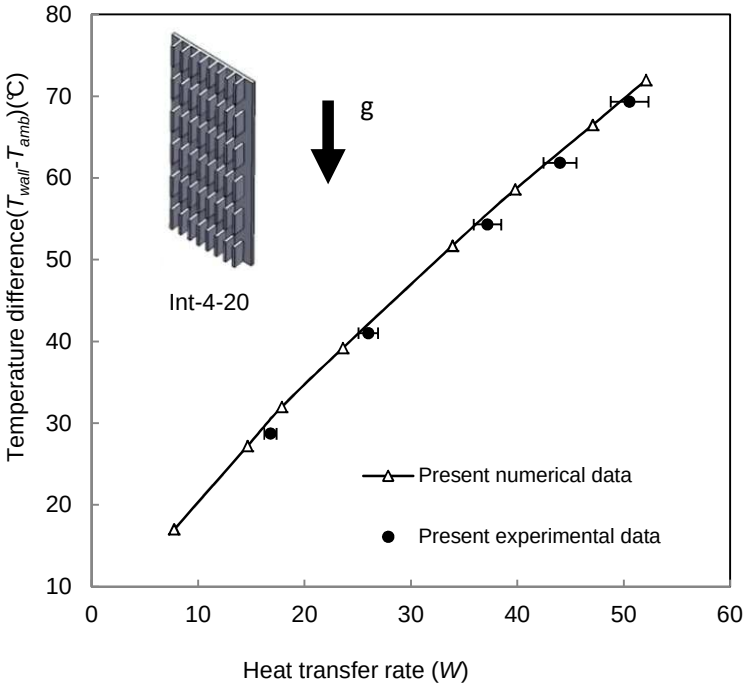

Figure 2-10: Numerical simulation validation; interrupted finned heatsink (n = 8, *s* = 9.5 mm, *L* = 305 mm, *H* = 17 mm, *l* = 37 mm, *G* = 30 mm).

Chapter 3.

Experimental Study

The objective of the experimental study is to investigate the effects of fin interruption length as well as fin spacing on the natural convection heat transfer from the considered rectangular vertical fins. To enable this investigation, two new custom-made testbed were designed and built at SFU. A number of heatsinks and single wall samples, with various geometrical parameters, were prepared. In total, two series of tests were undertaken. The first series of tests was designed to investigate the effect of interruptions and their comparison to the non-interrupted (continuous) channels. The second series of tests were undertaken to validate the numerical data used for calculating the Nusselt number for the vertical fins.

3-1 Testbed design

3-1-1 Testbed design for interrupted and continuous fins

A new testbed has been designed for measuring natural convection heat transfer from the finned heatsinks, as shown in Fig. 3-1 and 3-2. The set-up included an enclosure made of poly(methyl)methacrylate (PMMA) which was insulated by a layer of foam with a thickness of 15 mm. The testbed also included 20 cm long Chromalox strip heaters (120 V, 150 W) purchased from Omega Engineering (Toronto, ON), which were attached to

the backside of the fins base-plate, and a data acquisition system (DAQ), TAC80B-T supplied by Omega (Toronto, ON).

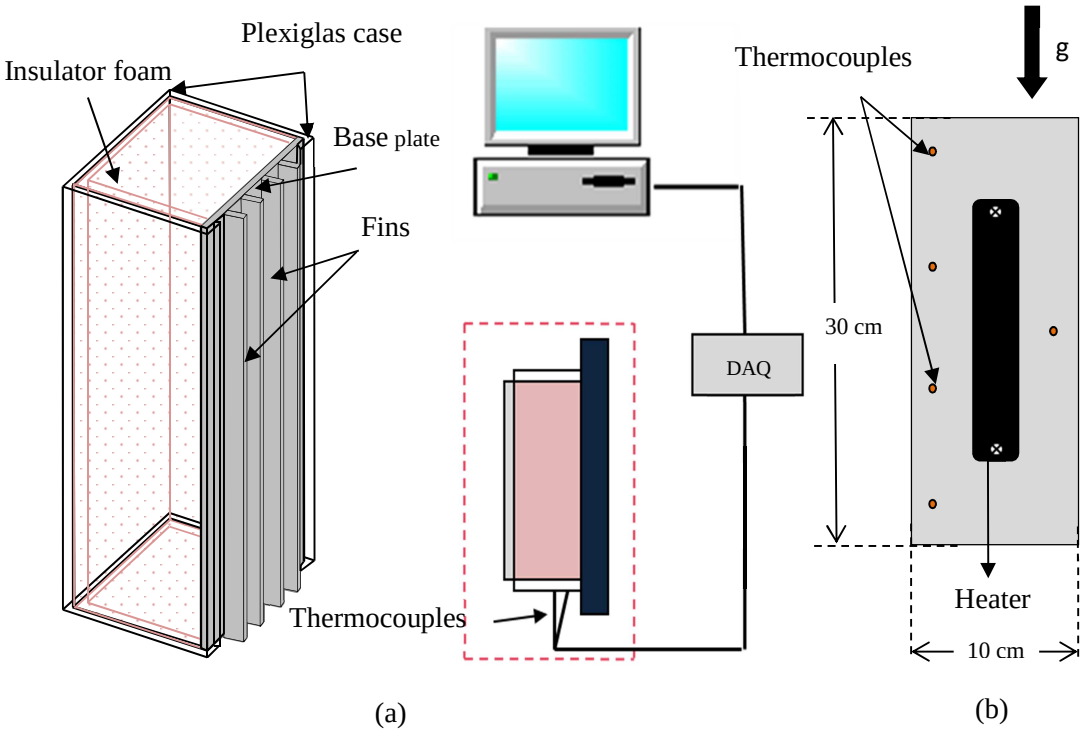

Figure 3-1: Schematic of the heatsink test-bed.

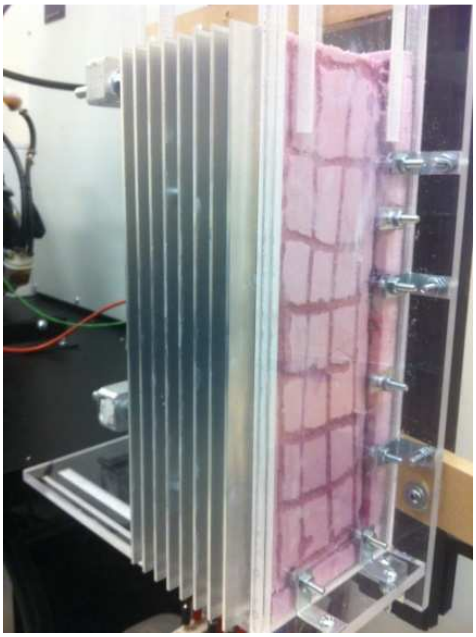

Figure 3-2: A continuous fin in the heatsink test-bed.

Thermal paste was used to decrease the thermal contact resistance between the heater and the heatsink base plate. The voltage and the current of the supplied power were measured with an EXTECH 430 digital multimeter.

3-2-2 Testbed design for interrupted single walls

Another new testbed was designed for measuring natural convection heat transfer from interrupted single wall heatsinks, as shown schematically in Fig. 3-4. The set-up included a metal framework from which samples were hung and an enclosure made of foam with a thickness of 20 mm to insulate the back side of the samples. The testbed also included a power supply, two electrical heaters, which were attached to the backside of the fins base-plate, and a DAQ system. Thermal paste (Omegatherm ®201) was used to decrease the thermal contact resistance between the heater and the heatsink base plate. Some of the testbed components are shown in Fig. 3-3.

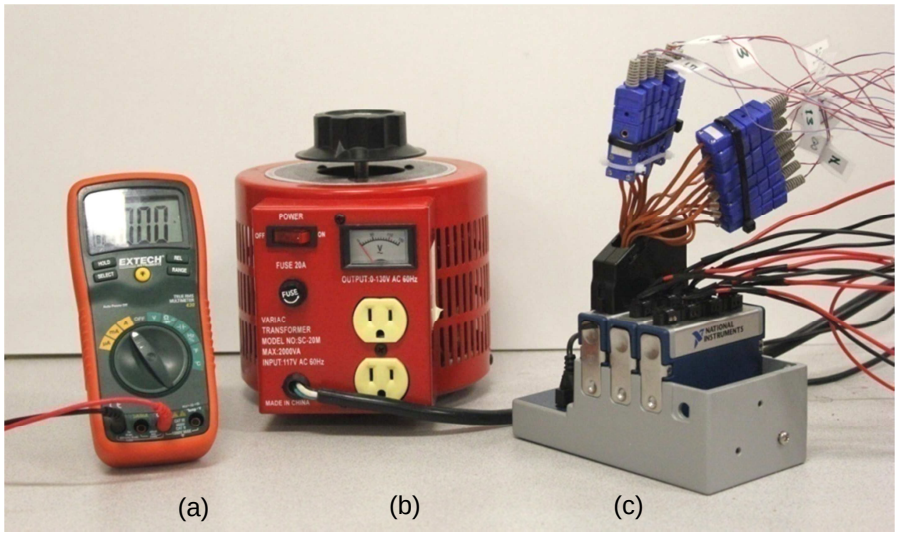

Figure 3-3: The testbed components: a) Extech 430 multimeter, b) SC-20MVariac, c)NI 9214DAQ system.

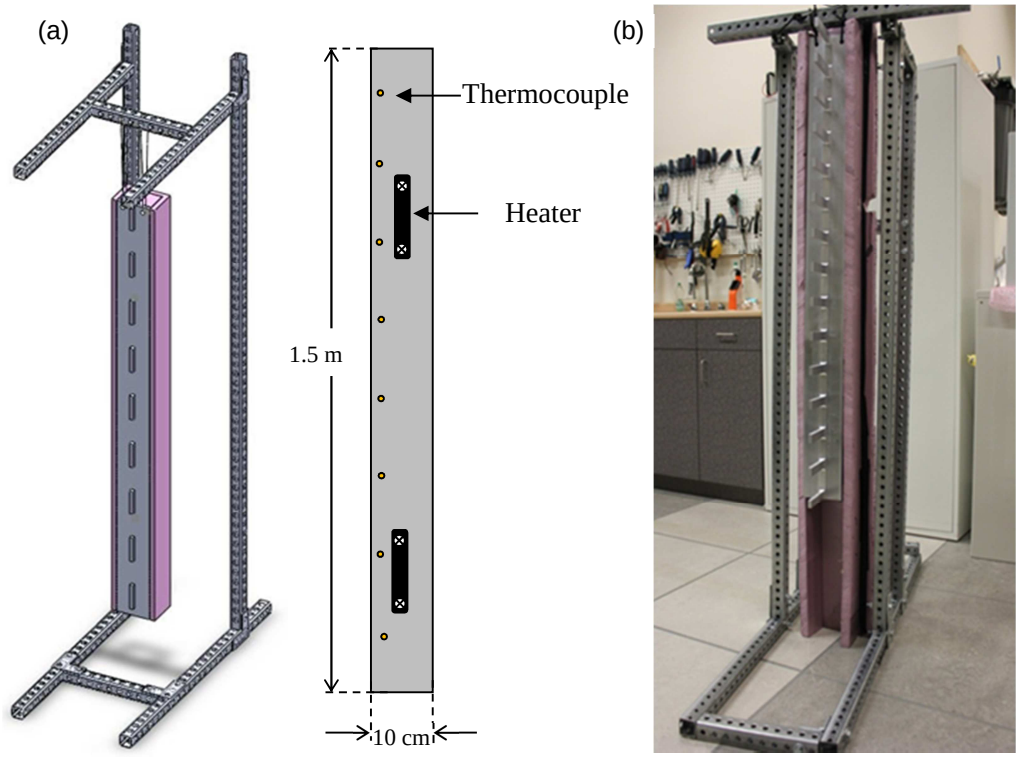

Figure 3-4: a) Schematic of the single wall test-bed; b) an interrupted single wall shown in the testbed.

3-2 Sample Preparation

3-2-1 Interrupted rectangular vertical fin arrays

Two sets of heatsinks featuring: i) continuous rectangular and ii) interrupted rectangular fins were prepared and tested to calibrate the testbed against the existing theoretical model of [15]. As shown in Figure 3-5, samples were machined by the industrial partner, Analytic Systems Ware (ASW), as requested by SFU team. The tested heatsinks were made from 6063-T5 aluminium alloy with a thermal conductivity of k = 130 W/mK at 20℃ and an emissivity of approximately ε = 0.8 at 20℃.

Base plate dimensions of the prepared samples were the same; however, the number and dimensions of the fins were different, as listed in Table 3-13-1 and Table 3-2 3-2.

The continuous fins were prepared to allow the calibration of the testbed with the existing experimental and theoretical results in the literature. More importantly, the continuous fins enabled verification and establishment of the optimum fin spacing, s, between the neighbouring fins. The verification is presented in Chapter 4, in Fig. 4-3.

Table 3-1: Dimensions of the finned plate samples, continuous fins.

Sample name	s (mm)	N	H (mm)	l (mm)
Cont-1-10-17	9.5	8	17	-
Cont-1-6-17	6.0	12	17	-
Cont-1-14-17	14.0	6	17	-
Cont-1-10-10	9.5	8	10	-
Cont-1-10-25	9.5	8	25	-

General note: Heatsink base length and width are constant in all the samples, L = 305mm and W = 101 mm.

The interrupted fin samples were prepared to investigate other salient fin geometric parameters, including length, interruption length, and the number of interruptions.

Table 3-2: Dimensions of finned plate samples, interrupted fins.

Sample name	s (mm)	N	H(mm)	l (mm)	n (number of interruptions)	G (mm)
Int-1-20	9.5	8	17.4	142.5	1	20
Int-2-20	9.5	8	17.4	88.3	2	20
Int-3-20	9.5	8	17.4	61.3	3	20
Int-4-20	9.5	8	17.4	45.0	4	20
Int-5-20	9.5	8	17.4	34.2	5	20
Int-4-30	9.5	8	17.4	37.0	4	30
Int-4-40	9.5	8	17.4	29.0	4	40

General note: Heatsink base length and width are constant in all the samples, L = 305 mm and W = 101 mm.

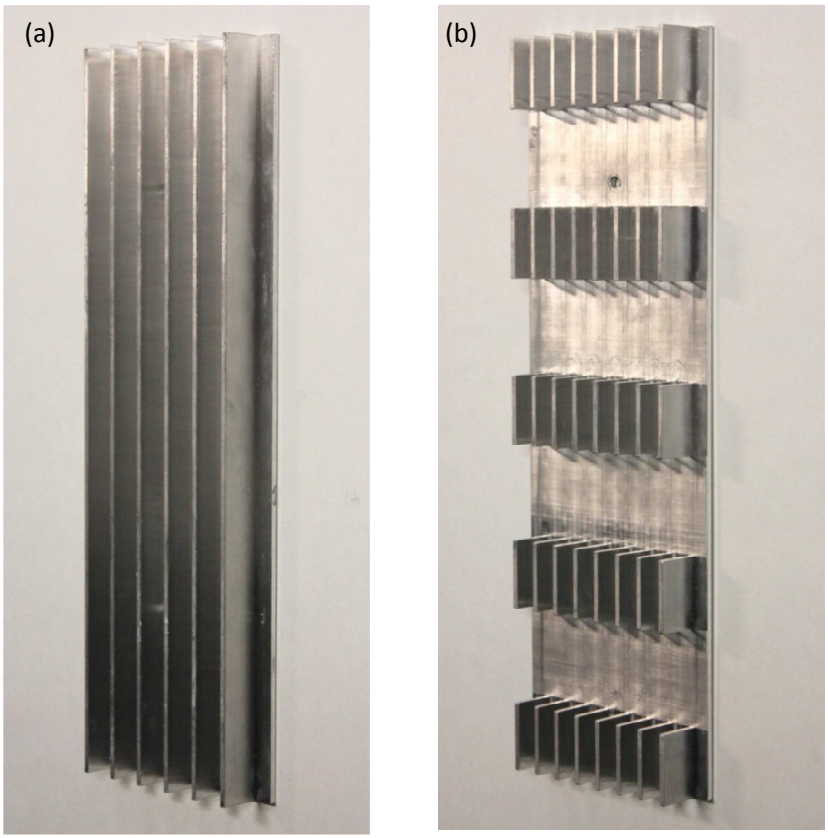

Figure 3-5: Examples of tested samples, a) continuous fins heatsink and b) interrupted fins heatsink.

3-2-2 Interrupted vertical wall

For the second series of tests, in which vertical fins were used, seven heatsinks with interrupted walls were prepared. The base plate width of the samples was the same; the number of fins was chosen such that the flow would reach a fully-developed state. To fully investigate the thermal boundary layer growth, dimensions of the fins and interruptions were varied, as listed in Table 3-3.

Table 3-3: Dimensions of finned plate samples; interrupted walls

Sample name #	*l* (mm)	*n*	*G* (mm)	*L*	*G/l*	*l/t*
SW-1	50	14	50	1.45	1	5
SW-2	50	7	150	1.45	3	5
SW-3	20	17	40	1.040	2	2
SW-4	20	14	60	1.14	3	2
SW-5	10	20	30	1.452	6.2	1
SW-6	50	17	25	1.325	0.5	5

General note: Fin length base land width are constant in all the samples, H = 100 mm, t = 10 mm, and W = 101 mm.

3-3 Test procedure and data collection

3-3-1 Vertical fin arrays

The enclosures were tested in a windowless room that had an environment free of air currents. During the experiments, the input power supplied to the heater and surface temperatures was measured at various locations at the back of the base-plate. Electrical power was applied using the AC power supply. The voltage and the current were measured with two digital Extech® 430 multimeters to determine the power input to the heater. The accuracy of voltage and current readings was 0.3% for both. Five self-adhesive, T-type, copper-constantan thermocouples with an accuracy of ± 1°C were installed in various locations on the surface of the enclosures, as shown in Fig. 3-2-b. All thermocouples were taped down to the inside surface of the enclosure, to prevent disturbing the buoyancy-driven air flow in front of the fins. An additional thermocouple was used to measure the ambient room temperature during the experiments. Thermocouples were plugged into the DAQ. Temperature measurements were performed at five points in order to monitor the temperature variation on the tested heatsinks. The average of these five readings was taken as the base plate temperature. Since the fin

heights were small, maximum fin height was 25 mm, they were assumed to be isothermal. For each of the twelve heatsinks, the experimental procedure was repeated for power inputs of 16, 25, 36, 42.2 and 49 W, respectively. The base-plate temperature T_W, the ambient temperature T_∞, and the power input to the heater $\dot{Q}$, considering that the power factor equals 1, were recorded at steady-state. The steady state was considered to be achieved when 100 minutes elapsed from the start of the experiment and the rate of temperature variations with respect to time, dT/dt for all the thermocouples were less than 0.1℃/hour. Figure 3-6 show the steady state experimental data from tested samples.

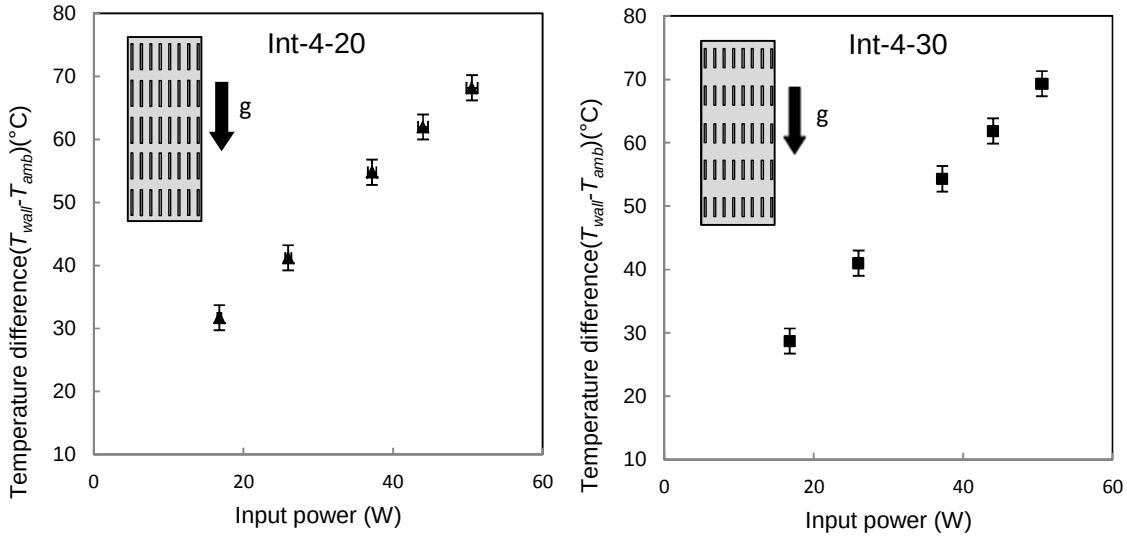

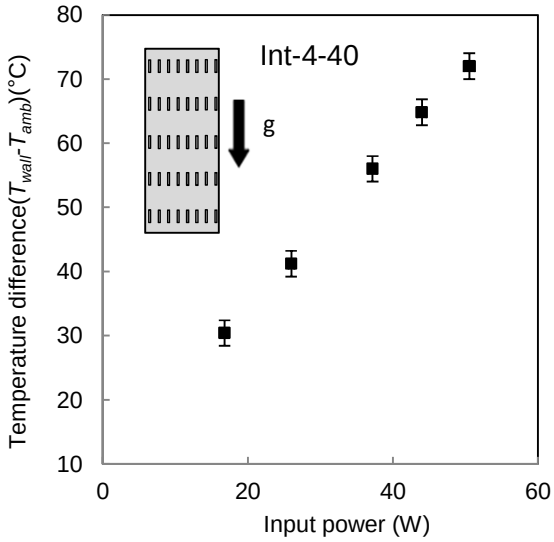
Int-4-40
g
Temperature difference(T_{wall}-T_{amb})(°C)
Input power (W)
80
70
60
50
40
30
20
10
0
20
40
60

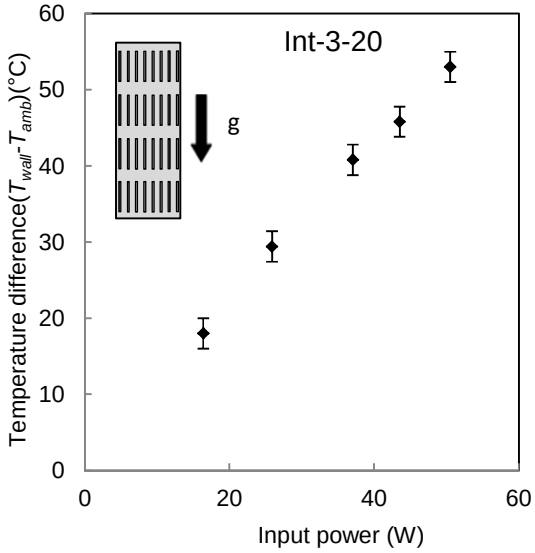
Int-3-20
g
Temperature difference(T_{wall}-T_{amb})(°C)
Input power (W)
60
50
40
30
20
10
0
20
40
60

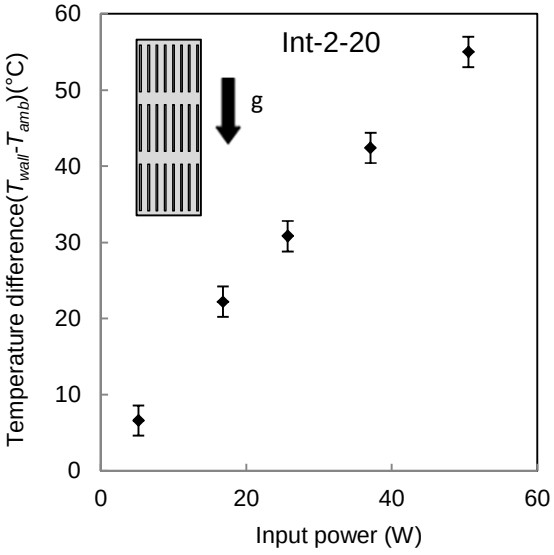
Int-2-20
g
Temperature difference(T_{wall}-T_{amb})(°C)
Input power (W)
60
50
40
30
20
10
0
20
40
60

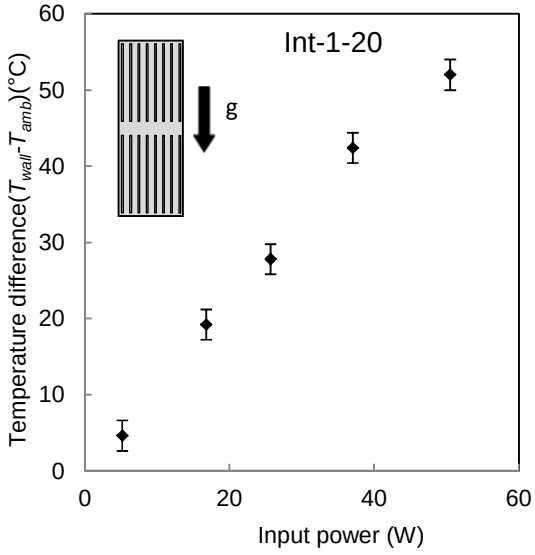
Int-1-20
g
Temperature difference(T_{wall}-T_{amb})(°C)
Input power (W)
60
50
40
30
20
10
0
20
40
60

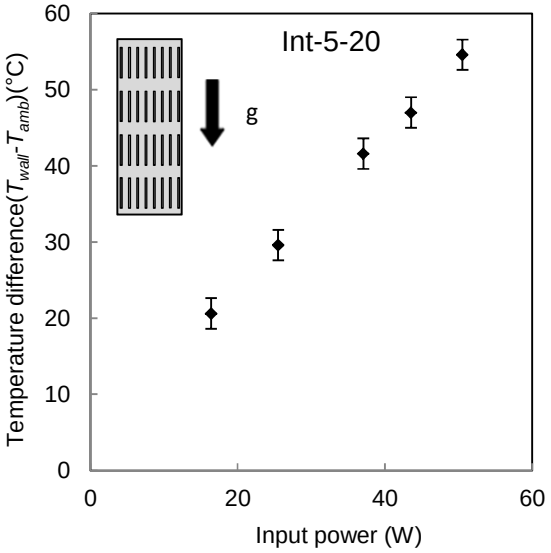
Int-5-20
g
Temperature difference(T_{wall}-T_{amb})(°C)
Input power (W)
0
10
20
30
40
50
60
0
20
40
60

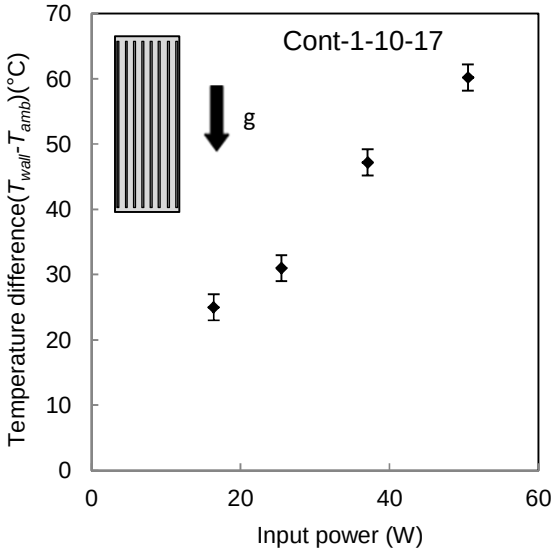
Cont-1-10-17
g
Temperature difference(T_{wall}-T_{amb})(°C)
Input power (W)
0
10
20
30
40
50
60
70
0
20
40
60

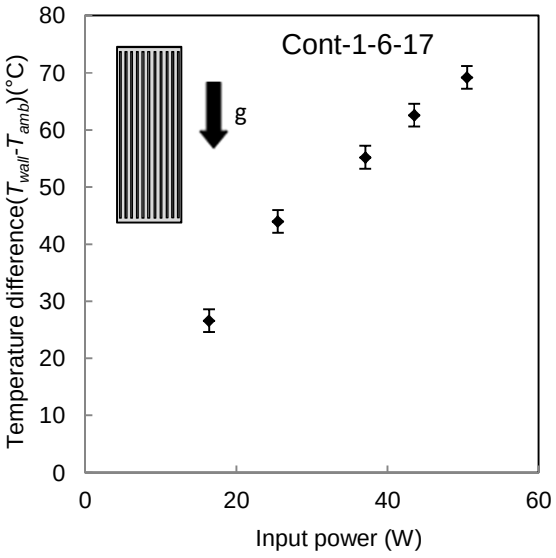
Cont-1-6-17
g
Temperature difference(T_{wall}-T_{amb})(°C)
Input power (W)
0
10
20
30
40
50
60
70
80
0
20
40
60

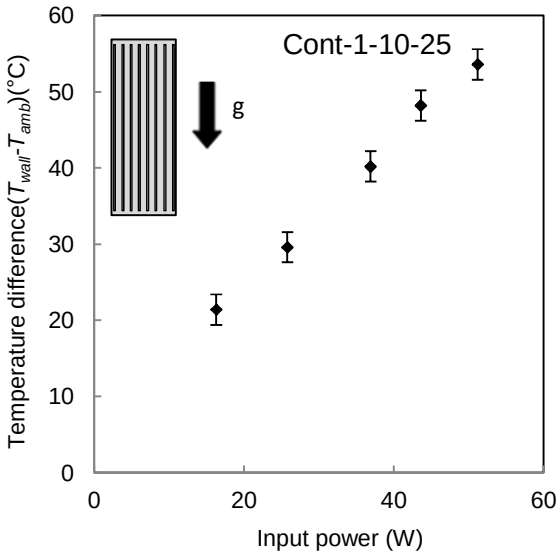
Cont-1-10-25
g
Temperature difference(T_{wall}-T_{amb})(°C)
Input power (W)
0
10
20
30
40
50
60
0
20
40
60

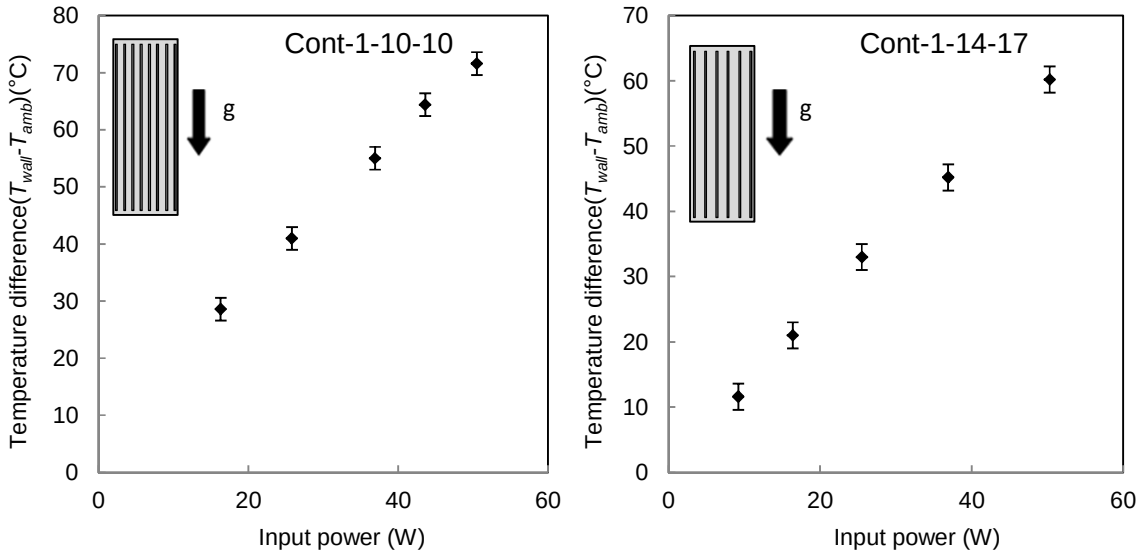

Figure 3-6: Experimental results for interrupted fins heatsinks.

It should be noted that the error bars corresponding to the power measurement uncertainty are not visible due to their relative small values as compared to the uncertainty values for the temperature difference. Also note that these are only raw experimental data, the results are discussed more in details in the next chapter.

3-3-2 Interrupted vertical single walls

Similar to the interrupted fins array experimental procedure explained in Section 3-3-1, during the experiments, the input power supplied to the heaters and surface temperatures were measured at various locations at the back of the base-plate. Electrical power was applied using a variable voltage transformer from Variac, model SC-20M (China). The voltage and the current were measured to determine the power input to the heater. Eight self-adhesive, T-type, copper-constantan thermocouples were installed in various locations on the backside surface of the aluminium samples, as in Fig. 3-2. All thermocouples were taped down to the backside surface of the enclosure to prevent

disturbing the buoyancy-driven air flow. An additional thermocouple was used to measure the ambient room temperature during the experiments. Thermocouples were plugged into an NI 9214 thermocouple module supplied by National Instruments (Austin, TX). Temperature measurements were performed at eight points in order to monitor the temperature variation on the heatsink. The average of these eight readings was taken as the base plate temperature. Since the measured temperature difference between the fins and the base plate was less than 1°C, the fins were assumed to be at the same temperature with the base plate. For each of the seven heatsinks, the experimental procedure was repeated for various power inputs. The base-plate temperature T_W , the ambient temperature T_{amb}, and the power input to the heater $\dot{Q}$, assuming that the power factor equals 1, were recorded at steady-state. The steady state was considered to be achieved when 150 minutes elapsed from the start of the experiment and the rate of temperature variations were less than 0.1℃/hour.

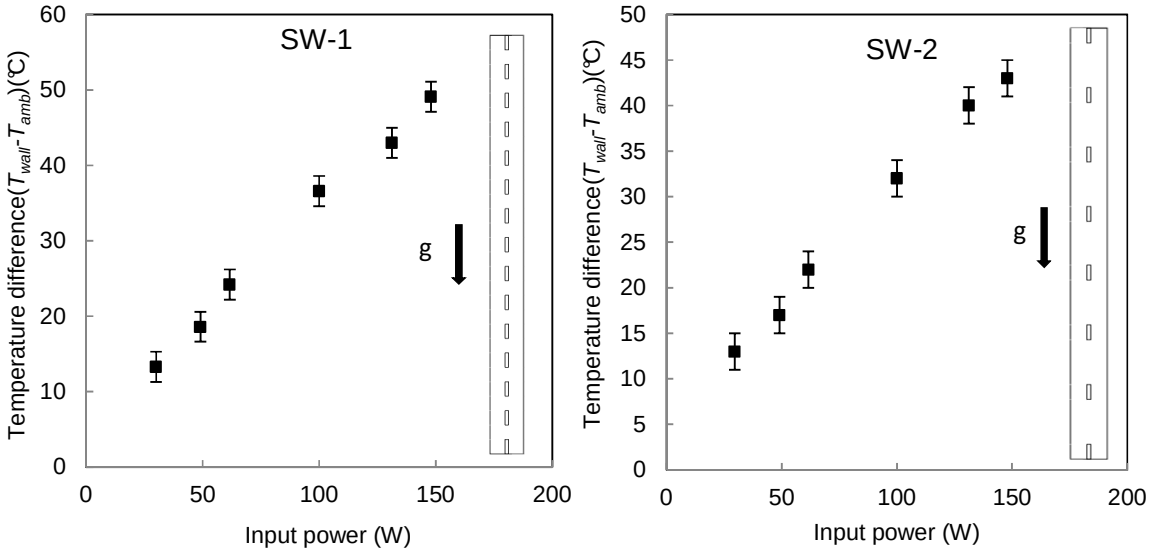

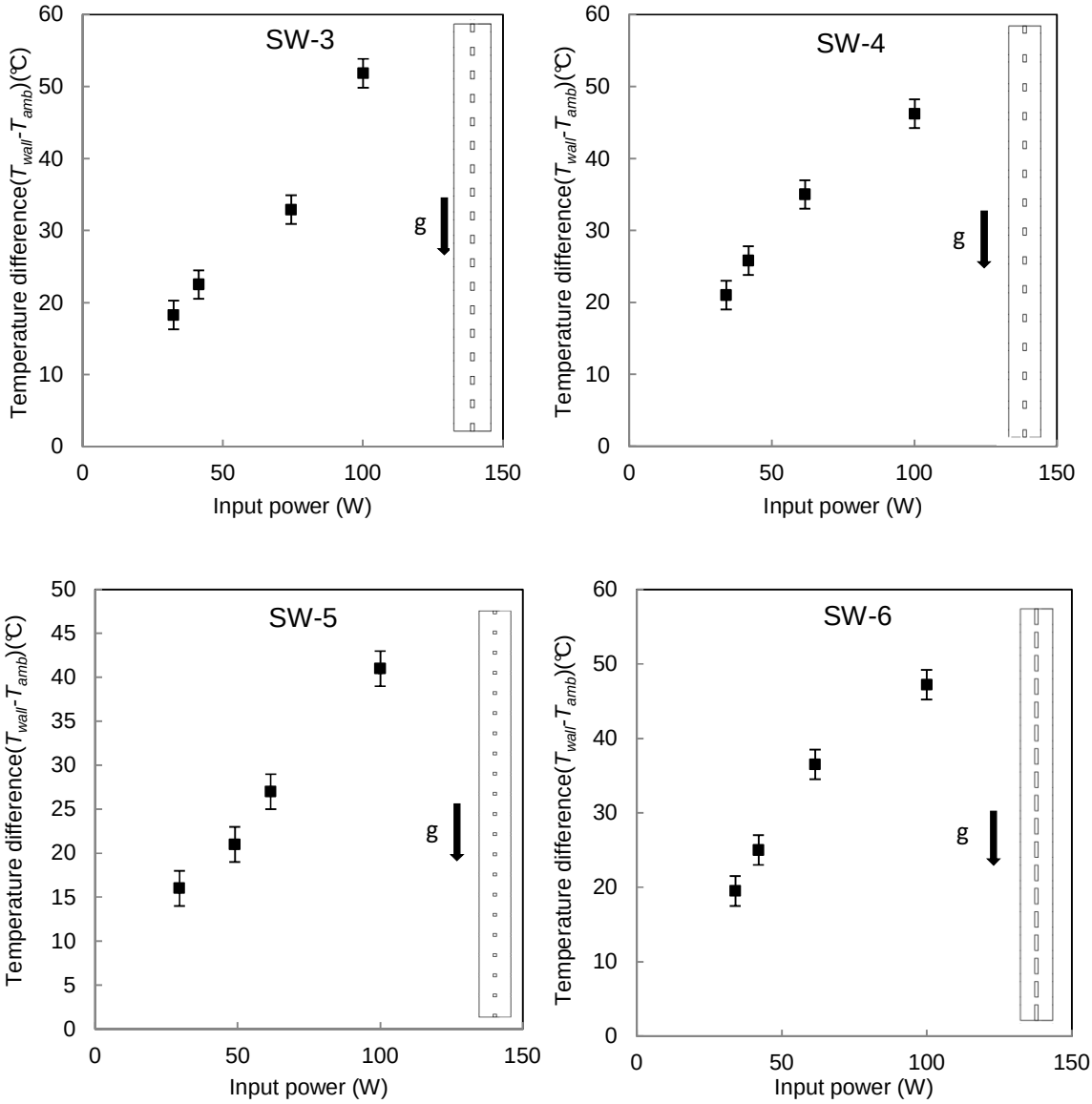

Figure 3-7: Experimental results for interrupted single walls.

Also note that the experimental data and the observed trends are discussed in Chapter 4 in detail.

3-4 Uncertainty analysis

Voltage (*V*) and current (*I*) were the electrical parameters measured in our experiments, from which the input power, P_{input}, can be calculated, see Eq. 3-3. The total accuracy in the measurements was evaluated based on the accuracy of the employed instruments, which was stated in subsection 3-3-1. The accuracy of the voltage and current readings were 0.3% for voltage and also 0.3% for the current, respectively, Extech® 430 multimeter. The reported accuracy values were given with respect to the instruments readings, and not the maximum value of the readings. The maximum uncertainty for the measurements can be obtained using the uncertainty concept provided in [52].

To calculate the uncertainty with the experimental measurements the following relation is used [52]:

$$\omega_R = \left[\sum \left(\frac{\partial R}{\partial x_i}\omega_i\right)^2\right]^{1/2} \quad 3\text{-}1$$

where ω_R is the uncertainty in results, $R(x_1, x_2 \ldots x_n)$, and ω_i is the uncertainty of the independent variable x_i . If the results function, $R(x_1, x_2 \ldots x_n)$, takes the form of a product of the independent variables, $R = x_1^{a1} x_2^{a2} \ldots x_n^{an}$, and Eq. 3-1 could be rewritten as:

$$\frac{\omega_R}{R} = \left[\sum \left(\frac{a_i}{x_i}\omega_i\right)^2\right]^{1/2} \quad 3\text{-}2$$

The final form of the uncertainty for the input power becomes, Eq.3-4 3-4:

$$P_{input} = V.I \qquad [W]\,, \tag{3-3}$$

$$\frac{\delta P_{input}}{P_{input}} = \sqrt{\left(\frac{\delta V}{V}\right)^2 + \left(\frac{\delta I}{I}\right)^2}\,, \tag{3-4}$$

$$\frac{\delta \dot{Q}_R}{\dot{Q}_R} = \sqrt{4\left(\frac{\delta T_w}{T_w}\right)^2 + 4\left(\frac{\delta T_{amb}}{T_{amb}}\right)^2 + \left(\frac{\delta l}{l}\right)^2 + \left(\frac{\delta H}{H}\right)^2 + \left(\frac{\delta t}{t}\right)^2}\,, \tag{3-5}$$

$$\dot{Q}_{NC} = P_{input} - \dot{Q}_R [W]\,, \tag{3-6}$$

Plugging the values for $V, I, T_w, T_{amb},\ l,\ H,$ and t, respectively, into 3-4 and 3-5 above, the maximum uncertainty value for $\dot{Q}_{NC}$ was calculated to be 8%. The calculated temperatures uncertainty ΔT was 2°C, which was twice the accuracy of the thermocouples. The calculated uncertainties for $\dot{Q}_{NC}$ and for ΔT were reported as error bars in the experimental results. It should be noted that the error bars corresponding to the power measurement uncertainty are not visible due to their relative small values as compared to the uncertainty values for the power.

Table 3-4: uncertainty analysis parameters

Parameter	Maximum uncertainty
$\delta V/V$	0.3%
$\delta I/I$	0.3%
$\delta P/P$	0.4%
δT	$\pm$1°C
δH	0.1 mm
δl	0.1 mm
δt	0.1 mm
$\delta \dot{Q}_R/\dot{Q}_R$	7.5%
$\delta \dot{Q}_{NC}/\dot{Q}_{NC}$	8%

Chapter 4.

Results and Discussion

In this chapter, the effects of different important geometrical parameters on the steady state natural convection heat transfer rate from both interrupted and continuous fins are discussed.

In the first Section, 4-1, the effects of parameters on the natural convective heat transfer rate from continuous rectangular fins are analysed as a parametric study. The impacts of fin spacing, s, fin height, H, for continuous fins on the average wall temperature are discussed in detail. Another important parameter is the fin interruption, G.The influence of this parameter on the natural convective heat transfer rate from interrupted rectangular walls is studied in Section 4-2. Later in this Section, a new closed form correlation is developed for Nusselt number based on the Rayleigh number for different values of γ and ζ, whereγ is a dimensionless parameter that represents the ratio of the interruption length, G, to the fin length, l, $\gamma = G/l$ and ζ is the aspect ratio of the fin length, l, over its thickness, t, $\zeta = l/t$. See Fig. 1-2.

In order to verify the numerical results, seven different heatsinks with interrupted fin arrays, and six different heatsinks with interrupted walls were prepared and studied experimentally, as described in detail in Chapter 3. The averaged surface temperature was measured for various heat dissipation rates. The average surface temperature was

calculated using the existing relationships for natural convection and radiation heat transfer rate; please see Chapter 1 for more details.

4-1 Continuous finned heatsinks

In the present experimental study, five different continuous finned plates were investigated and the results were compared to the analytical existing model of [15]. To investigate the effect of geometrical parameters, heat transfer rates from the prepared heatsinks are plotted as a function of average wall temperature. Figures 4-1 and 4-2 show the heat transfer rates obtained when varying the fin height *H* from 10 to 17 and to 25 mm, and keeping the fin length *L* constant at 305 mm; the fin spacing *s*, was varied from 6.0 to 9.5, and to 14.0 mm as shown in Table 3-1. As expected, the heat transfer rate from the heatsinks depends on the fin height, fin spacing and the average wall temperature. The conclusion is that the heat transfer rate is increasing with an increase in the fin height and wall temperature. Heat transfer rates measured from three different fin heights are close to each other at low wall temperatures, while at higher wall temperatures,$i.e., T_{wall} \approx$ 100℃, the heat transfer rates tend to diverge, as shown in Fig. 4-1. As it can be seen in Fig. 4-1, the experimental data and analytical model of [15] are in good agreement; the mean relative difference is 4.6 % and the maximum relative difference is 14 %. To calculate the total heat transfer rate from the heatsink to the ambient, we have to calculate the convective heat transfer rate using Eq. 1-1; then, the heat transfer rate from base plate and the radiation heat transfer rate, from Eq. 2-14 are also added.

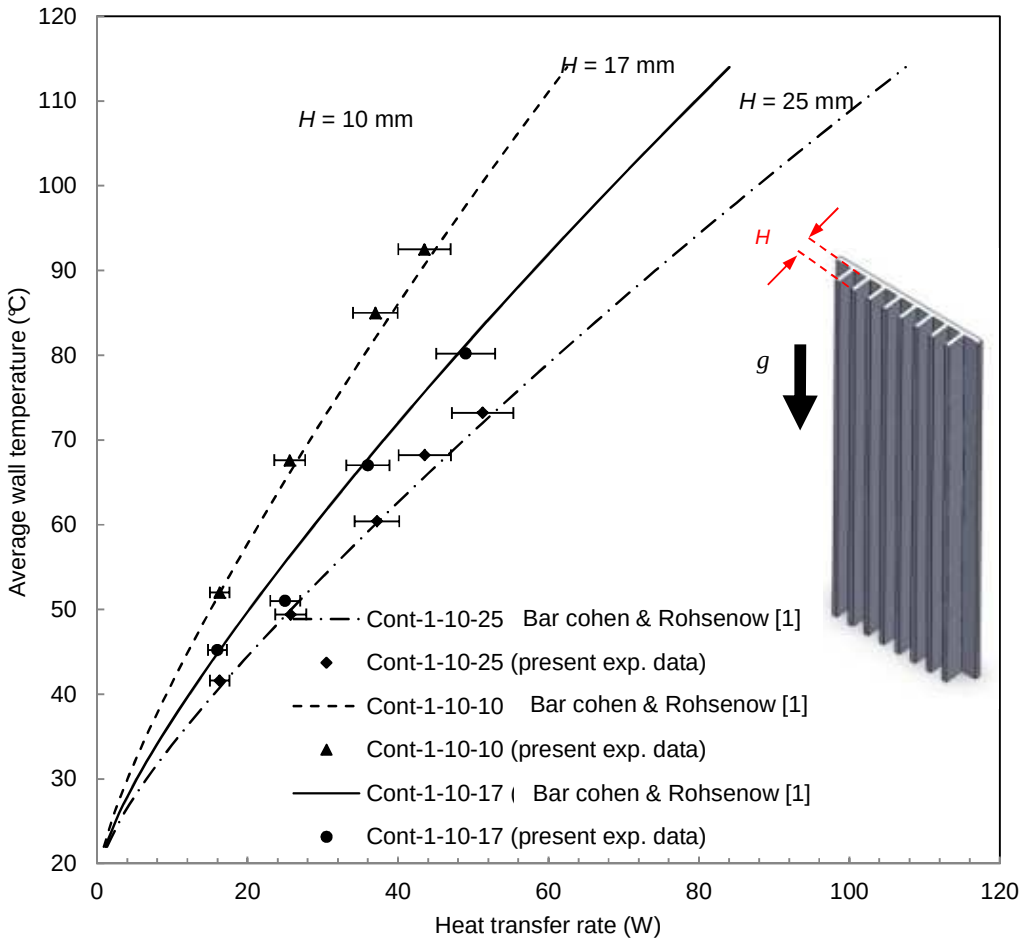

Figure 4-1: Comparison of the present experimental data with the theoretical predictions of [15] for different fin heights-continuous finned heatsinks; see Table 3-1 for the dimensions of the heatsinks.

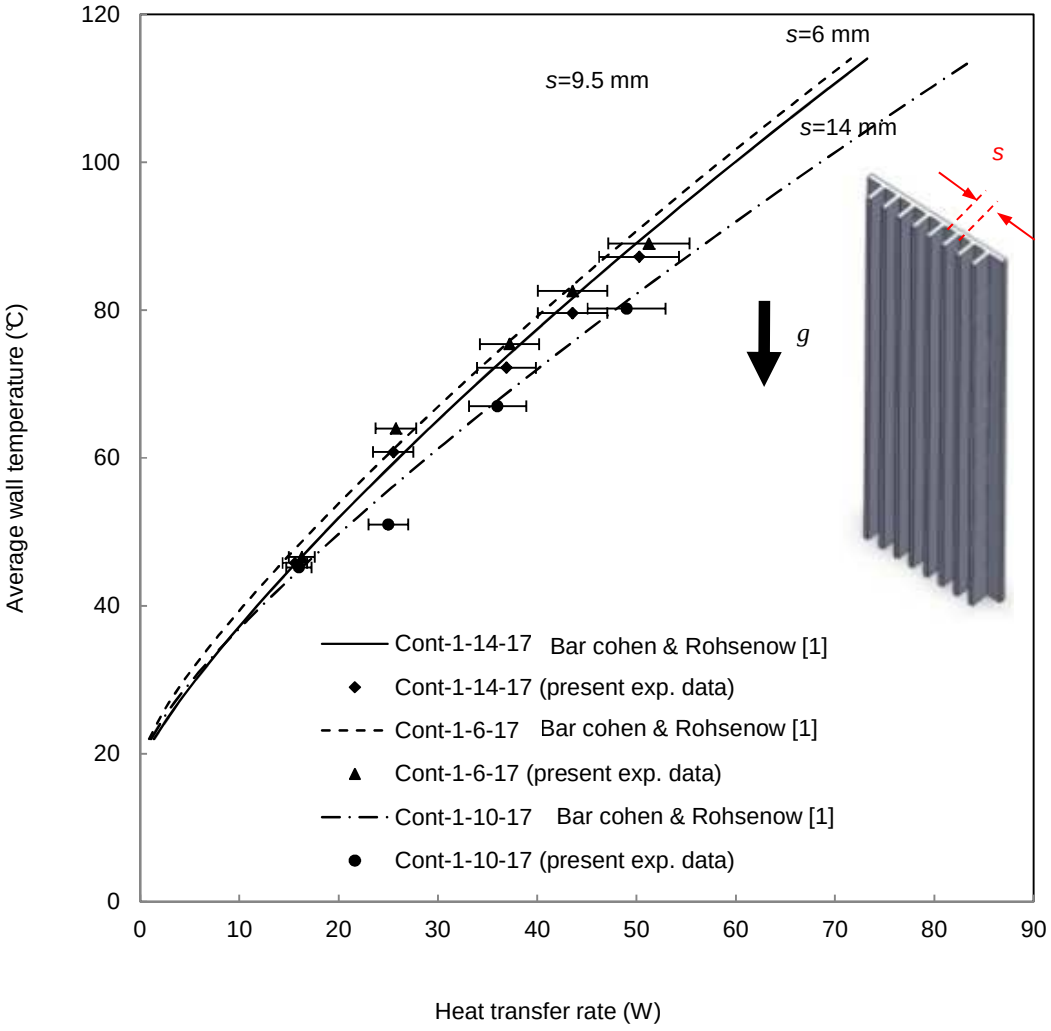

Figure 4-2: Comparison of the present experimental data with the theoretical predictions of [1] for different fin spacing-continuous finned heatsinks; see Table 3-1 for the dimensions of the heatsinks.

4-2 Effect of fin spacing on heat transfer rate

One of the most crucial parameters in designing a heatsink is the fin spacing, *s*. Closely packed fins will have greater surface area for heat transfer, but a smaller heat transfer coefficient, since for closely spaced fins or for relatively long channels, the fluid velocity attains its fully developed profile, leading to an increased heat transfer

resistance. A heatsink with widely spaced fins will have a higher heat transfer coefficient but smaller surface area, due to wide spacing. As such, the fins appear to have little influence upon one another and a developing flow regime occurs. Thus, an optimum spacing exists that maximizes the natural convection from the heatsink to the surroundings [15].

Heat transfer rate and heatsink mass are plotted as a function of the fin spacing for the samples considered in this study in Fig. 4-3. The data are for heatsinks with fin lengths of L = 305 mm, fin heights of H = 17 mm and fin spacing of s = 6, 9.5, and 14 mm, respectively, as shown in Table 1-1.

The power input to the heater was kept constant at $P_{input} = 40$ W. As can be seen in Fig. 4-3, there is an optimum fin spacing that maximizes the heat transfer rate for different average surface temperatures. It should be noted that the present experimental data are in good agreement when compared against the analytical and experimental results reported by Bar-Cohen and Rohsenow [15] and Tamayol *et al.* [51] for optimum fin spacing.

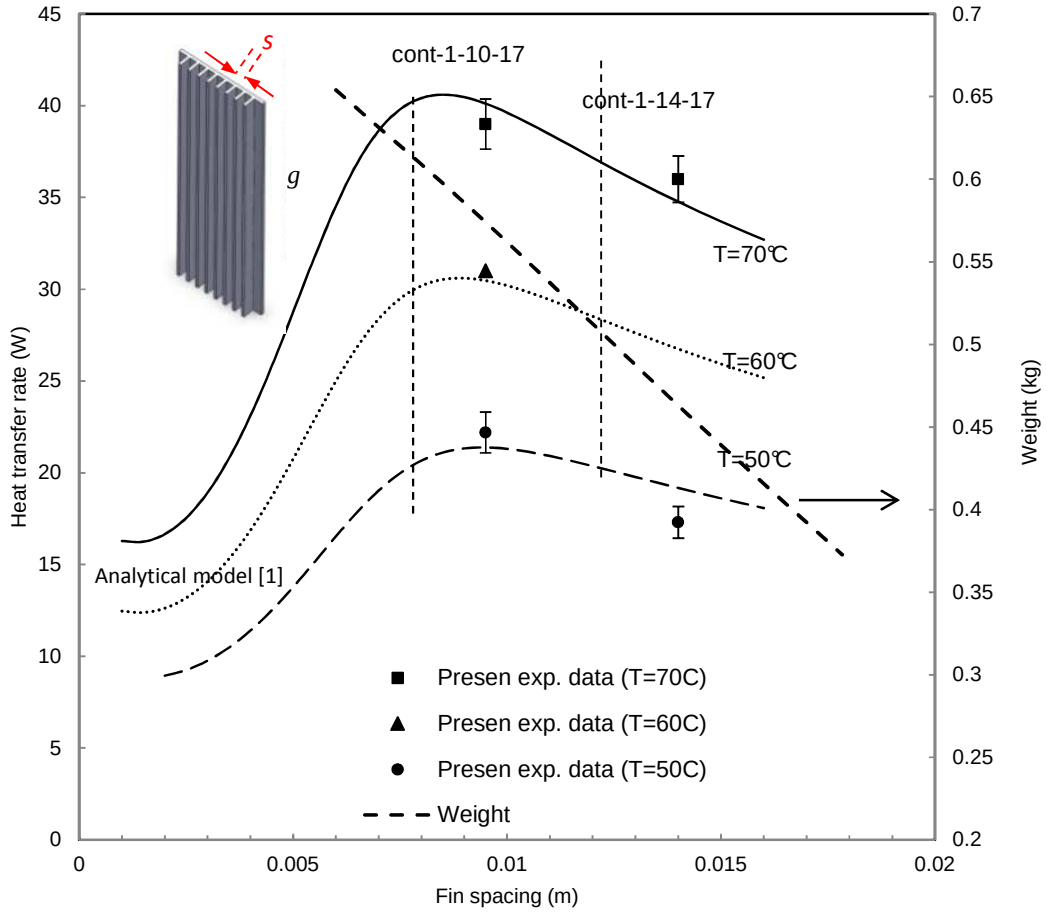

Figure 4-3: Heat transfer rate and heatsink mass versus fin spacing for different average surface temperatures, fin base lengths *L* = 305 mm, heights *H* = 17 mm; see Table 3-1 for more detail on samples.

Selection of a proper fin-spacing is very important, since fin spacing could lead to an inefficient heat transfer and a voluminous heatsink. Tamayol *et al* [51] tested three different heatsinks with non-optimized fin spacing and compared the sample's weight and their heat transfer rate to the same samples with no fins on the surface. They showed that due to small fin spacing in the tested samples, fins did not increase natural convection

heat transfer. However, the weight of the closely finned surfaces was 84% higher because of the additional material used.

4-3 Effects of fin interruption on natural convection heat transfer

4.2.1 Optimum interruption length to the fin length ratio

Heat flux from heatsinks with interrupted fins as a function of average wall temperature for fin length of L = 305 mm, fin spacing of s = 9.5 mm, and fin height of H = 17 mm are plotted in Figs. 4-4 and 4-5. These figures show the effect of interruption length on natural convection heat transfer. In this case, four interruptions were made along the fin array and the interruption length was varied in steps of 10 mm, from G = 20 mm to G = 40 mm, as shown in Table 3-3.As it was expected, the heatflux improves as G increases. In Fig. 4-5 the effect of number of interruptions is shown; the interruption length was kept constant at 20 mm, and one, two, three, four, and five interruptions were added to the fins, respectively. Both Figs 4-4 and 4-5 show the present experimental data and the comparison with our numerical results. As can be seen from Fig. 4-5, increasing the number of interruptions would cause an increase in heat flux, which is a result of the frequent resets, which are imposed on the thermal boundary layer due to adding interruption along the fins.

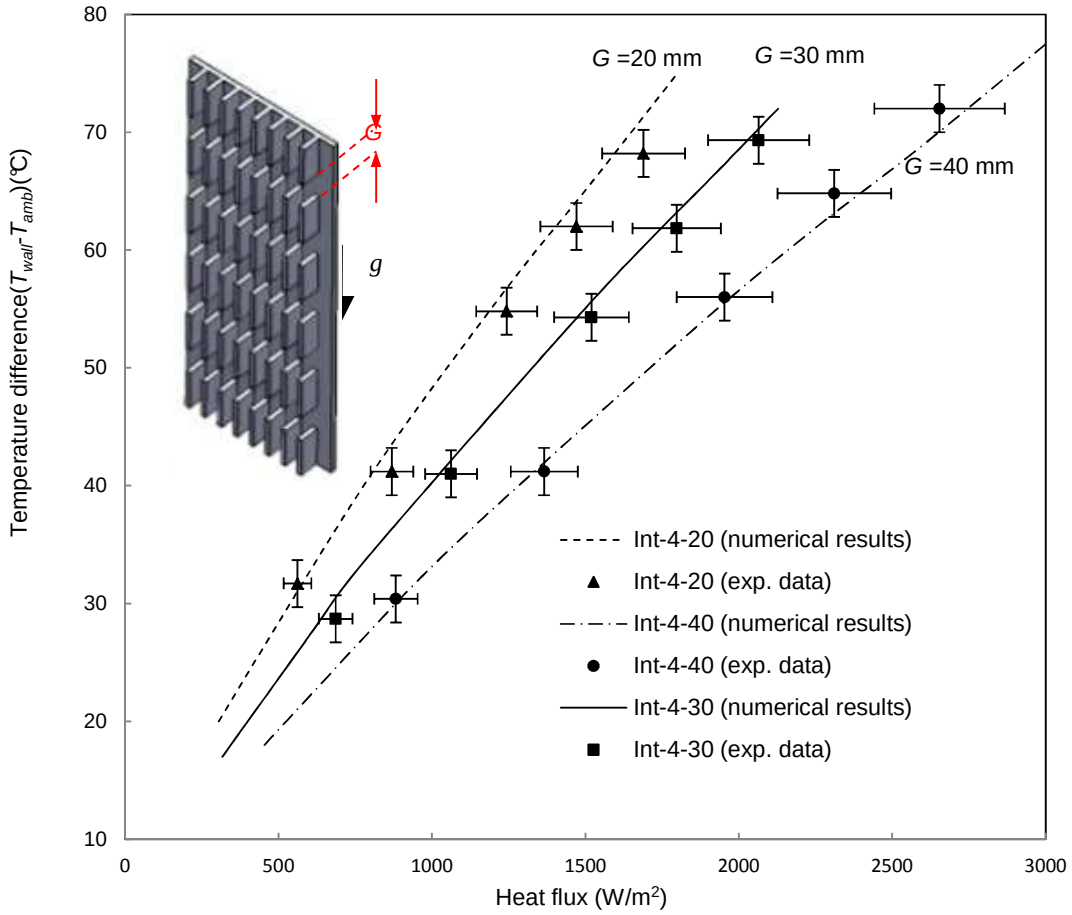

Figure 4-4: Comparison between the present experimental data and numerical results for different fin interruption lengths (i.e., 20, 30 and 40 mm) for constant number of fins in a row *N* = 4 interruptions; see Table 3-2 for more detail on samples.

Figure 4-4 shows the results of the numerical simulation as discussed in Chapter 2, which accounts for the effect of fin interruption on the heat transfer rate from the fins. The interruption sizes started from zero, the limiting case which represented the continuous fins.

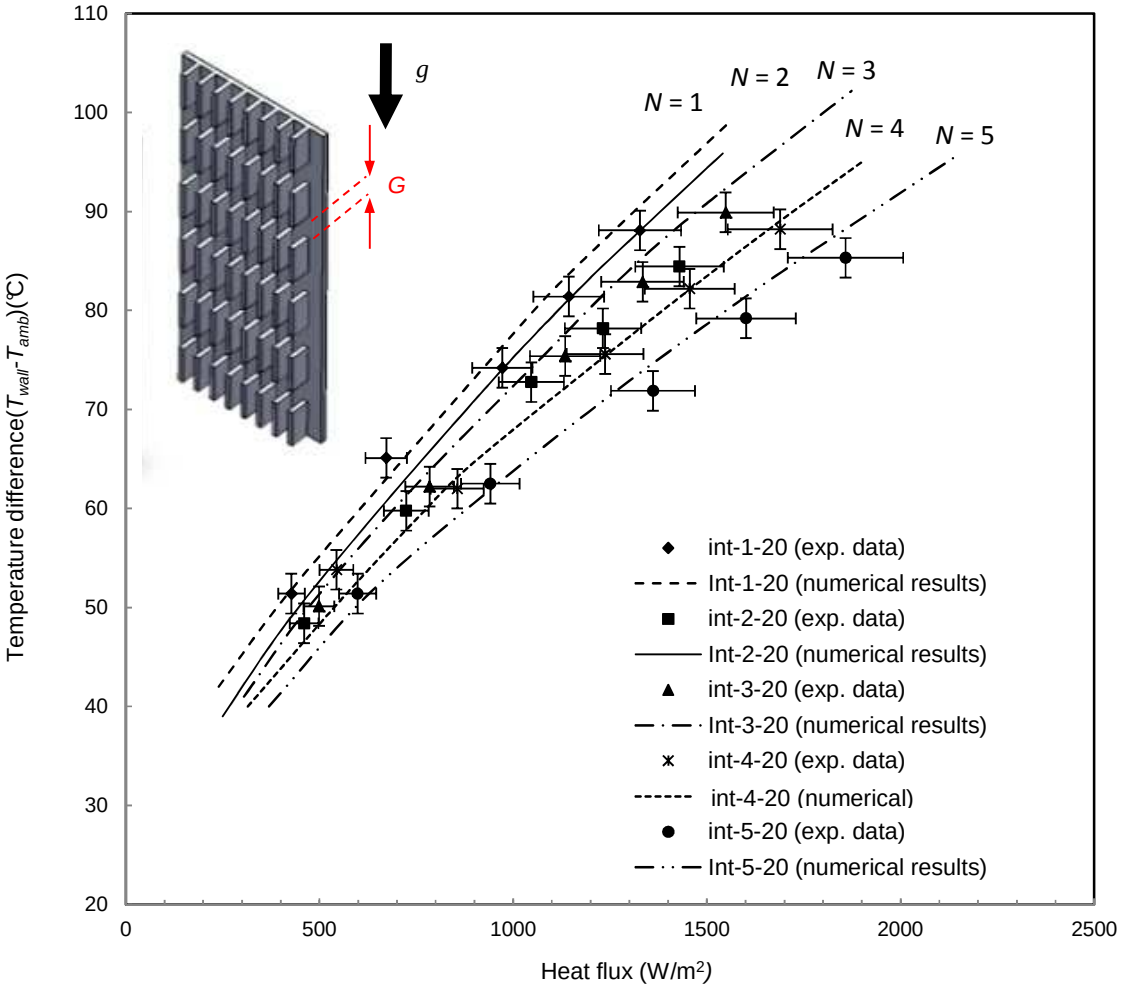

Figure 4-5: Comparison between experimental data and the present numerical results for different number of interruptions (*N*) for constant interruption value of *G* = 20 mm; see Table 3-2 for more detail on samples.

The following can be concluded from Figs. 4-4 and 4-5:

- Increasing the fin interruption length causes an increase in the heat flux because of "better" interruption in the thermal boundary layer.
- Increasing the number of interruptions increases the heat flux as well, which is a result of the frequent resets imposed on to the thermal boundary layer.

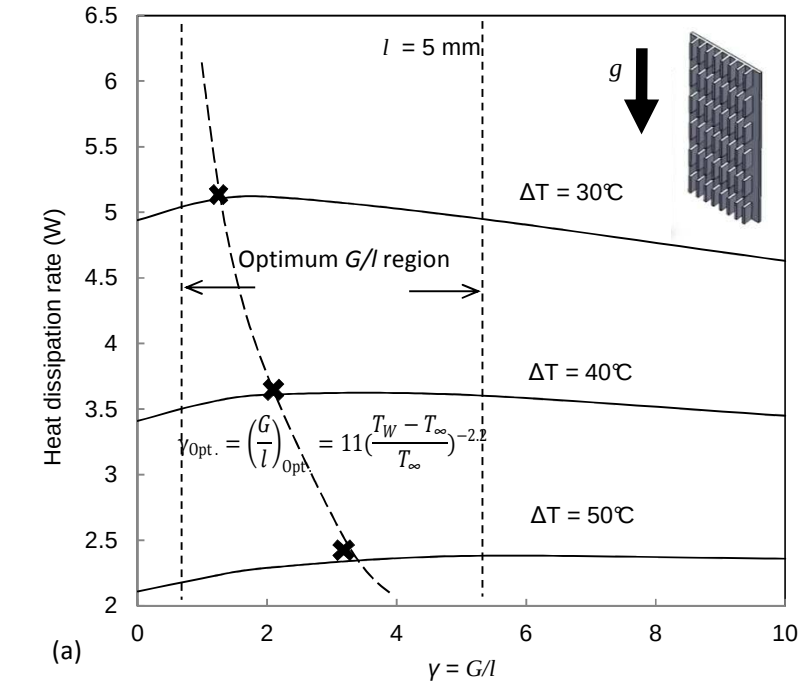

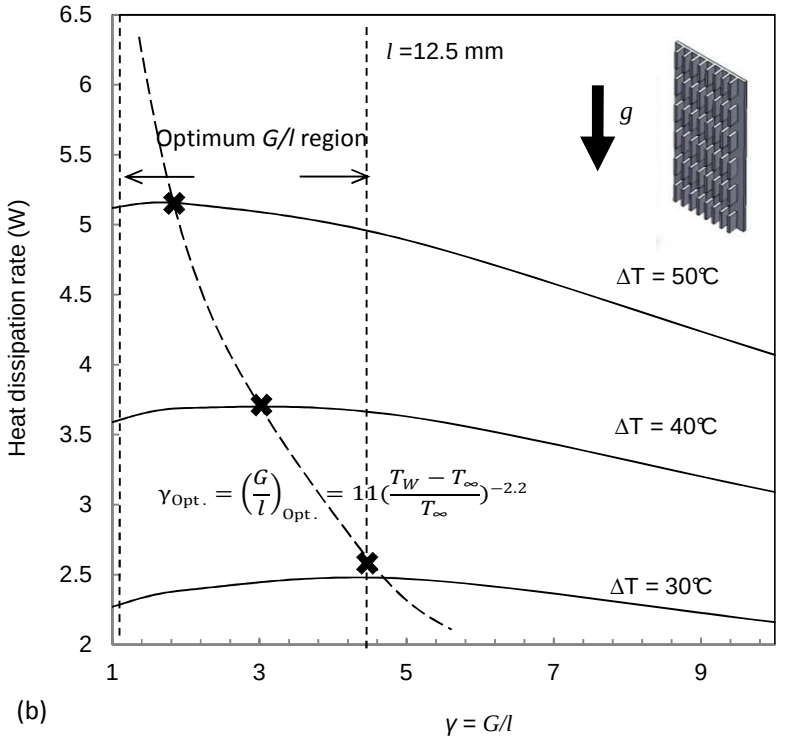

Figure 4-6: Effect of the interruption length on the total natural convection heat transfer from the fins (numerical results): a) fin length l = 5 mm and b) fin length l = 12.5 mm. ($\Delta T = T_s - T_{amb}$)

In Figure 4-6 the non-dashed lines show the numerical data for heat transfer rate from each fin, and the dashed curve lines show the relationship fitted to the maximum points of each curve for different temperature difference (Eq. 4-1) Since the results show a rather flat curvature in the vicinity of the optimum point, and more importantly, that the heatsinks work over a range of temperature difference, the optimum $\gamma = G/l$, is demarcated as a region - as marked with dashed lines on Figure 4-6.

One can conclude the following from Fig. 4-6:

- There is an optimum interruption length that maximizes the total heat transfer rate from the heatsink.
- The optimum interruption length is a function of surface temperature and fin length. In this study, a new compact correlation is developed that can accurately predicts the optimum fin interruption as a function of surface temperature for different lengths (2.5 mm < l < 25 mm) and fin surface temperatures , as follows:

$$\gamma_{\text{Opt.}} = \left(\frac{G}{l}\right)_{\text{Opt.}} = 11\left(\frac{T_W - T_{amb}}{T_{amb}}\right)^{-2.2}. \qquad 4\text{-}1$$

4-4 Model development for interrupted vertical walls

We seek a solution for steady-state laminar natural convective heat transfer rate from an interrupted single wall.

A new concept, effective wall length, is introduced to calculate the Nusselt number for the natural convective heat transfer rate along the interrupted vertical walls. The effective length is defined so that the heat transfer rate from an equivalent continuous

vertical wall with the effective length would be equal to the heat transfer rate from the interrupted (actual) walls. For this purpose, the calculated heat transfer rate from the interrupted walls is made equal to the heat transfer rate from a continuous wall with effective length, and from that mathematical expression the effective length is calculated. The heat transfer from an isothermal vertical wall can be calculated from the relationship proposed in [11]:

$$Nu_{L_{eff}} = 0.59\left(Ra_{L_{eff}}\right)^{\frac{1}{4}}, \qquad 4\text{-}2$$

knowing that

$$Nu_{Leff} = \frac{h.L_{eff}}{k}, \qquad 4\text{-}3$$

Replacing $h = \frac{\dot{Q}}{A.\Delta T}$ in Eq. 4-3, yields:

$$L_{eff} = \left(\frac{\dot{Q}}{0.59\ k}\right)^{2}\left(\frac{\alpha\vartheta}{g\beta}\right)^{\frac{1}{2}}\Delta T^{-5/2}, \quad [m] \qquad 4\text{-}4$$

We introduce $\zeta = l/t$, which is a non-dimensional number equal to the ratio of the wall length *l*, to the wall thickness, *t*:

$$\zeta = l/t\ , \qquad 4\text{-}5$$

and γ is equal to the ratio of the interruption length, *G*, to the wall length, *l*,

$$\gamma = G/l\ , \qquad 4\text{-}6$$

In order to develop a general model for various amounts of γ, two asymptotes are recognized and a blending technique [53] is implemented to develop a compact

relationship for the wall effective length and the corresponding Nusselt number. The first asymptote is developed for small γ , where $\gamma \to 0$, for which the flow behaviour resembles the flow over a vertical plate that has no interruptions with a total length of

$$L = N.l \qquad [m], \tag{4-7}$$

where *N* is the number of walls. The second asymptote is when $\gamma \to \infty$; that is the limiting case where the walls are located far enough from each other, leading to an individual wall limit; in other words, the walls boundary layer will not be affected by the previous walls boundary layers. For the first asymptote, $\gamma \to 0$, the effective length is correlated using the present numerical data.

$$\frac{L_{eff,\ \gamma \to 0}}{N.l} = 0.22\gamma + 1\ , \tag{4-8}$$

For the asymptote $\gamma \to \infty$, Eqs. 4-10 through 4-12 available in literature [7, 11] are used to calculate the heat transfer from walls. Natural convective heat transfer from the walls in this asymptote is obtained by calculating the heat transfer from each side of the wall and adding them up. The relationships used for calculating the heat transfer from the upper and lower and vertical sides of the wall are given in [54] and they are the same as Eqs. 4-10 and 4-12.

$$\dot{Q}_t\ = \dot{Q}_{horizontal\ sides} + \dot{Q}_{vertical\ sides}\ , \qquad [W] \tag{4-9}$$

$$Nu_{vertical\ sides} = Nu_l = \ 0.59Ra_l^{\frac{1}{4}}\ , \tag{4-10}$$

$$Nu_{horizontal\ sides} = Nu_{up} = 0.56Ra_t^{\frac{1}{4}}\ , \tag{4-11}$$

$$Nu_{low} = 0.27Ra_t^{\frac{1}{4}}\ , \tag{4-12}$$

The natural convective heat transfer, $\dot{Q}$, as calculated from the equations above, could be substituted in Eq. 4-4 in order to calculate the asymptote of L_{eff} for larger values of γ, $L_{eff,\gamma\to\infty}$. As a result, for the upper, lower and vertical sides of the walls, we can calculate the ratio of the effective length to *N.l* as:

$$\frac{L_{eff,\gamma\to\infty}}{N.l} = N^{\frac{1}{3}}\left[0.83\left(\frac{1}{\zeta}\right)^{\frac{3}{4}}+1\right]^{4/3}, \qquad 4\text{-}13$$

Having $L_{eff,\gamma\to\infty}$ and $L_{eff,\gamma\to 0}$ available, a compact relationship for L_{eff} can be developed by using a blending technique, introduced by Churchill and Usagi [53].

$$L_{eff} = \left[\left(L_{eff,\ \gamma\to 0}\right)^{-c} + \left(L_{eff,\ \gamma\to\infty}\right)^{-c}\right]^{-1/c}, \qquad [m], \qquad 4\text{-}14$$

where *c* is a fitting parameter, and its value is found by comparison with the present numerical data to be *c* = 3. This fitting parameter minimizes the maximum percent difference between the model and the exact solution, as is shown in Fig. 4-8.

$Nu_{L_{eff}}$ is calculated by substituting L_{eff} into Eq. 2-9. The final relationship is a function of γ, ζ, $N$and the Rayleigh number, which, in turn, is a function of temperature difference, as shown below:

$$Nu_{L_{eff}} = \frac{hL_{eff}}{k} = 0.59\,Ra_l^{1/4}N^{3/4}\left\{(0.22\gamma+1)^{-3} + \left[N\left(0.83\left(\frac{1}{\zeta}\right)^{\frac{3}{4}}+1\right)^{4}\right]^{-1}\right\}^{-1/4}, \qquad 4\text{-}15$$

where l is the wall length, ζ is the aspect ratio of the wall length of the wall thickness, $\zeta = l/t$, γ is the ratio of the interruption length to the wall length, $\gamma = G/l$. N is the number of walls and Ra_l is the Rayleigh number based on wall length, respectively.

$$Ra_l = \frac{g\beta\ \Delta T l^3}{\alpha\vartheta}, \qquad 4\text{-}16$$

L_{eff} is the effective length for the walls, the relationship proposed for $Nu_{L_{eff}}$ is valid for the following range: ($5 < \zeta = \frac{l}{t} < 15$).

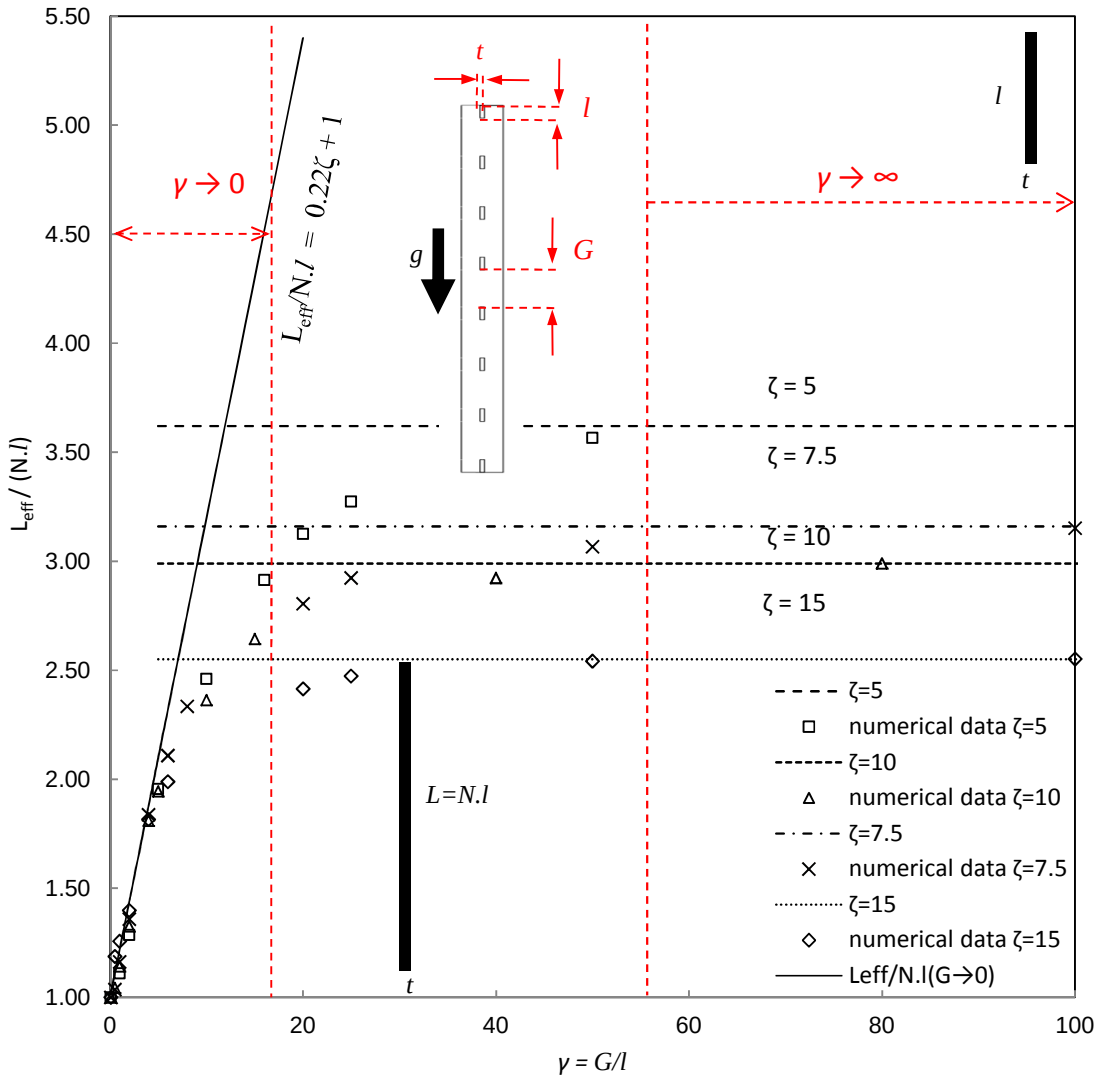

Figure 4-7: Numerical data and asymptotes for natural convective heat transfer from interrupted walls.

Figure 4-7 highlights the tendencies that the two asymptotes, introduced in Chapter 2, exhibit based on γ. Two different trends can be seen in the present data for the extreme values of γ, where γ is the ratio of the interruption length to the wall length, $\gamma = G/l$. The first trend is showing small values of γ and it can be seen that the data in this region have been collapsed, as shown in Fig. 4-8. The second trend of data, which

corresponds to relatively large values of γ, shows a plateau. i.e., data converge to a specific value, which is the asymptote for walls with effective length equal to the wall length ($L_{eff} = l$), see Chapter 2 for more explanation.

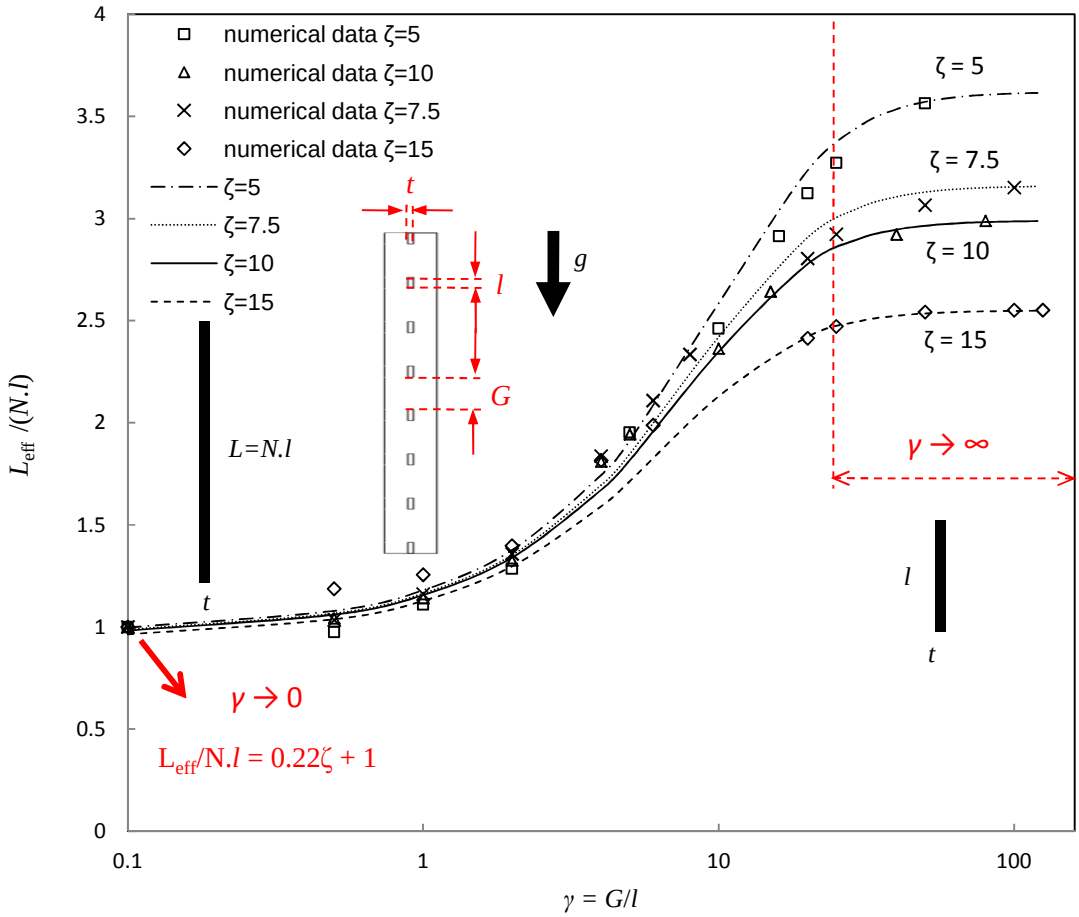

Figure 4-8: Numerical data and analytical relationship - natural convective heat transfer from interrupted walls.

A new general relationship, Eq. 4-17, is developed to determine the Nusselt number that characterizes the natural heat transfer from interrupted walls. The calculation is performed using a blending technique [53] based on the non-dimensional geometrical

parameters $\gamma = G/l$ and $\zeta = l/t$. This Nusselt number can be used to calculate the heat transfer rate for any rectangular interrupted wall in the range of $5 < \zeta = \frac{l}{t} < 15$.

$$Nu_{L_{eff}} = 0.59\, Ra_l^{1/4} N^{3/4} \left\{ (0.22\gamma + 1)^{-3} + \left[N \left(0.83 \left(\frac{1}{\zeta} \right)^{\frac{3}{4}} + 1 \right)^4 \right]^{-1} \right\}^{-1/4}, \qquad \text{4-17}$$

where l is the wall length, $\boldsymbol{\zeta}$ is the aspect ratio of the wall length of the wall thickness, $\boldsymbol{\zeta = l/t}$, $\boldsymbol{\gamma}$ is the ratio of the interruption length to the wall length, $\boldsymbol{\gamma = G/l}$. N is the number of walls and $\boldsymbol{Ra_l}$ is the Reyleigh number based on wall length, respectively.

It should be noted that since the Nusselt numbers are based on the wall effective length, which is an effective length, the value of these Nusselt numbers are not in the normal range of natural convection Nusselt number. Experimental data obtained from interrupted wall samples is compared against Eq. 4-17 in Fig. 4-9. It should be noted that out of six samples tested, three of them could not be used since their fin aspect ratios were out of the applicable range of the proposed Eq. 4-17; however the experimental data were reported along with the other samples in Appendix 1.

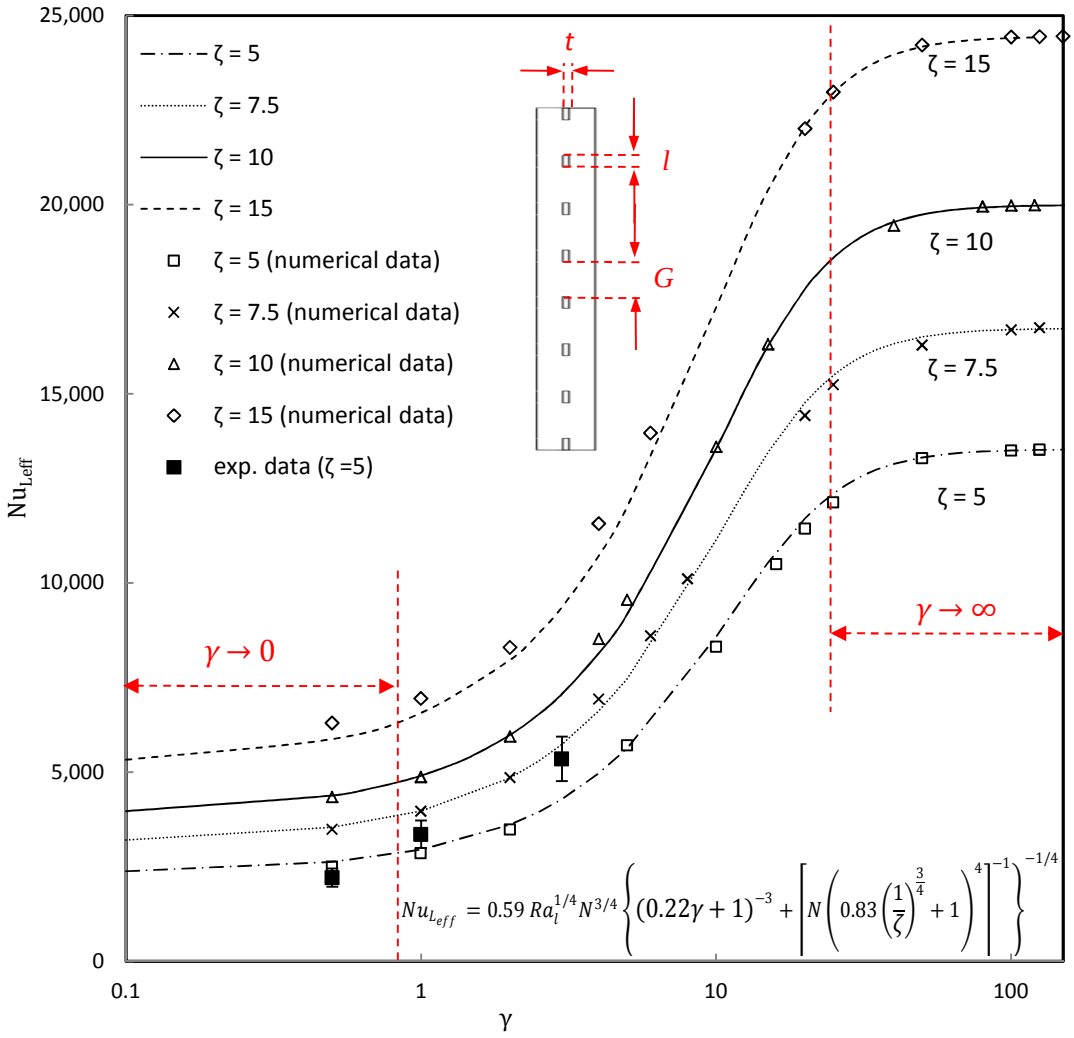

Figure 4-9: Comparison between the present numerical data and the proposed compact relationship for Nusselt number of interrupted walls. ($\zeta = l / t$)

The second approach for calculating the Nusselt number was to correlate the numerical data based on the dimensionless numbers of $\gamma = G/l$ and $\zeta = l/t$. The corresponding data for each case of ζ were non-dimensionalized with respect to the Nusselt number data for $= l/t = 1$, which represents the pin-fins geometry. The following new correlation is developed for the Nusselt number based on the square root of area, $Nu_{\sqrt{A}}$, as a function of γ and ζ. The area is defined as follows:

$$A = (l + t)H \qquad [m^2] \tag{4-18}$$

where *A* is the walls area Since all the calculations are done based on the unit depth of the interrupted wall, *H* will be equal to 1 m.

$$Nu_{\sqrt{A}}/Nu_{pin} = \frac{0.0125\zeta + 1}{1 - (0.02\,\zeta + 0.17)e^{(-0.0012\,\zeta - 0.032)(\gamma)}} \tag{4-19}$$

where l is the wall length, ζ is the aspect ratio of the wall length of the wall thickness, $\zeta = l/t$, γ is the ratio of the interruption length to the wall length, $\gamma = G/l$.

The proposed Nusselt number shown in Eq. 4-19 is compared to the present experimental and numerical data in Fig. 4-10. The relative difference between the Nusselt number from the correlation given in Eq. 4-19 and the data is within 10%.

From the numerical data Nu_{pin} is calculated and a correlation is fitted to the data as follows:

$$Nu_{pin} = \frac{187 + 45.73\,\gamma^{1.06}}{13.56 + \gamma^{1.06}} \tag{4-20}$$

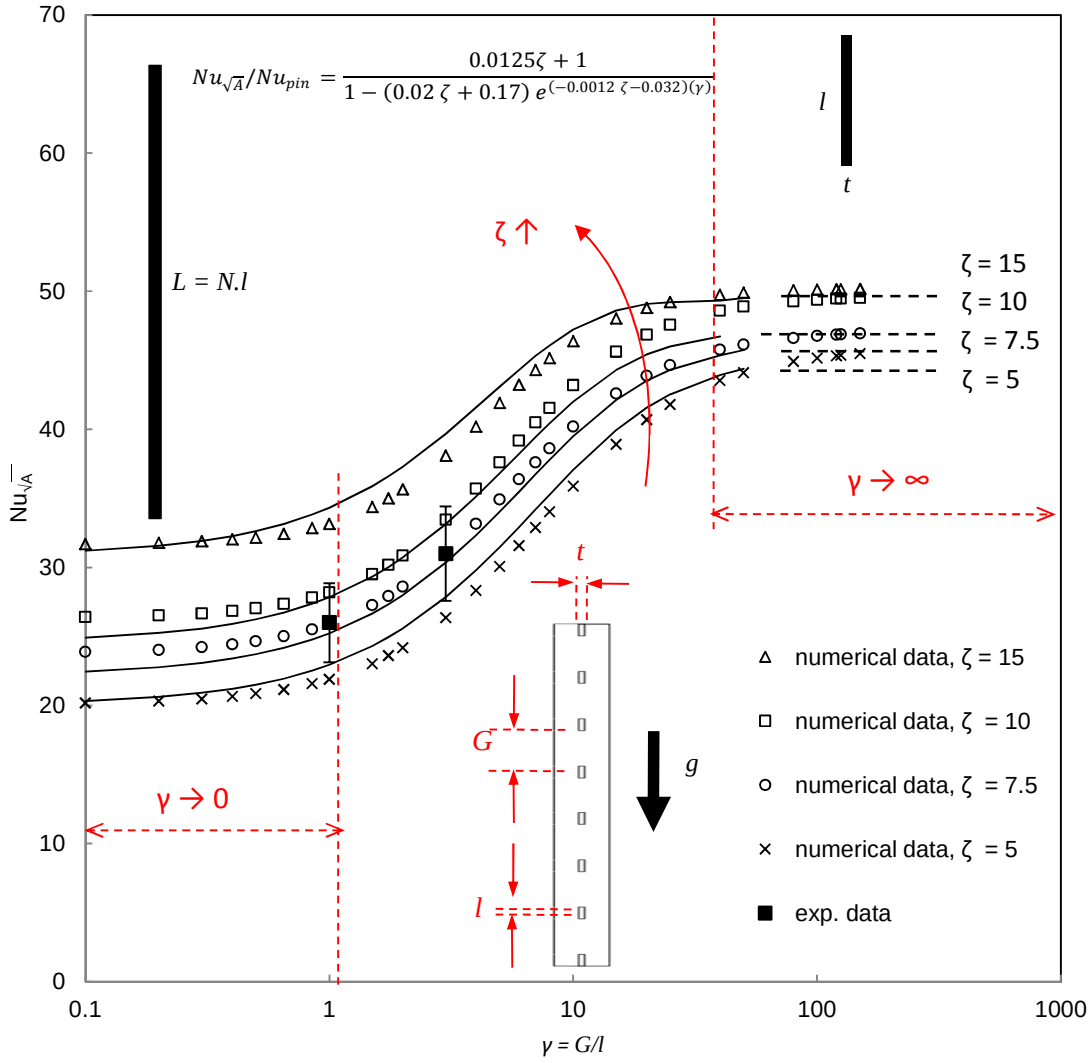

Figure 4-10: Comparison between the present numerical and experimental data against the new compact relationship for the natural convective heat transfer from interrupted walls. (ζ = *l*/*t*)

Chapter 5.

Conclusion

Experimental, numerical and analytical studies were performed in order to establish optimized geometrical fin parameters for natural convection heat transfer from vertically-installed interrupted rectangular fin arrays. Two new custom-designed testbeds were developed at SFU. An experimental investigation was planned in close collaboration with the project industrial partner, Analytic System Ware (ASW). Twelve fin arrays and interrupted wall samples were prepared to verify the developed numerical and analytical models over the entire range of fin geometrical parameters, and also to provide a proof-of-concept demonstration for the proposed new enclosure designs. The prepared samples were tested in the lab and collected data were compared with the numerical and analytical models developed in this study. The numerical and analytical results were successfully verified by experimental data; the mean relative difference found was 4.6% and the maximum relative difference was 14%. Optimum fin spacing was calculated and compared to the existing data and models available in the literature.

The most important element of the present work is the determination of the interruption length in natural convection fin arrays. The purpose of these interruptions is to reset the thermal boundary layer associated with the fin in order to decrease thermal resistance [55] [21]. After implementing an optimum fin interruption, the experimental and numerical results show a considerable increase in the heat flux from a heatsink

compared to the equivalent continuous heat flux from heatsink. A comprehensive parametric study has been conducted to investigate the effect of various fin array geometrical parameters on natural convection heat transfer. Our parametric studies show an optimum interruption length which lead to the maximum natural heat transfer from the fin array. A new correlation is developed for this optimum fin interruption and the associated heat transfer coefficient.

The following highlights this project finding:

- There is an optimum interruption length that maximizes the total natural convection heat transfer from vertically installed fin arrays.
- The optimum interruption length is a function of both the temperature at the fin surface and the fin length. The following new correlation is proposed for different fin lengths (2.5mm < l < 25mm) and fin surface temperatures:

$$\left(\frac{G}{l}\right)_{\text{Opt.}} = 11\left(\frac{T_W - T_{amb}}{T_{amb}}\right)^{-2.2}$$

- The above proposed correlation is successfully verified with experimental and numerical data. A mean relative difference of 4.6% and a maximum relative difference of 14% are observed, predicting the optimum natural convection heat transfer coefficients.
- A new general and compact relationship is developed for the Nusselt number for natural convection heat transfer from interrupted fins using a blending technique based on the non-dimensional geometrical parameters $\gamma = G/l$ and $\zeta = l/t$. This relationship can be used for calculating heat transfer rate for any rectangular interrupted fin in the range of $5 < \zeta = \frac{l}{t} < 15$.

$$Nu_{L_{eff}} = 0.59\, Ra_l^{1/4} N^{3/4} \left\{ (0.22\gamma + 1)^{-3} + \left[N \left(0.83 \left(\frac{1}{\zeta} \right)^{\frac{3}{4}} + 1 \right)^4 \right]^{-1} \right\}^{-1/4}$$

- The collected numerical data were correlated, and the relationship for the Nusselt number ratio to the Nusselt number of pin-fins was presented based on the square root of area of the walls as a function of γ and ζ, $5 < \zeta = \frac{l}{t} < 15$.

$$\frac{Nu}{Nu_{pin}} = \frac{0.0125\zeta + 1}{1 - (0.02\,\zeta + 0.17) e^{(-0.0012\,\zeta - 0.032)\left(\frac{G}{l}\right)}}$$

Future work

The following directions can be considered as the continuation of this dissertation:

1. Perform an analytical solution for finding natural convective heat transfer and a corresponding Nusselt number for interrupted fin arrays. The methods could be integral solution or similarity solution.
2. Extend the analysis to other fin orientations, such as inclined fins, or staggered orientation.
3. Extend the analysis to conductive heat transfer inside the heatsink and fins.
4. Investigate the effects of thermal load variations, i.e., the transient natural convection heat transfer from interrupted fins.

Bibliography

[1] S. P. Gurrum, S. K. Suman and J. Y. K., " Thermal issues in next-generation integrated circuits," *IEEE Transactions on device and materials reliability,* vol. 4, no. 4, pp. 709-714, 2004.

[2] R. Remsburg, Advanced Thermal Design of Electronic Equipment, Chapman & Hall, 1998.

[3] Available at: www.bccresearch.com/report/thermal-management-technologies-market..

[4] R. J. McGlen, R. Jachuck and S. Lin, " Integrated thermal management techniques for high power electronic devices," *Applied thermal engineering,* vol. 24, no. 8, pp. 1143-1156 , 2004.

[5] Y. Wang and K. Vafai, "An experimental investigation of the thermal performance of an asymmetrical flat plate heat pipe," *International journal of heat and mass transfer,* vol. 43, no. 15, pp. 2657-2668, 2000.

[6] R. Chu and R. Simons, "Recent development of computer cooling technology," *International symposium on transport phenomena in thermal engineering,* vol. 5, pp. 17-25, 1993.

[7] H. Yuncu and G. Anbar, "An experimental investigation on performance of fins on a horizontal base in free convection heat transfer," *Journal of heat and mass transfer,* vol. 33, no. 5-6, pp. 507-514, 1998.

[8] B. Yazicioglu and H. Yuncu, "Optimum fin spacing of rectangular fins on a vertical base in free convection heat transfer," *Journal of heat and mass transfer,* vol. 44, no. 1, pp. 11-21, 2007.

[9] F. Harahap and H. McManus, "Natural convection heat transfer from horizontal rectangular fin arrays," *Journal of heat transfer,* vol. 89, no. 1, pp. 32-39, 1967.

[10] S. Anandan and V. Ramalingam, " Thermal management of electronics: a review of literature.," vol. 2, 2008.

[11] S. Ostrach, "An analysis of free convection flow and heat transfer about a flat plate parallel to the direction of the generating of the body force," NACA, 1953.

[12] E. Sparrow and J. L. Gregg, "Laminar free convection from a vertical flat plate," *ASME,* vol.

80, pp. 435-440 , 1956.

[13] S. Churchill and H. Chu, "Correlating equations for laminar and turbulent free convection from a vertical plate," *International journal of heat and mass transfer,* vol. 18, no. 11, pp. 1323-1329, 1975.

[14] W. Elenbaas, "Heat dissipation of parallel plates by free convection," *Journal of Physica,* vol. 9, no. 1, pp. 1-28, 1942.

[15] A. Bar-Cohen and W. Rohsenow, "Thermally optimum spacing of vertical, natural convection cooled, parallel plates," *Journal of heat transfer,* vol. 106, no. 1, pp. 116-124, 1984.

[16] J. Culham, M. M. Yovanovich and S. Lee, "Thermal modeling of isothermal cuboids and rectangular heat sinks cooled by natural convection," *IEEE transaction on components, packaging and manufacturing technology,* vol. 18, no. 3, pp. 559-566, 1995.

[17] Y. M., "Natural convection from isothermal spheroids in the conductive to laminar flow regimes," in *AIAA Thermophysics conference*, Honolulu, 1987.

[18] M. Yovanovich, "On the effect of shape, aspect ration and orientation upon natural convection from isothermal bodies," in *ASME*, Boston, 1987.

[19] J. Bodoia and J. Osterle, "The development of free convection betwen heated vertical plates," *Journal of heat transfer,* vol. 84, pp. 40-44, 1962.

[20] O. Olusoji and H. Hetherington, "Application of the finite element method to natural convection heat transfer from the open vertical channel," *International journal of heat and mass transfer,* vol. 20, no. 11, pp. 1195-1204, 1977.

[21] M. Fujii, "Enhancement of natural convection heat transfer from a vertical heated plate using inclined fins," *Heat Transfer—Asian Research,* vol. 36, no. 6, pp. 334-344, 2007.

[22] K. Starner and H. N. McManus, "An experimental investigation of free-convection heat transfer from rectangular-fin arrays," *Journal of heat tranfer,* vol. 85, no. 3, pp. 273-278, 1963.

[23] J. Welling and C. Wooldridge, "Free convection heat transfer coefficients from rectangular vertical fins," *Journal of heat transfer,* vol. 87, no. 4, pp. 439-445, 1965.

[24] B. Chaddock, "Free convection heat transfer from vertical rectangular fin arrays," *ASHRAE journal,* vol. 12, pp. 53-60, 1970.

[25] T. Alhara, "Natural convection heat transfer from vertical rectangular-fin arrays: Part 2, heat transfer from fin-edges," *Bulletin of the JSME,* pp. 1182-1120, 1970.

[26] T. Alhara, "Convection heat transfer from vertical rectangular-fin arrays (part 3, heat transfer

from fin-flats)," *Bulletin of JSME,* pp. 1192-, 1970.

[27] C. Leung and S. Probert, "Heat exchanger performance: effect of orientation," *Journal of applied energy,* vol. 33, no. 4, pp. 235-252, 1989.

[28] C. Leung and S. Probert, "Natural-convective heat exchanger with vertical rectangular fins and base: design criteria," *Journal of mechanical engineering science,* vol. 201, no. 5, pp. 365-372, 1987.

[29] C. Leung, S. Probert and M. Shilston, "Heat exchanger design: Optimal uniform separation between rectangular fins protruding from a vertical rectangular base," *Journal of applied energy,* vol. 19, no. 4, pp. 287-299, 1985.

[30] C. Leung, S. Probert and M. Shilston, "Heat exchanger design: Thermal performances of rectangular fins protruding from vertical or horizontal rectangular bases," *Journal of applied energy,* vol. 20, no. 2, pp. 123-140, 1985.

[31] C. Leung, S. Probert and M. Shilston, "Heat transfer performance of vertical rectangular fins protruding from bases: effect of fin length," *Journal of applied energy,* vol. 22, no. 4, pp. 313-318, 1986.

[32] D. Van de Pol, "Free convective heat transfer from vertical fin arrays," *IEEE transaction on parts, hybrids and packaging,* vol. 10, no. 4, pp. 267-271, 1974.

[33] J. Edwards and J. Chaddock, "An experimental investigation of the radiation and free convection heat transfer from a cylindrical disk extended surface," *ASHRAE transactions,* vol. 69, pp. 313-322, 1963.

[34] E. Sparrow and S. Acharya, "A natural convection fin with a solution-determined nonmonotonically varying heat transfer coefficient," *Journal of heat transfer,* vol. 103, no. 2, pp. 218-226, 1981.

[35] N. Saikhedkar and S. Sukhatme, "Heat transfer from rectangular cross-sectioned vertical fin arrays," in *Proceedings of the sixth national heat and mass transfer conference, India,* 1981.

[36] E. Sparrow and S. Vemuri, "Natural convection/radiation heat transfer from highly populated pin fin arrays," *Journal of heat transfer,* vol. 107, no. 1, pp. 190-198, 1985.

[37] E. Sparrow and S. Vemuri, "Orientation effects on natural convection/radiation heat transfer from pin-fin arrays," *International journal of heat and mass transfer,* vol. 29, no. 3, pp. 359-368, 1986.

[38] H. Azarkish, S. Sarvari and A. Behzadmehr, "Optimum geometry design of a longitudinal fin with volumetric heat generation under the influences of natural convection and radiation," *Journal of energy conversion and management,* vol. 51, no. 10, pp. 1938-1946, 2010.

[39] V. Dharma Rao, S. Naidu, B. Govinda Rao and K. Sharma, “Heat transfer from a horizontal fin array by natural convection and radiation-A conjugate analysis,” *International journal of heat and mass transfer,* vol. 49, no. 19-20, pp. 3379-3391, 2006.

[40] K. Karki and S. Patankar, “Cooling of a vertical shrouded fin array by natural convection: a numerical study,” *Journal of heat transfer,* vol. 109, pp. 671-676, 1987.

[41] Y. Cengel and T. Ngai, “Cooling of vertical shrouded-fin arrays of rectangular profile by natural convection: an experimental study,” *Journal of heat transfer engineering,* vol. 12, no. 4, pp. 27-39, 1991.

[42] C. Leung and S. Probert, “Thermal effectiveness of short-protrusion rectangular heat exchanger fins,” *Journal of applied energy,* vol. 34, no. 1, pp. 1-8, 1989.

[43] T. A. A. Daloglu, “Natural convection in a periodically finned vertical channel,” *International Communications in Heat and Mass Transfer,* vol. 26, no. 8, p. 1175–1182, 1999.

[44] S. Nada, “Natural convection heat transfer in horizontal and vertical closed narrow enclosures with heated rectangular finned base plate,” vol. 50, 2007.

[45] A. Nakhi and A. Chamkha, “Conjugate natural convection in a square enclosure with inclined thin fin of arbitrary length,” *International journal of thermal sciences,* vol. 46, no. 5, p. 467–478, 2007.

[46] A. Bejan, Convection heat transfer, Prentice Hall, 1984.

[47] D. F. Young, B. R. Munson, T. H. Okiishi and W. W. Huebsch, A Brief Introduction to Fluid Mechanics, John Wiley & Sons, 2010.

[48] T. Aihara and S. Maruyama, “Free convective/radiative heat transfer from pin-fin arrays with a vertical base plate (general representation of heat transfer performance),” *International journal of heat and mass transfer,* vol. 33, no. 6, pp. 1223-1232, 1990.

[49] “ANSYS Fluent, computational fluid dynamics CAD tool (Ver. 12.1.4)”.

[50] COMSOL Multiphysics Finite Element Analysis Software (4.2).

[51] A. Tamayol, F. McGregor, E. Demian, E. Trandafir, P. Bowler and M. Bahrami, “Assessment of thermal performance of electronic enclosures with rectangular fins: A passive thermal solution,” in *ASME pacific rim technical conference and exhibition on packaging and Integration of electronic and photonic systems*, Portland, Oregon, USA, 2011.

[52] J. P. Holman, Experimental Methods for Engineering, 7th ed., New York: McGrawHill, 2001.

[53] S. W. Churchill and R. Usagi, " A general expression for the correlation of rates of transfer and other phenomenon," *AIChE,* vol. 18, no. 6, p. 1121–1128, 1972.

[54] R. J. Goldstein, E. M. Sparrow and D. C. Jones, "Natural convection mass transfer adjacent to horizontal plates," *Int. journal of heat mass transfer,* vol. 16, pp. 1025-1035, 1973.

[55] A. C. A.B.-Nakhi, "Conjugate natural convection in a square enclosure with inclined thin fin of arbitrary length," vol. 46, 2007.

[56] A. Guvenc and H. Yuncu, "An experimental investigation on performance of fins on a horizontal base in free convection heat transfer," *Journal of heat and mass transfer,* vol. 37, no. 4-5, pp. 409-416, 2001.

[57] M. Mobedi and H. Yuncu, "A three dimensional numerical study on natural convection heat transfer from short horizontal rectangular fin array," *Journal of heat and mass transfer,* vol. 39, no. 4, pp. 267-275, 2003.

[58] S. Churchill, "A comprehensive correlating equation for Buoyancy-Induced flow in channels," *Letters in heat and mass transfer,* vol. 4, pp. 193-199, 1977.

[59] C. Leung, S. Probert and M. Shilston, "Heat exchanger: optimal separation for vertical rectangular fins protruding from a vertical rectangular base," *Journal of applied energy,* vol. 19, no. 2, pp. 77-85, 1985.

[60] J. Taylor, An introduction to error analysis: the study of uncertainties in physical measurements, University Science Books, 1996.

[61] A. Shanmuga and V. Ramalingam, "Thermal managment of electronics, a review of literature," in *Thermal Science*, National library of Serbia, 2008, pp. 5-26.

[62] A. Daloglu and T. Ayhan, "Natural convection in a periodically finned vertical channel," *International Communications in Heat and Mass Transfer,* vol. 26, no. 8, p. 1175–1182, 1999.

[63] A. Nakhi and A. Chamkha, "Conjugate natural convection in a square enclosure with inclined thin fin of arbitrary length," vol. 46, 2007.

[64] A. Daloglu and T. Ayhan, "Natural convection in a periodically finned vertical channel," *International Communications in Heat and Mass Transfer,* vol. 26, no. 8, p. 1175–1182, 1999.

[65] O. Miyatake and T. Fujii, "Free convection heat transfer between vertical parallel plates - one plate isothermally heated and the other thermally insulated,," *Heat transfer Japan,* vol. 1, pp. 30-38, 1972.

Appendices

Appendix 1. Experimental Data

A-1-1 Experimental data for continuous fins

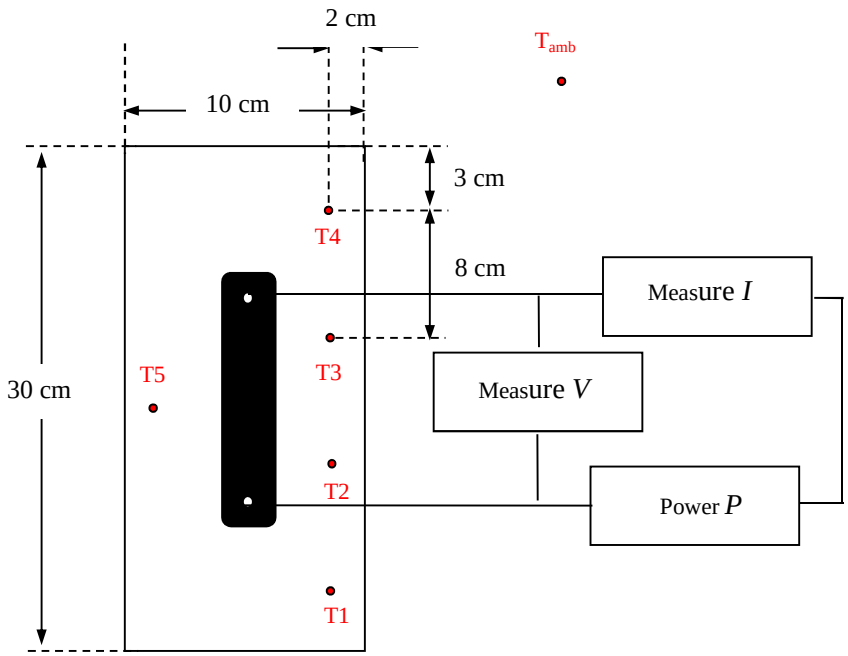

Figure A1-0-1: Testbed configuration for heatsinks with fin array (both continuous and interrupted)

Note that the samples dimensions are shown in Tables 3-1, 3-2 and 3-3.

Sample# cont-1-10-25					
V(V)	40	50	60	65	70
I(A)	0.407	0.515	0.615	0.67	0.732
Power(W)	**16.3**	**25.8**	**36.9**	**43.6**	**51.2**
T_{amb} (°C)	21	21	21	20	20
T1 (°C)	39	45	57	64	71
T2 (°C)	40	50	58	67	71
T3 (°C)	41	49	60	69	73
T4 (°C)	46	53	65	72	80
T5 (°C)	41	51	61	69	73
T_{ave} (°C)	**41.4**	**49.6**	**60.2**	**68.2**	**73.6**

Sample# cont-1-10-10					
V(V)	40	50	60	65	70
I(A)	0.409	0.512	0.617	0.67	0.722
Power(W)	**16.4**	**25.6**	**37.0**	**43.6**	**50.5**
T_{amb} (°C)	21	20	21	20	19.5
T1 (°C)	44	58	71	81	87
T2 (°C)	47	59	73	83	90
T3 (°C)	52	62	78	85	93
T4 (°C)	54	66	80	90	98
T5 (°C)	46	60	73	83	90
T_{ave} (°C)	**48.6**	**61**	**75**	**84.4**	**91.6**

Sample# cont-1-10-17				
V(V)	40	50	60	70
I(A)	0.41	0.51	0.615	0.718
Power(W)	**16.4**	**25.5**	**36.9**	**50.3**
T_{amb} (°C)	21	21	21	21
T1 (°C)	44	50	65	77
T2 (°C)	44	50	68	80
T3 (°C)	45	51	66	81
T4 (°C)	50	57	73	86
T5 (°C)	42	47	64	77
T_{ave} (°C)	**45**	**51**	**67.2**	**80.2**

Sample# cont-1-14-17					
V(V)	30	40	50	60	70
I(A)	0.305	0.41	0.51	0.615	0.718
Power(W)	**9.2**	**16.4**	**25.5**	**36.9**	**50.3**
T_{amb} (°C)	21	21	20	20	20
T1 (°C)	28	38	49	62	77
T2 (°C)	31	40	52	63	80
T3 (°C)	32	41	53	65	81
T4 (°C)	34	45	58	70	86
T5 (°C)	33	41	53	66	77
T_{ave} (°C)	**31.6**	**41**	**53**	**65.2**	**80.2**

Sample# cont-1-6-17					
V(V)	40	50	60	65	70
I(A)	0.41	0.51	0.615	0.67	0.718
Power(W)	**16.4**	**25.5**	**36.9**	**43.6**	**50.3**
T_{amb} (°C)	21	20	20	20	20
T1 (°C)	43	60	72	80	86
T2 (°C)	46	63	73	80	89
T3 (°C)	47	63	74	82	90
T4 (°C)	49	70	81	88	95
T5 (°C)	48	64	76	83	86
T_{ave} (°C)	**46.6**	**64**	**75.2**	**82.6**	**89.2**

Sample calculation for sample# Cont-1-10-17:

The aim is to calculate the Nusselt number for natural convective heat transfer rate from the fins from our experimental data and compare it to the Nusselt number by [9].

Known and measured parameters:

$$k = 0.026\, W/m.K,\ \ Pr = 0.7,\ \ \sigma = 5.67\ 10^{-8}\, W/m^2.K^4,\ \ \varepsilon = 0.75$$

$$l = 0.3 \text{ m},\ \ s = 0.0095 \text{ m},\ \ W = 0.1 \text{ m},\ \ N = 8,\ \ t = 2.5 \text{ mm},\ \ H = 0.017 \text{ m}$$

$$l = 0.3 \text{ m},\ \ s = 0.0095 \text{ m},\ \ W = 0.1 \text{ m},\ \ N = 8,\ \ t = 2.5 \text{ mm}$$

Solution:

$\dot{Q}_{NC} = \dot{Q}_{total} - \dot{Q}_{rad} \quad [W]$,

$P = V.I = \dot{Q}_{total}$ (In a steady state condition)

$$\dot{Q}_{rad} = \sigma\varepsilon\left({T_w}^4 - {T_\infty}^4\right)\sum_{i=1}^{3} A_i F_{i4} \quad [W],$$

$$\sum_{i=1}^{3} A_i F_{i4} = N.l\left\{0.4\, s + 2H\left[1 + \left(\frac{S}{H}\right) - 0.5\left(1 + \left(\frac{S}{H}\right)^2\right)^{0.5}\right]\right\} = 0.0277$$

$P = V.I = 25.5\, W$

$\dot{Q}_{rad} = 6.06\, W$

$\dot{Q}_{NC} = \dot{Q}_{total} - \dot{Q}_{rad} = 19.5\, W$

$\dot{Q}_{fins} = \dot{Q}_{NC} - \ \dot{Q}_{fin\ tips} \ \ [W]$,

$\dot{Q}_{fin\ tips} \ = h_{ft}\, A_{ft}\, \Delta T \ \ [W]$

$$h_{ft} = \frac{Nu_l.k}{l},$$

$$Ra_l = \frac{g\beta\, \Delta T l^3}{\alpha\vartheta} = 8 \times 10^7$$

$$Nu_l = \left(0.825 + \frac{0.387 Ra_l^{1/6}}{(1 + (0.492/Pr)^{9/16})^{8/27}}\right)^2 = 57.56$$

$A_{ft} = N.t.l = 0.006\, m^2$

$$Nu_s = \frac{h_s.s}{k},$$

$$h_s = \frac{\dot{Q}_{fins}}{A_f \Delta T},$$

$A_f = l[2.N.H + (w - N.t)] = 0.112\ m^2$

$$Nu_s = 1.73$$

And the Nusselt number from [9] is calculated by Eq. 1-6

$$Nu_s = \frac{h\ s}{k} = \left[\frac{576}{\left(\frac{Ra_s s}{L}\right)^2} + \frac{2.873}{\left(\frac{Ra_s s}{L}\right)^{0.5}}\right]^{-0.5} = 1.58$$

A-1-2 Experimental data for interrupted fins

Sample# Int-4-20					
V(V)	40	50	60	65	70
I(A)	0.409	0.512	0.617	0.67	0.722
Power(W)	**16.4**	**25.6**	**37.0**	**43.6**	**50.5**
T_{amb} (°C)	20	20	20	21	20
T1 (°C)	37	49	56	64	68
T2 (°C)	40	50	59	66	73
T3 (°C)	42	52	58	63	69
T4 (°C)	44	54	64	72	78
T5 (°C)	41	51	62	70	75
T_{ave} (°C)	**40.8**	**51.2**	**59.8**	**67**	**72.6**

Sample# Int-4-30					
V(V)	40	50	60	65	70
I(A)	0.41	0.512	0.617	0.669	0.72
Power(W)	**16.4**	**25.6**	**37.0**	**43.5**	**50.4**
T_{amb} (°C)	21	20	20	21	20
T1 (°C)	38	51	65	71	75
T2 (°C)	39	53	63	74	81
T3 (°C)	41	52	65	73	80
T4 (°C)	42	57	66	80	85
T5 (°C)	42	57	66	77	82
T_{ave} (°C)	**40.4**	**54**	**65**	**75**	**80.6**

Sample# Int-4-40					
V(V)	40	50	60	65	70
I(A)	0.409	0.512	0.617	0.671	0.722
Power(W)	**16.4**	**25.6**	**37.0**	**43.6**	**50.5**
T_{amb} (°C)	20	21	20	21	20
T1 (°C)	52	62	62	73	76
T2 (°C)	55	64	67	74	78
T3 (°C)	58	66	70	77	80
T4 (°C)	60	69	73	81	85
T5 (°C)	56	65	68	75	82
T_{ave} (°C)	**56.2**	**65.2**	**68**	**76**	**80.2**

Sample# Int-1-20					
V(V)	22.6	40.5	50	60	70
I(A)	0.23	0.415	0.513	0.618	0.72
Power(W)	**5.2**	**16.8**	**25.7**	**37.1**	**50.4**
T_{amb} (°C)	21	20	20	20	19
T1 (°C)	22	35	43	54	66
T2 (°C)	24	36	48	66	74
T3 (°C)	25	41	49	66	75
T4 (°C)	27	43	52	68	76
T5 (°C)	25	41	47	58	69
T_{ave} (°C)	**24.6**	**39.2**	**47.8**	**62.4**	**72**

Sample# Int-2-20					
V(V)	22.6	40.5	50	60	70
I(A)	0.23	0.415	0.513	0.618	0.72
Power(W)	**5.2**	**16.8**	**25.7**	**37.1**	**50.4**
T_{amb} (°C)	21	20	20	20	20
T1 (°C)	24	37	47	57	70
T2 (°C)	26	40	50	63	76
T3 (°C)	27	44	52	66	78
T4 (°C)	29	46	55	68	79
T5 (°C)	27	44	50	58	72
T_{ave} (°C)	**26.6**	**42.2**	**50.8**	**62.4**	**75**

Sample# Int-3-20					
V(V)	40	50	60	65	70
I(A)	0.409	0.517	0.619	0.67	0.722
Power(W)	**16.4**	**25.9**	**37.1**	**43.6**	**50.5**
T_{amb} (°C)	20	21	20	20	20
T1 (°C)	34	45	55	60	68
T2 (°C)	36	48	59	63	71
T3 (°C)	38	51	64	70	76
T4 (°C)	42	53	65	71	78
T5 (°C)	40	50	61	65	72
T_{ave} (°C)	**38**	**49.4**	**60.8**	**65.8**	**73**

Sample# Int-5-20					
V(V)	40	50	60	65	70
I(A)	0.41	0.51	0.618	0.67	0.722
Power(W)	**16.4**	**25.5**	**37.1**	**43.6**	**50.5**
T_{amb} (°C)	20	20	20	21	21
T1 (°C)	35	45	57	64	65
T2 (°C)	39	47	59	66	70
T3 (°C)	40	50	62	70	75
T4 (°C)	47	54	66	63	85
T5 (°C)	42	52	64	72	78
T_{ave} (°C)	**40.6**	**49.6**	**61.6**	**67**	**74.6**

A-1-3 Experimental data for interrupted walls

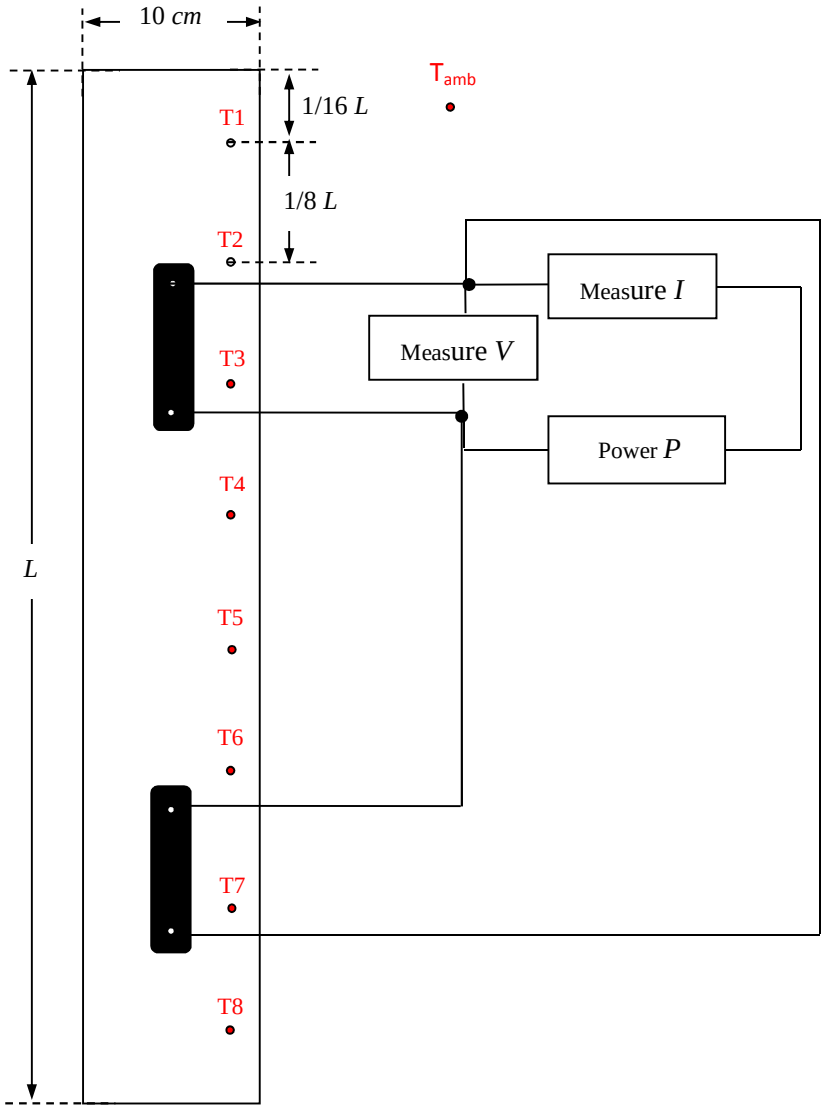

Figure A1-0-2: Testbed configuration for heatsinks with interrupted walls

Sample# SW-1						
V (V)	38	45	55	70	80	85
I (A)	0.79	1.09	1.12	1.14	1.64	1.74
Power (W)	**30.02**	**49.05**	**61.6**	**79.8**	**131.2**	**147.9**
T_{amb} (°C)	22.4	22.4	22.3	21.5	22.2	22.1
T1 (°C)	37.5	42.9	48.9	60.7	68.7	74.2
T2 (°C)	35.2	40.6	46.7	62.2	69.7	78.1
T3 (°C)	37.2	42.9	48.8	62	67.8	76.4
T4 (°C)	39.3	46	52.9	67.3	76.3	83.2
T5 (°C)	40.8	48.4	56.3	71.9	82.8	89.8
T6 (°C)	34.5	39.1	43.8	52	59.3	62.3
T7 (°C)	32.2	35.7	39.3	46.3	51.2	54.2
T8 (°C)	29.4	32.1	34.9	42.4	46	51.6
T_{ave} (°C)	**35.8**	**41.0**	**46.5**	**58.1**	**65.2**	**71.2**

Sample# SW-2						
V (V)	38	45	55	70	80	85
I (A)	0.78	1.09	1.12	1.14	1.64	1.74
Power (W)	**29.6**	**49.05**	**61.6**	**79.8**	**131.2**	**147.9**
T_{amb} (°C)	24	25	23	22	22	23
T1 (°C)	38	44	47	57	66	71
T2 (°C)	37	42	44	53	59	64
T3 (°C)	39	42	43	52	58	63
T4 (°C)	40	46	50	63	73	77
T5 (°C)	38	43	46	56	64	69
T6 (°C)	36	40	45	55	62	67
T7 (°C)	35	42	44	54	61	66
T8 (°C)	35	39	39	45	50	54
T_{ave} (°C)	**37**	**42**	**45**	**54**	**62**	**66**

Sample# **SW-3**				
V (V)	40	45	60	70
I (A)	0.81	0.92	1.24	1.43
Power (W)	**32.4**	**41.4**	**74.4**	**100.1**
T_{amb} (°C)	22.5	23	22.3	21.5
T1 (°C)	44	50	60	81.5
T2 (°C)	42	48	57.3	77.5
T3 (°C)	42	48	57	77.3
T4 (°C)	41.5	47	56.5	75.5
T5 (°C)	41	44.5	55.5	73.4
T6 (°C)	40	43	54	70.5
T7 (°C)	39	42	52	68
T8 (°C)	36.5	41.5	48.5	63
T_{ave} (°C)	**40.8**	**45.5**	**55.1**	**73.3**

Sample# **SW-4**				
V (V)	40	44	60	70
I (A)	0.85	0.95	1.24	1.43
Power (W)	**34**	**41.8**	**61.6**	**100.1**
T_{amb} (°C)	22	24	24	21
T1 (°C)	47.3	53	62	76.5
T2 (°C)	45.5	51	59	72
T3 (°C)	44.5	50	58	70
T4 (°C)	43.5	49	57.4	69
T5 (°C)	43	48.5	56	67
T6 (°C)	43	48	56	65
T7 (°C)	40	46	53	62.5
T8 (°C)	41.5	44.5	51	59.5
T_{ave} (°C)	**43.5**	**48.8**	**57.3**	**67.7**

Sample# **w-int-5**				
V (V)	38	45	55	70
I (A)	0.78	1.09	1.12	1.43
Power (W)	**29.6**	**49.05**	**61.6**	**100**
Tamb (°C)	24	25	23	22
T1 (°C)	39	44	47	57
T2 (°C)	38	43	46	56
T3 (°C)	37	42	45	55
T4 (°C)	37	42	45	54
T5 (°C)	38	42	44	54
T6 (°C)	36	40	44	53
T7 (°C)	35	42	43	52
T8 (°C)	35	39	39	45
Tave (°C)	**40.0**	**46.0**	**50.0**	**63**

Sample# **w-int-6**				
V (V)	40	44	60	70
I (A)	0.85	0.95	1.24	1.43
Power (W)	**34**	**41.8**	**61.6**	**100.1**
T_{amb} (°C)	22	24	26	21
T1 (°C)	47.3	54	64	79.5
T2 (°C)	45.5	52	61	75
T3 (°C)	44.5	51	60	72.5
T4 (°C)	43.5	50.2	59.2	72
T5 (°C)	43	49.5	58.3	70
T6 (°C)	43	49	58.1	65.2
T7 (°C)	40	48	55	61.5
T8 (°C)	41.5	44.5	54	58
T_{ave} (°C)	**43.5**	**49.8**	**59.4**	**69.2**

Sample calculation for sample# SW-2 :

The aim is to calculate the Nusselt number for natural convective heat transfer rate from the interrupted walls from our experimental data.

Known and measured parameters:

$$T_w = 45°C,\ T_{amb} = 23°C,\quad V = 55\ V,\ I = 1.12\ A$$
$$k = 0.026\ W/m.K,\ Pr = 0.7,\ \sigma = 5.67\ 10^{-8}\ W/m^2.K^4,\ \varepsilon = 0.75$$
$$\vartheta = 1.58\ 10^{-5},\quad g = 9.81\ m/s^2$$
$$l = 0.05\ m,\ L = 1.45\ m,\ W = 0.1\ m,\ n = 7,\ t = 10\ mm,\ H = 0.1\ m$$

Solution:

Calculation of natural convective heat transfer rate is very similar to the calculations in the previous sub-section. After calculating $\dot{Q}_{fins}$, L_{eff} is obtained as following:

$$L_{eff} = \left(\frac{\dot{Q}_{fins}}{0.59\ k}\right)^{4/3} \left(\frac{\alpha\vartheta}{g\beta}\right)^{\frac{1}{3}} .\Delta T^{-\frac{5}{3}}\ \ [m]$$

$$Nu_{L_{eff}} = 0.59\ Ra_{L_{eff}}^{\frac{1}{4}} = 3120$$

Appendix 2. ASW Reports

This section contains the reports by SFU provided for ASW for their naturally cooled enclosures. Each part contains the geometrical specifications for their former design of the enclosures and a recommended design by SFU.

Report Number:	**ASW-0811-1/1**
Report Date:	**November 3rd 2011**
Sample Name:	**Extrusion4-Vertical Test**

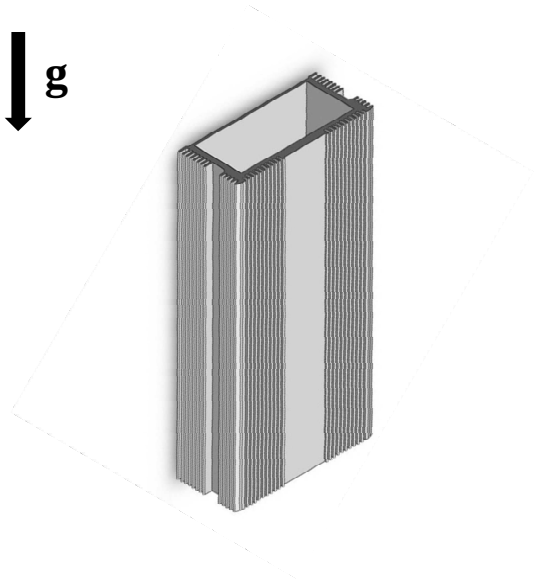

Figure A2-1-1a: Extrusion4 Current Design

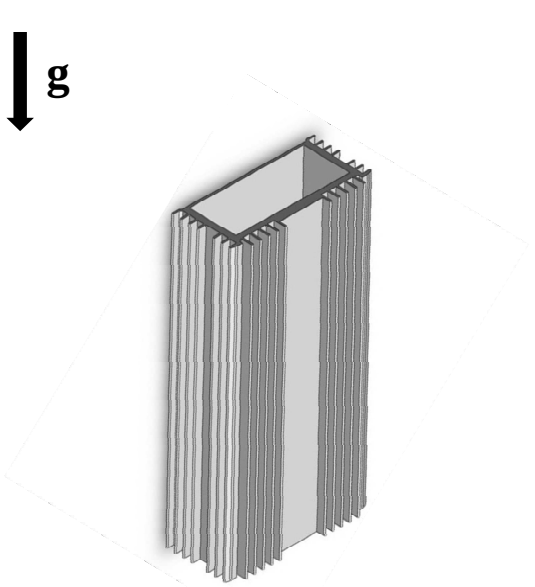

Figure A2-1-1b: Extrusion4 Recom. Design

Figure A2-1-2: Real picture of the current design enclosure

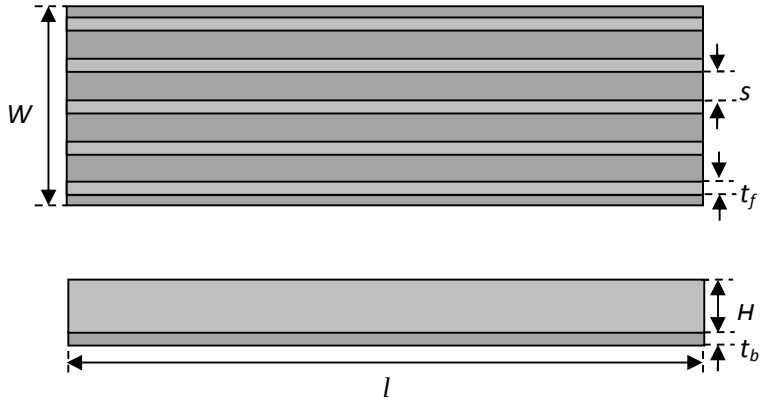

Figure A2-1-3: Top and side view of the fin array with geometric parameters

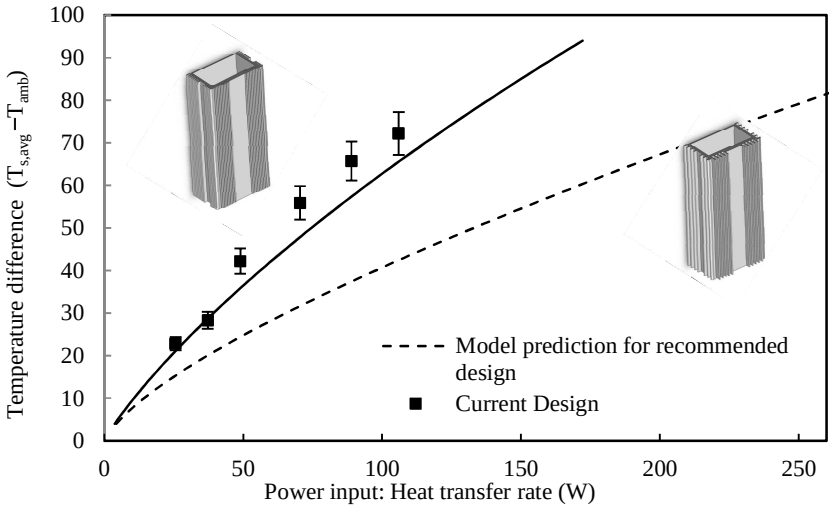

Figure A2-1-4: Comparison between current and recommended design

Current Design Dimensions							
Top Plate	n (#Fins)	s (mm)	H (mm)	W (mm)	L (mm)	t_b (mm)	t_f (mm)
	20	2.7	7	160	406	3.5	2.5
Side Plate	n (#Fins)	s (mm)	H (mm)	W (mm)	L (mm)	t_b (mm)	t_f (mm)
	26	2.7	7	75	406	3.5	2.5
Caps	n (#Fins)	s (mm)	H (mm)	W (mm)	L (mm)	t_b (mm)	t_f (mm)
	-	-	-	75	160	1.7	-

Test Results: Current Design						
Power (W)	106	89	70	49	37	26
$T_{s,avg}$ (˚C)	96	89	79	69	52	46
T_{amb} (˚C)	21	22	21	21	22	22

Recommended Design Dimensions							
Top Plate	n* (#Fins)	s* (mm)	H* (mm)	W (mm)	L (mm)	t_b (mm)	t_f (mm)
	10	9	15	160	406	3.5	2.5
Side Plate	n* (#Fins)	s* (mm)	H (mm)	W (mm)	L (mm)	t_b (mm)	t_f (mm)
	14	9	10	75	406	3.5	2.5
Caps	n (#Fins)	s (mm)	H (mm)	W (mm)	L (mm)	t_b (mm)	t_f (mm)
	-	-	-	75	160	1.7	-

Estimated Results: Recommended Design							
Power (W)	150	106	89	70	49	37	26
$T_{s,avg}$ (˚C)	74	62	57	52	45	40	36

Current vs. Recommended Design: Thermal Performance Improvement							
Power (W)	150	106	89	70	49	37	26
$T_{current}$(˚C)	105	86	77	67	56	49	41
T_{recom}(˚C)	74	62	57	52	45	40	36
ΔT (˚C)	**31**	**23**	**20**	**16**	**11**	**9**	**6**

Summary
• 30˚C potential reduction in average surface temperature of enclosure @ 150 W

Report Number:	**ASW-0811-1/1**
Report Date:	**August 31st 2011**
Sample Name:	**Extrusion5-Vertical Test**

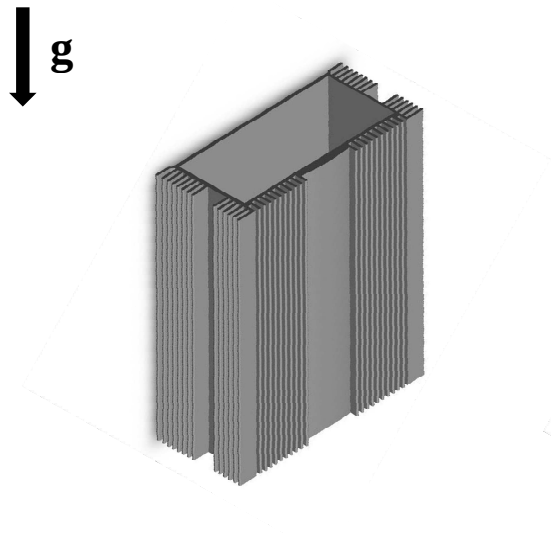

Figure A2-2-1a: Extrusion5 Current Design, Weight: 1490 g

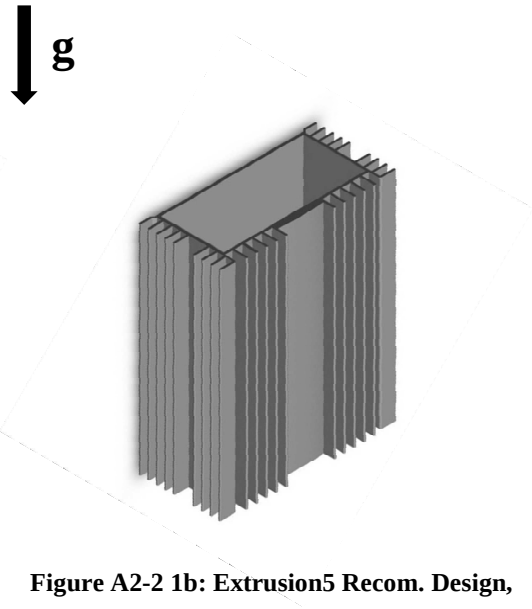

Figure A2-2 1b: Extrusion5 Recom. Design, Weight: 1220 g

Figure A2-2-2: Real picture of the current design enclosure

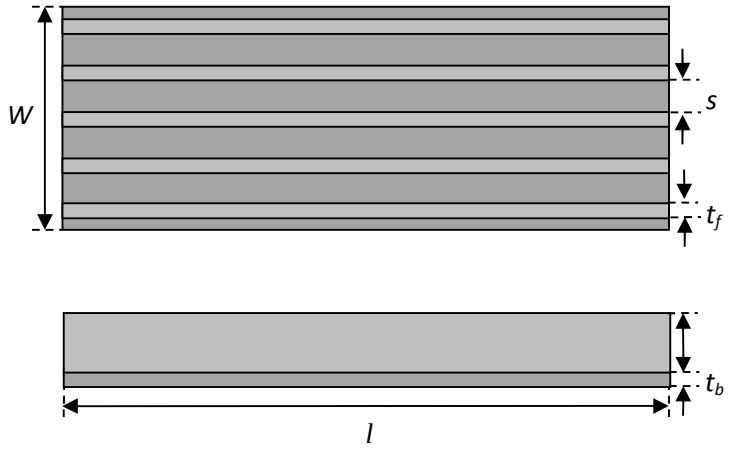

Figure A2-2-3: Top and side view of the fin array with geometric parameters

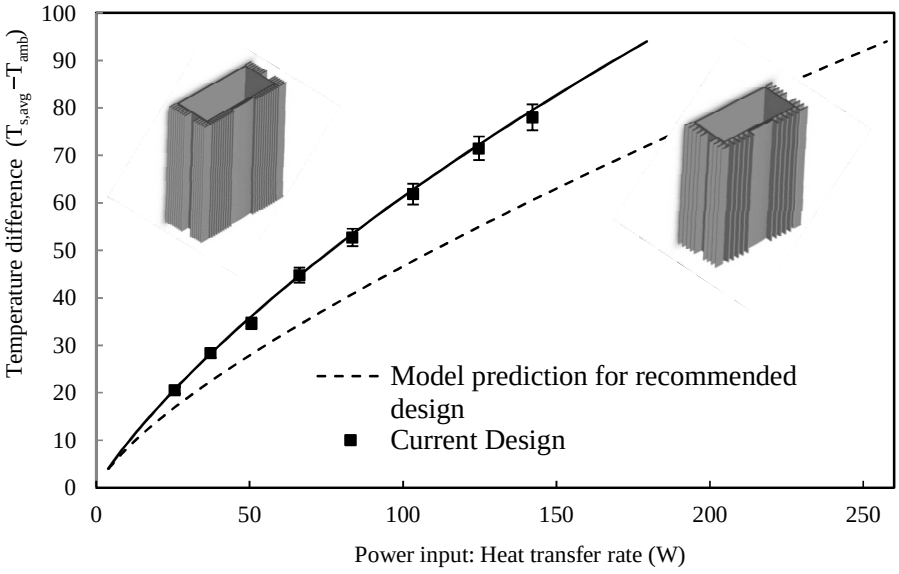

Figure A2-2-4: Comparison between current and recommended design

Current Design Dimensions							
Top Plate	n (#Fins)	s (mm)	H (mm)	W (mm)	L (mm)	t_b (mm)	t_f (mm)
	20	2.7	10	160	241	3.5	2.5
Side Plate	n (#Fins)	s (mm)	H (mm)	W (mm)	L (mm)	t_b (mm)	t_f (mm)
	26	2.7	15	75	241	3.5	2.5
Caps	n (#Fins)	s (mm)	H (mm)	W (mm)	L (mm)	t_b (mm)	t_f (mm)
	-	-	-	75	160	1.7	-

Test Results: Current Design							
Power (W)	142	125	103	84	66	51	37
$T_{s,avg}$ (˚C)	101	97	85	76	66	57	51
T_{amb} (˚C)	23	26	23	24	21	22	23

Recommended Design Dimensions							
Top Plate	n* (#Fins)	s* (mm)	H* (mm)	W (mm)	L (mm)	t_b (mm)	t_f (mm)
	12	8	15	160	241	3.5	2.5
Side Plate	n* (#Fins)	s* (mm)	H (mm)	W (mm)	L (mm)	t_b (mm)	t_f (mm)
	18	8	15	75	241	3.5	2.5
Caps	n (#Fins)	s (mm)	H (mm)	W (mm)	L (mm)	t_b (mm)	t_f (mm)
	-	-	-	75	160	1.7	-

Estimated Results: Recommended Design							
Power (W)	142	125	103	84	66	51	37
$T_{s,avg}$ (˚C)	84	81	71	63	55	50	45

Current vs. Recommended Design: Thermal Performance Improvement							
Power (W)	142	125	103	84	66	51	37
$T_{current}$(˚C)	101	97	85	76	66	57	51
T_{recom}(˚C)	84	81	71	63	55	50	45
ΔT (˚C)	**17**	**17**	**14**	**13**	**11**	**7**	**6**

Summary
• 20˚C potential reduction in average surface temperature of enclosure @ 150 W
• 18% enclosure weight reduction

Report Number:	**ASW-0811-1/1**
Report Date:	**August 6th 2011**
Sample Name:	**TPS-Extrusion**

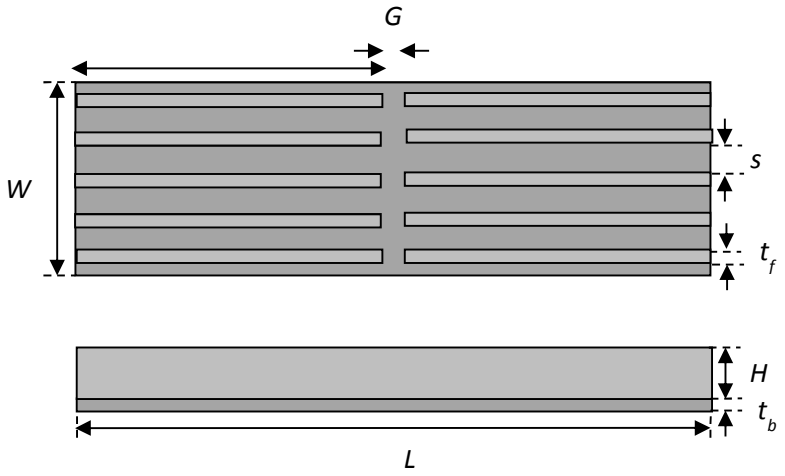

Figure A2-3-2: Top and side view of the fin array with geometric parameters

Dimensions									
Top Plate	n (#Fins)	s (mm)	H (mm)	W (mm)	L (mm)	t_b (mm)	t_f (mm)	*l* (mm)	G (mm)
	4*37	6.5	17.7	240	355	3.5	2.5	44.5	18.7
Side Plate	n (#Fins)	s (mm)	H (mm)	W (mm)	L (mm)	t_b (mm)	t_f (mm)	*l* (mm)	G (mm)
	8	6.7	12.7	95	240	3.5	2.5	95	-

Test Results: Current Design							
Power (W)	142	125	103	84	66	51	37
$T_{s,avg}$ (˚C)	51	47	41	38	37	32	28
T_{amb} (˚C)	23	22	21	21	21	21	20

Recommended Design Dimensions									
Top Plate	n (#Fins)	s (mm)	H (mm)	W (mm)	L (mm)	t_b (mm)	t_f (mm)	*l* (mm)	G (mm)
	4*37	6.5	17.7	240	355	3.5	2.5	43	22
Side Plate	n (#Fins)	s (mm)	H (mm)	W (mm)	L (mm)	t_b (mm)	t_f (mm)	*l* (mm)	G (mm)
	18	8	15	75	241	3.5	2.5	-	-

Estimated Results: Recommended Design							
Power (W)	142	125	103	84	66	51	37
$T_{s,avg}$ (˚C)	49	46	40	37	36	32	28

Current vs. Recommended Design: Thermal Performance Improvement							
Power (W)	142	125	103	84	66	51	37
$T_{current}$(˚C)	51	47	41	38	37	32	28
T_{recom}(˚C)	49	46	40	37	36	32	28
ΔT (˚C)	**2**	**1**	**1**	**1**	**1**	**0**	**0**

Summary
• 3˚C potential reduction in average surface temperature of enclosure @ 150 W
•5-6% enclosure weight reduction

Report Number:	**ASW-0811-1/1**
Report Date:	**August 6th 2011**
Sample Name:	**VMC-Extrusion**

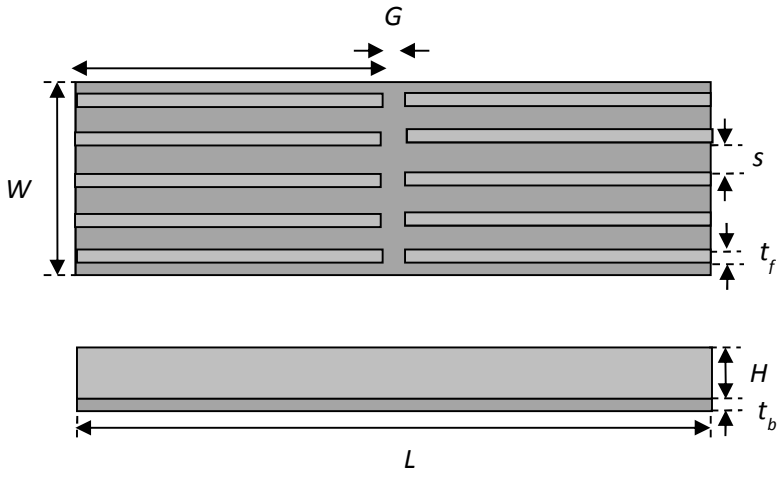

Figure A2-4-2: Top and side view of the fin array with geometric parameters

Dimensions									
Top Plate	n (#Fins)	s (mm)	H (mm)	W (mm)	L (mm)	t_b (mm)	t_f (mm)	*l* (mm)	G(mm)
	4*37	6.5	17.7	240	355	3.5	2.5	44.5	18.7
Side Plate	n (#Fins)	s (mm)	H (mm)	W (mm)	L (mm)	t_b (mm)	t_f (mm)	*l* (mm)	G (mm)
	8	6.7	12.7	95	240	3.5	2.5	95	-

Test Results: Current Design							
Power (W)	142	106	87	70	49	37	24
$T_{s,avg}$ (˚C)	55	51	43	39	32	30	28
T_{amb} (˚C)	21	22	21	20	20	20	20

Recommended Design Dimensions									
Top Plate	n (#Fins)	s (mm)	H (mm)	W (mm)	L (mm)	t_b (mm)	t_f (mm)	*l* (mm)	G(mm)
	4*37	6.5	17.7	240	355	3.5	2.5	44.5	18.7
Side Plate	n (#Fins)	s (mm)	H (mm)	W (mm)	L (mm)	t_b (mm)	t_f (mm)	*l* (mm)	G (mm)
	18	8	15	75	241	3.5	2.5	95	-

Summary
Fin spacing and gap length are within the optimum range